

# Stress singularities in classical elasticity—II: Asymptotic identification

**GB Sinclair**

*Department of Mechanical Engineering, Louisiana State University, Baton Rouge, LA 70803-6413; sinclair@me.lsu.edu*

This review article (Part II) is a sequel to an earlier one (Part I) that dealt with means of removal and interpretation of stress singularities in elasticity, as well as their asymptotic and numerical analysis. It reviews contributions to the literature that have actually effected asymptotic identifications of possible stress singularities for specific configurations. For the most part, attention is focused on 2D elastostatic configurations with constituent materials being homogeneous and isotropic. For such configurations, the following types of stress singularity are identified: power singularities with both real and complex exponents, logarithmic intensification of power singularities with real exponents, pure logarithmic singularities, and log-squared singularities. These identifications are reviewed for the in-plane loading of angular elastic plates comprised of a single material in Section 2, and for such plates comprised of multiple materials in Section 3. In Section 4, singularity identifications are examined for the out-of-plane shear of elastic wedges comprised of single and multiple materials, and for the out-of-plane bending of elastic plates within the context of classical and higher-order theory. A review of stress singularities identified for other geometries is given in Section 5, axisymmetric and 3D configurations being considered. A limited examination of the stress singularities identified for other field equations is given as well in Section 5. The paper closes with an overview of the status of singularity identification within elasticity. This Part II of the review has 227 references. [DOI: 10.1115/1.1767846]

## 1 INTRODUCTION

This article is a sequel to another one on stress singularities in classical elastostatics which considers their removal, interpretation, and analysis (Sinclair [1]—hereinafter referred to simply as Part I). Both papers share the recognition that it is an exercise in futility to perform a stress analysis without appreciating the presence of a singularity when one occurs. In Part I, some methods for determining when a singularity is present, and possibilities for dealing with it when it is, are drawn from the literature and discussed. Here, in Part II, the literature is reviewed for contributions that have actually effected determinations of when singularities may occur.

The means by which these determinations are made is asymptotic identification. It is therefore necessary, if Part II is to be fairly self-contained, that we recap key results attending the asymptotic identification of stress singularities. These are available in the literature and a description of their development is given in Part I, Sections 4.1 and 4.2. The particular approach considered in some detail there is via the Airy stress function and separation of variables (after Williams [2]): There are other approaches which can lead to the same results (complex potentials, Mellin transforms).

To fix ideas, we consider an angular elastic plate in exten-

sion (Fig. 1). The basic separable fields used to analyze such plates are given in Williams [2] and Part I, Section 4.1. In terms of cylindrical polar coordinates  $r$  and  $\theta$ , the stresses  $\sigma_r$ ,  $\sigma_\theta$ , and  $\tau_{r\theta}$  and displacements  $u_r$  and  $u_\theta$  in these fields are

$$\begin{aligned} \sigma_r &= -\lambda r^{\lambda-1} [c_1 \cos(\lambda+1)\theta + c_2 \sin(\lambda+1)\theta \\ &\quad + (\lambda-3)(c_3 \cos(\lambda-1)\theta + c_4 \sin(\lambda-1)\theta)] \\ \sigma_\theta &= \lambda r^{\lambda-1} [c_1 \cos(\lambda+1)\theta + c_2 \sin(\lambda+1)\theta \\ &\quad + (\lambda+1)(c_3 \cos(\lambda-1)\theta + c_4 \sin(\lambda-1)\theta)] \\ \tau_{r\theta} &= \lambda r^{\lambda-1} [c_1 \sin(\lambda+1)\theta - c_2 \cos(\lambda+1)\theta \\ &\quad + (\lambda-1)(c_3 \sin(\lambda-1)\theta - c_4 \cos(\lambda-1)\theta)] \quad (1.1) \\ u_r &= \frac{-r^\lambda}{2\mu} [c_1 \cos(\lambda+1)\theta + c_2 \sin(\lambda+1)\theta \\ &\quad + (\lambda-\kappa)(c_3 \cos(\lambda-1)\theta + c_4 \sin(\lambda-1)\theta)] \\ u_\theta &= \frac{r^\lambda}{2\mu} [c_1 \sin(\lambda+1)\theta - c_2 \cos(\lambda+1)\theta \\ &\quad + (\lambda+\kappa)(c_3 \sin(\lambda-1)\theta - c_4 \cos(\lambda-1)\theta)] \end{aligned}$$

Transmitted by Editorial Advisory Board member R. C. Benson

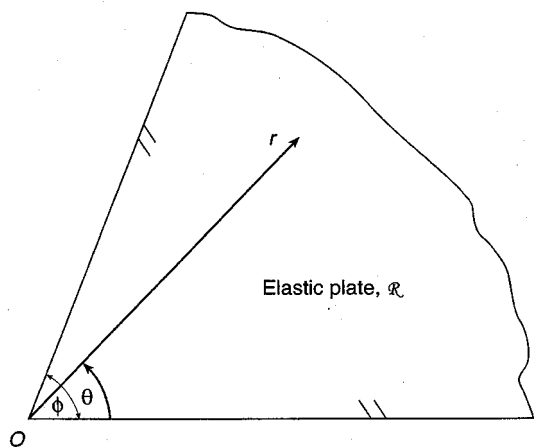


Fig. 1 Geometry and coordinates for the angular elastic plate

In (1.1),  $\mu$  is the shear modulus and  $\kappa$  equals  $3-4\nu$  for plane strain and  $(3-\nu)/(1+\nu)$  for plane stress,  $\nu$  being Poisson's ratio. Further,  $c_i$  ( $i=1,\dots,4$ ) are constants and  $\lambda$  is the separation-of-variables parameter. This parameter may be complex. Then the real and imaginary parts of (1.1) each constitute acceptable fields which may have distinct sets of constants from one another. It is also possible to have auxiliary fields participate in the asymptotic analysis. These fields can be generated by differentiating with respect to  $\lambda$  as in Dempsey and Sinclair [3], and are given in Part I, Section 4.2. By way of example, the  $\sigma_\theta$  stress component in these fields is

$$\begin{aligned} \sigma_\theta = r^{\lambda-1} & [(1+\lambda \ln r)(\hat{c}_1 \cos(\lambda+1)\theta + \hat{c}_2 \sin(\lambda+1)\theta) \\ & + (2\lambda+1+\lambda(\lambda+1)\ln r)(\hat{c}_3 \cos(\lambda-1)\theta \\ & + \hat{c}_4 \sin(\lambda-1)\theta) - \lambda\theta(\hat{c}_1 \sin(\lambda+1)\theta - \hat{c}_2 \cos(\lambda+1)\theta) \\ & + (\lambda+1)(\hat{c}_3 \sin(\lambda-1)\theta - \hat{c}_4 \cos(\lambda-1)\theta)] \end{aligned} \quad (1.2)$$

In (1.2), the carets atop constants serve to distinguish them from those of (1.1)

Introducing the fields in (1.1) into a set of four homogeneous boundary conditions holding on the two edges of the angular plate results in a homogeneous system of equations in the four constants  $c_i$ . Call the coefficient matrix of this system  $A$  and its determinant  $D$ . Then, also entertaining the possibility of the participation of the fields attending (1.2) leads to the following set of conditions for the singular stresses that are possible with homogeneous boundary conditions. For any stress component  $\sigma$ , as  $r \rightarrow 0$ :

$$\sigma = O(r^{\xi-1} \cos(\eta \ln r)) + O(r^{\xi-1} \sin(\eta \ln r)) \quad \text{when } D=0$$

for complex  $\lambda = \xi + i\eta$  ( $0 < \xi < 1$ )

$$\sigma = O(r^{\lambda-1} \ln r) + O(r^{\lambda-1}) \quad \text{when } D=0, \frac{\partial^n D}{\partial \lambda^n} = 0$$

for  $n=1, \dots, n_A - r_A$  and real  $\lambda$  ( $0 < \lambda < 1$ )

$$\sigma = O(r^{\lambda-1}) \quad \text{when } D=0 \text{ for real } \lambda (0 < \lambda < 1) \quad (1.3)$$

$$\sigma = O(\ln r) \quad \text{when } D=0, \frac{\partial^n D}{\partial \lambda^n} = 0$$

for  $n=1,\dots,n_A - r_A$  and  $\lambda=1$  with

$$\hat{c}_1^2 + \hat{c}_2^2 + \hat{c}_3^2 \neq 0 \quad \text{in the stress field attending (1.2)}$$

$$\sigma = O(\cos(\eta \ln r)) + O(\sin(\eta \ln r)) \quad \text{when } D=0$$

for complex  $\lambda = 1 + i\eta$

Herein,  $\lambda$  has taken on the role of an eigenvalue of the asymptotic problem,  $n_A$  is the order of the matrix  $A$ , and  $r_A$  is its rank when  $\lambda$  is an eigenvalue. For a plate made of a single material,  $n_A=4$  at most; for a bimaterial plate,  $n_A=8$ , and so on. The last stress in (1.3) is not singular as  $r \rightarrow 0$ , being bounded under this limit. However, it is undefined as  $r \rightarrow 0$ . Hence, to a degree, it shares with singular stresses some of the difficulties attending interpretation as  $r \rightarrow 0$ .

The conditions in (1.3) apply to angular plates in extension. Adaptation of (1.3) to states of antiplane shear follows directly (see Sections 4.1 and 4.2). Adaptation of (1.3) to bending is less direct but nonetheless fairly straightforward (see Sections 4.3 and 4.4). Adaptation of (1.3) to other configurations is discussed in Section 5.

With inhomogeneous boundary conditions, further auxiliary fields can participate. These fields follow from a further differentiation with respect to  $\lambda$ ; stresses are given in Part I, Section 4.2. By way of example, the  $\sigma_\theta$  stress component in these fields is

$$\begin{aligned} \sigma_\theta = r^{\lambda-1} & [(\lambda \ln^2 r + 2 \ln r - \lambda \theta^2)(\tilde{c}_1 \cos(\lambda+1)\theta \\ & + \tilde{c}_2 \sin(\lambda+1)\theta) + (\lambda+1)(\tilde{c}_3 \cos(\lambda-1)\theta \\ & + \tilde{c}_4 \sin(\lambda-1)\theta) + O(\ln r) + O(1)] \end{aligned} \quad (1.4)$$

as  $r \rightarrow 0$ . In (1.4), tildes atop constants distinguish them from those of (1.1) or (1.2). All three sorts of field in concert lead to the following set of conditions for the singular stresses that are possible with uniform tractions/ linear displacements applied. For any stress component  $\sigma$ , as  $r \rightarrow 0$ :

$$\sigma = \text{ord}(\ln^2 r) + \text{ord}(\ln r) \quad \text{when } D=0, \frac{\partial^n D}{\partial \lambda^n} = 0$$

for  $n=1,\dots,n_A - r_A$  with

$$\tilde{c}_1^2 + \tilde{c}_2^2 + \tilde{c}_3^2 \neq 0 \quad \text{in the stresses attending (1.4)}$$

$$\sigma = \text{ord}(\ln r) \quad \text{when } D=0, \frac{\partial^n D}{\partial \lambda^n} = 0, \text{ for } n=1,\dots, n_A - r_A \quad (1.5)$$

with  $\tilde{c}_1 = \tilde{c}_2 = \tilde{c}_3 = 0$  in the stresses attending (1.4)

$$\sigma = \text{ord}(\ln r) \quad \text{when } D=0, \frac{\partial^n D}{\partial \lambda^n} \neq 0, \text{ for } n=n_A - r_A$$

with  $\hat{c}_1^2 + \hat{c}_2^2 + \hat{c}_3^2 \neq 0$  in the stresses attending (1.2)

provided throughout (1.5),  $\lambda=1$  and  $r_A \neq r_{A'}$ , where  $r_{A'}$  is the rank of the augmented matrix formed by combining  $A$  with the nontrivial forcing vector associated with the inhomogeneous boundary conditions. Given such a nontrivial vector, the singularities in (1.5) occur irrespective of far-field boundary conditions. Hence the use of the ord notation in

(1.5) instead of the large order  $O$  notation of (1.3).<sup>1</sup> The singularity conditions in (1.5) apply directly to angular plates in extension: Adaptation to other configurations is discussed in Sections 4 and 5.

In what follows, we review asymptotic analyses that employ (1.3), (1.5), or their equivalents to identify stress singularities. We begin in Section 2 with angular elastic plates made of a single material under in-plane loading (ie, in extension). In Section 3, we review the singularities identified when such plates are made of multiple materials. In Section 4, we consider out-of-plane shear and bending. In Section 5, we consider a variety of other circumstances: axisymmetric and 3D configurations within classical elasticity, and a limited review of the effects of other field equations. Finally, in Section 6, we close with some remarks on the general character of results, and the overall state of investigations into singularity identification.

## 2 STRESS SINGULARITIES FOR THE IN-PLANE LOADING OF AN ELASTIC PLATE MADE OF A SINGLE MATERIAL

### 2.1 Formulation and eigenvalue equations

Here we obtain the eigenvalue equations governing the possible stress singularities that can occur at the vertex of an angular elastic plate subjected to different homogeneous boundary conditions on its edges.

To formally state the class of problems under consideration, we continue to employ cylindrical polar coordinates  $r$  and  $\theta$  with origin  $O$  at the plate vertex (Fig. 1). In terms of these coordinates, the open angular region of interest  $\mathfrak{R}$  is given by

$$\mathfrak{R} = \{(r, \theta) | 0 < r < \infty, 0 < \theta < \phi\} \tag{2.1}$$

where  $\phi$  is the angle subtended at the vertex of the plate. With these geometric preliminaries in place, we can formulate our class of problems as follows.

In general, we seek the planar stress components  $\sigma_r$ ,  $\sigma_\theta$ , and  $\tau_{r\theta}$  and their companion displacements  $u_r$  and  $u_\theta$ , as functions of  $r$  and  $\theta$  throughout  $\mathfrak{R}$ , satisfying: the *stress equations of equilibrium* in the absence of body forces,

$$\begin{aligned} \frac{\partial \sigma_r}{\partial r} + \frac{1}{r} \frac{\partial \tau_{r\theta}}{\partial \theta} + \frac{\sigma_r - \sigma_\theta}{r} &= 0 \\ \frac{1}{r} \frac{\partial \sigma_\theta}{\partial \theta} + \frac{\partial \tau_{r\theta}}{\partial r} + \frac{2\tau_{r\theta}}{r} &= 0 \end{aligned} \tag{2.2}$$

on  $\mathfrak{R}$ ; the *stress-displacement relations* for a linear elastic plate which is both homogeneous and isotropic,

$$\begin{aligned} \begin{Bmatrix} \sigma_r \\ \sigma_\theta \end{Bmatrix} &= \mu \begin{bmatrix} 2\Theta \\ \kappa - 1 \end{bmatrix} \begin{Bmatrix} + \\ - \end{Bmatrix} \left( \frac{\partial u_r}{\partial r} - \frac{1}{r} \frac{\partial u_\theta}{\partial \theta} - \frac{u_r}{r} \right) \\ \tau_{r\theta} &= \mu \left[ \frac{1}{r} \frac{\partial u_r}{\partial \theta} + \frac{\partial u_\theta}{\partial r} - \frac{u_\theta}{r} \right] \end{aligned} \tag{2.3}$$

<sup>1</sup>A definition of ord is given in Part I, Section 1.2. The essential difference between ord and  $O$  is that, with the former, the coefficient of the related singularity cannot be zero, whereas with the latter it can.

**Table 1. Homogeneous boundary conditions for in-plane loading**

Identifying Roman numeral	Boundary conditions	Physical description
I	$\sigma_\theta=0, \tau_{r\theta}=0$	Stress free
II	$u_\theta=0, u_r=0$	Clamped
III	$u_\theta=0, \tau_{r\theta}=0$	Symmetry
IV	$u_r=0, \sigma_\theta=0$	Antisymmetry
V	$u_\theta=0, \tau_{r\theta}=f\sigma_\theta$	Contact with friction
VI	$\sigma_\theta=ku_\theta, \tau_{r\theta}=k'u_r$	Cohesive stress-separation laws

with

$$\Theta = \frac{\partial u_r}{\partial r} + \frac{1}{r} \frac{\partial u_\theta}{\partial \theta} + \frac{u_r}{r} \tag{2.4}$$

on  $\mathfrak{R}$ , wherein  $\Theta$  is the dilatation while  $\mu$  continues as the shear modulus and  $\kappa$  continues to equal  $3 - 4\nu$  for plane strain and  $(3 - \nu)/(1 + \nu)$  for plane stress,  $\nu$  being Poisson's ratio; any one of the admissible sets of *boundary conditions* listed in Table 1 on the plate edge at  $\theta=0$ , together with another such set on the edge at  $\theta=\phi$  or bisector at  $\theta=\phi/2$  as appropriate, for  $0 < r < \infty$ ; and the *regularity requirements* at the plate vertex,

$$u_r = O(1), \quad u_\theta = O(1), \quad \text{as } r \rightarrow 0 \tag{2.5}$$

on  $\mathfrak{R}$ . In particular, we are interested in the local behavior of the fields complying with the foregoing in the vicinity of the plate vertex  $O$ .

The *boundary conditions* of Table 1 merit some discussion. Conditions I and II apply on  $\theta=0$  or  $\phi$  and are the classical conditions for a stress-free surface and one clamped to a rigid attachment. The clamped conditions also admit to interpretation as the homogeneous complement to the conditions attending indentation by a rigid punch with no slip permitted. Such indentation is also sometimes associated with a “rough” or “adhesive” punch in the literature.

When the same conditions apply on both plate edges ( $\theta = 0, \phi$ ), it is useful to distinguish between symmetric and antisymmetric response about the plate bisector. In the first instance, it is useful because the analysis can be easier by virtue of leading to a  $2 \times 2$  determinant for the eigenvalue equation instead of a  $4 \times 4$ . In the second instance, it is useful because it can restrict the number of singular stress states possible in a given global configuration before undertaking its global analysis. Conditions III and IV enable one to make this distinction. For the present plate configuration, they apply on  $\theta = \phi/2$  when used in this role.<sup>2</sup>

Conditions III can also be interpreted as the homogeneous complement to indentation by a frictionless rigid punch. In this role, they apply on  $\theta=0$  or  $\phi$  and are usually adjoined with the condition that the normal stress not be tensile in the contact region. That is,

$$\sigma_\theta \leq 0 \tag{2.6}$$

<sup>2</sup>With symmetry,  $u_r$  is an even function of  $\theta$  about  $\phi/2$ ,  $u_\theta$  on odd; with antisymmetry, vice versa. Hence, on drawing on (2.3), (2.4), the boundary conditions given in III and IV.

on  $\theta=0$  or  $\phi$ , for  $0 < r < \infty$ . The indenter shape can lead to further constraints outside the contact region to prevent interpenetration.

Conditions IV can also be interpreted as those for a thin stiff reinforcement (Rao [4]). The reinforcement is sufficiently relatively stiff to prevent extension ( $u_r=0$ ), but not so stiff as to prevent bending because of its thinness ( $u_\theta \neq 0$ ).

Conditions V extend the contact conditions of III to permit finite friction via Amonton's law.<sup>3</sup> Herein  $f$  has the magnitude of the coefficient of friction. For these conditions, in addition to seeking to apply the contact constraint (2.6) and any external displacement constraints, we must try to ensure that the shear stress opposes any slipping. This may be possible by selecting the sign of  $f$  appropriately.

Conditions VI apply cohesive stress-separation laws. Thus  $k$  and  $k'$  are the stiffnesses associated with relative transverse and lateral displacements between material on the two sides of the ray on which the conditions are applied. When applied on  $\theta=0$  in Fig. 1, both  $k$  and  $k'$  are positive: on  $\theta = \phi$ , negative. In some instances it may be possible to set one or the other of these stiffnesses to zero. For example,  $k'$  can be taken as zero when loading is symmetric. In contrast, if  $k$  and  $k'$  are let tend to infinity, Conditions II are recovered. In general,  $k$  and  $k'$  are of constant magnitude in the elastic regime and should both be consistent with the elastic moduli of the surrounding continuum.

Conditions VI can also be interpreted as those for a plate on an elastic foundation. Usually then  $k'$  is taken as zero giving Winkler conditions (Winkler [6]; Oravas [7] has that these conditions were given earlier in Euler [8]).

In either role, Conditions VI differ from the others in Table 1 in that a single boundary condition involves both a stress and a displacement. Such mixed boundary conditions would seem to be fairly rare in elasticity. One further instance occurs for the elastic angular plate reinforced by a beam column—see Nuller [9].

All of the foregoing boundary conditions are applied along radial rays emanating from the plate vertex. That is, on straight boundaries. If instead they are applied on curved boundaries that smoothly make tangents to the straight at the vertex, the same singular eigenvalues can be expected. Companion eigenfunctions differ, however. See Ting [10].

Some further comments on the preceding formulation are also appropriate. First, regarding the absence *requirements at infinity* on  $\mathfrak{R}$ . This renders fields complying with our formulation nonunique. Since the principal attribute of these fields is the characterization of all possible responses at the plate vertex, including especially all possible stress singularities there, such a lack of uniqueness is to be desired rather than regulated against. In any configuration of *finite* extent locally containing one of the configurations admitted by our formulation, conditions on the other boundaries in the finite geometry should make its solution unique.

Second, regarding *dimensions*. There is no length scale in

the problems formulated. This is also something provided by associated finite problems. However, this does not mean that there need be concern as to the dimensional consistency of the asymptotic analysis. To see this, observe that the field equations (2.2), (2.3), and (2.4) are equidimensional in  $r$ , and that  $u_r$  and  $u_\theta$  occur "divided" by  $r$ . Thus  $r$ ,  $u_r$ , and  $u_\theta$  can be replaced by  $r/L$ ,  $u_r/L$ , and  $u_\theta/L$ , where  $L$  is any length scale, and leave the equations unchanged. Hence any asymptotic solutions obtained can be regarded as being in terms of  $r/L$  and thereby made dimensionally consistent.

Third, regarding *material constants*. These are constrained to the physically applicable ranges,  $0 < \mu < \infty$  and  $0 \leq \nu \leq 1/2$ . However, for plane strain with an incompressible material ( $\nu=1/2$ ), we have  $\kappa=1$  and the stress-displacement relations of (2.3) and (2.4) are no longer directly applicable. Under these circumstances we require  $\Theta = 0$  in (2.4) and modify (2.3) by removing the  $\Theta$  terms.

Fourth, regarding the *regularity requirements*, (2.5). These ensure bounded displacements at the plate vertex and bounded forces on rays radiating from the vertex. Such fields definitely appeal as being more physical than those with unbounded displacements or forces. This, though, is not the reason for (2.5). If physical appropriateness in itself were to serve as sufficient justification, then we would want to prohibit unbounded stresses as well. We cannot do this. This is because then the formulation does not admit a sufficiently broad class of fields to enable its solution in general: That is, the fields so admitted are incomplete. In contrast, we can prohibit unbounded displacements because the fields so admitted are complete. This is explicitly shown for Conditions I, and indicated for the remaining conditions in Table 1, in Gregory [11].<sup>4</sup>

For problems wherein the completeness of elastic fields with bounded displacements holds true, the regularity requirements of (2.5) are not just a nice option. Rather, they are essential if any companion finite problems are to have unique solutions. To explain further, consider the elementary problem of a circular elastic plate of unit radius under all-around uniform pressure  $p$ . Absent regularity requirements as  $r \rightarrow 0$ , two solutions are possible:

$$\sigma_r = \sigma_\theta = -p, \quad u_r = -\frac{pr}{4\mu}(\kappa - 1) \quad (2.7)$$

or

$$\sigma_r = -\sigma_\theta = -\frac{p}{r^2}, \quad u_r = \frac{p}{2\mu r} \quad (2.8)$$

Requiring bounded displacements eliminates (2.8) and renders the problem well posed by making it have a unique solution. Analogously, uniqueness for singular stress fields with bounded displacements in completely formulated problems for finite regions occurs: The proof of this follows from

<sup>3</sup>Also termed Coulomb's law in the literature. See Ch 13, Johnson [5] for conditions under which there is some physical support for the use of this law.

<sup>4</sup>From the abstract and introduction in Gregory [11], one might think that the original Williams' eigenfunctions are complete for the boundary conditions in Williams [2]. As is demonstrated in Section 2.3, this is not so. Further reading of [11], though, reveals that it recognizes the need to supplement the fields of (1.1) with those attending (1.2) for completeness.

**Table 2. Eigenvalue equations for symmetric response about  $\theta = \phi/2$**

Boundary conditions on $\theta=0, \phi$	Eigenvalue equation	Equation number
I or VI-I or VI	$\lambda \sin \phi = -\sin \lambda \phi$	(2.9)
II-II	$\lambda \sin \phi = \kappa \sin \lambda \phi$	(2.10)
III-III	$\cos \phi = \cos \lambda \phi$	(2.11)
V-V	$f[(1-\kappa)\sin \lambda \phi + (1+\kappa+2\lambda)\sin \phi]$ $= (1+\kappa)(\cos \lambda \phi - \cos \phi)$	(2.12)

**Table 3. Eigenvalue equations for antisymmetric response about  $\theta = \phi/2$**

Boundary conditions on $\theta=0, \phi$	Eigenvalue equation	Equation number
I or VI-I or VI	$\lambda \sin \phi = \sin \lambda \phi$	(2.13)
II-II	$\lambda \sin \phi = -\kappa \sin \lambda \phi$	(2.14)
III-III	$\cos \phi = -\cos \lambda \phi$	(2.15)
V-V	$f[(1-\kappa)\sin \lambda \phi - (1+\kappa+2\lambda)\sin \phi]$ $= (1+\kappa)(\cos \lambda \phi + \cos \phi)$	(2.16)

**Table 4. Eigenvalue equations for mixed problems**

Boundary conditions on $\theta=0, \phi$	Eigenvalue equation	Equation number
I or VI-II	$4[\kappa \sin^2 \lambda \phi + \lambda^2 \sin^2 \phi] = (1+\kappa)^2$	(2.17)
I or VI-V	$2f[(1-\kappa)\sin^2 \lambda \phi - \lambda(1+\kappa+2\lambda)\sin^2 \phi]$ $= (1+\kappa)(\sin 2\lambda \phi + \lambda \sin 2\phi)$	(2.18)
II-V	$2f[\kappa(1-\kappa)\sin^2 \lambda \phi + \lambda(1+\kappa+2\lambda)\sin^2 \phi]$ $= (1+\kappa)(\kappa \sin 2\lambda \phi - \lambda \sin 2\phi)$	(2.19)

the boundedness of attendant strain energies and the usual Kirchhoff argument (see Knowles and Pucik [12]).

On occasion, further support for the bounded displacement conditions derives from solving a singular problem as the limit of a sequence of nonsingular problems, the analogue of the approach adopted in concentrated load problems and for generalized functions in general in Lighthill [13]. An example is the plate under uniform remote tension with an elliptical hole. As the height of the hole parallel to the tension goes to zero, the nonsingular stress fields can be shown to recover the inverse-square-root stress singularity of a stress-free mathematically-sharp crack (Kolosoff [14,15] and Inglis [16]). This singularity has bounded displacements. The same is true of other singular configurations realized in this way: see, for example, Neuber [17].

The analysis of the class of asymptotic problems formulated proceeds routinely on using the approach outlined in the Introduction here, and described in some detail in Part I, Section 4.1. This yields the eigenvalue equations set out in Tables 2, 3, and 4 for symmetric, antisymmetric, and mixed configurations, respectively. These eigenvalue equations are typically available in the literature as described next: Here, they are independently derived largely as a check.

The free-free equations (2.9) and (2.13) in Tables 2 and 3, the clamped-clamped equations (2.10) and (2.14) in Tables 2 and 3, and the clamped-free equation (2.17) in Table 4 all effectively appear in Williams [2] and Kitover [18].<sup>5</sup> Equivalent equations to those for frictionless contact-frictionless

contact, (2.11) and (2.15) in Tables 2 and 3, are given in Kalandia [19]. Equations for these conditions which are exactly the same as (2.11) and (2.15) are provided in Seweryn and Molski [20]. Two further frictionless contact equations for such conditions in combination with free and with clamped conditions can be obtained by setting  $f=0$  in (2.18) and (2.19) of Table 4, respectively: These two are given in Kalandia [19]. The equation for contact with friction acting with itself symmetrically, (2.12), would not appear to be readily available in the literature; the equation when this action is antisymmetric, (2.16), is essentially the same as the corresponding equation in Dempsey [21]. The contact with friction-free equation of (2.18) in Table 4 can be obtained from Gdoutos and Theocaris [22]. It follows on setting “ $G_2$ ” in [22] to infinity to reflect a rigid punch, and “ $q$ ” =  $-f$  because the friction conditions therein hold on a negative  $\theta$ -edge. The contact with friction-clamped equation of (2.19) in Table 4 is essentially given in Dempsey [21]. The equivalence of stress-free conditions with those for cohesive stress-separation laws as far as the foregoing eigenvalue equations are concerned is basically argued in Sinclair [23].

When Conditions IV are interpreted as being for a thin stiff reinforcement, eigenvalue equations for these conditions with others and a plate of vertex angle  $\phi/2$  are given in Table 4. When Conditions IV act in this role on both edges of a plate of vertex angle  $\phi$ , the eigenvalue equation can be formed as a product of (2.11) and (2.15).<sup>6</sup>

**2.2 Power singularities with homogeneous boundary conditions**

For the homogeneous boundary conditions of Table 1, the associated eigenvalue equations of Tables 2–4 can give rise to stresses with power singularities when their eigenvalues are less than one—see (1.1). To be in accordance with the regularity requirements (2.5), these eigenvalues must not be less than zero. An eigenvalue equal to zero corresponds to a rigid body displacement in (1.1) and therefore is not of interest because associated stresses are not singular: The same value leads to unbounded displacements for the fields associated with (1.2) and therefore is not admissible. Thus the eigenvalue range for *power singularities* is

$$0 < \lambda < 1 \tag{2.20}$$

We review eigenvalues within this range for a variety of configurations in this section.

The solution of the eigenvalue equations within the singular range typically cannot be done completely analytically. Accordingly it usually proceeds numerically except for a few select instances. The results so found are compared with those in the literature. For all sources given in what follows, they are consistent. Thus their calculation here may be viewed as independently confirming values already determined in the cited sources.

In presenting results we introduce the *singularity exponent*  $\gamma$  defined by

<sup>5</sup>The eigenvalue equations in Kitover [18] are correct for plane strain, but appear to have typographical errors for plane stress.

<sup>6</sup>That is, by rearranging (2.11), (2.15) so that they have expressions on one side of the =, zero on the other, then setting the product of these expressions = 0. The so-obtained equation is given in Rössle [24]. This reference also gives nine further eigenvalue equations. These equations are contained in, and are consistent with, those in Tables 2–4.

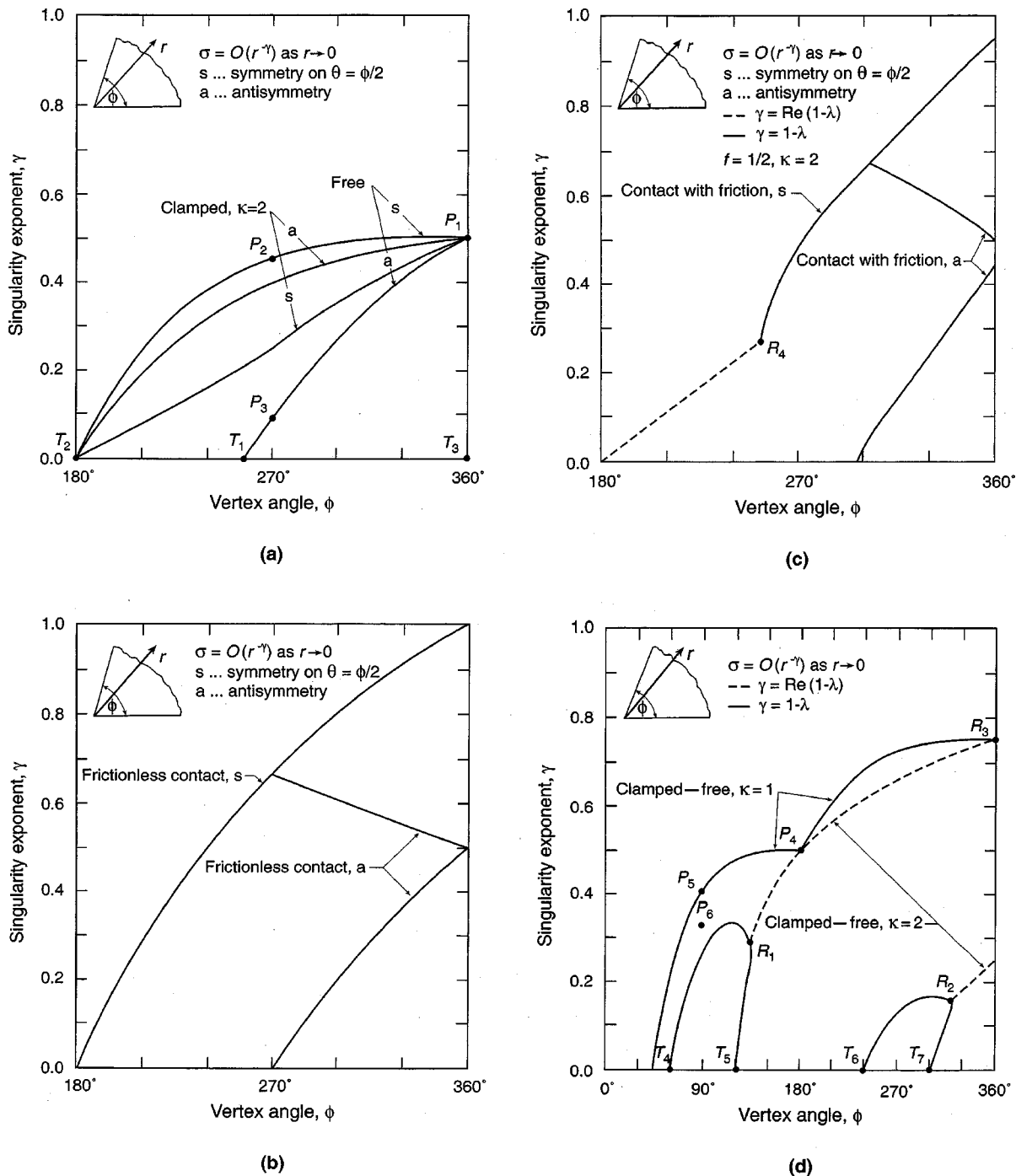


Fig. 2 Singularity exponents for varying vertex angles: a) free-free and clamped-clamped (from (2.9), (2.13) and (2.10), (2.14), respectively), b) frictionless contact-frictionless contact (from (2.11), (2.15)), c) contact with friction-contact with friction (from (2.12), (2.16)), d) clamped-free (from (2.17)), e) contact-free (from (2.18)), f) contact-clamped (from (2.19))

$$\gamma = 1 - \lambda \tag{2.21}$$

Then (1.1) has stresses which behave in accordance with

$$\sigma = O(r^{-\gamma}) \text{ as } r \rightarrow 0 \tag{2.22}$$

where  $\sigma$  is any stress component. That is, stresses are singu-

lar for  $\gamma$  positive, and the larger  $\gamma$  the more singular. The limits on the nature of this power singularity are, from (2.20) and (2.21),

$$0 < \gamma < 1 \tag{2.23}$$

In the event that  $\lambda$  is complex, we have stress singularities as

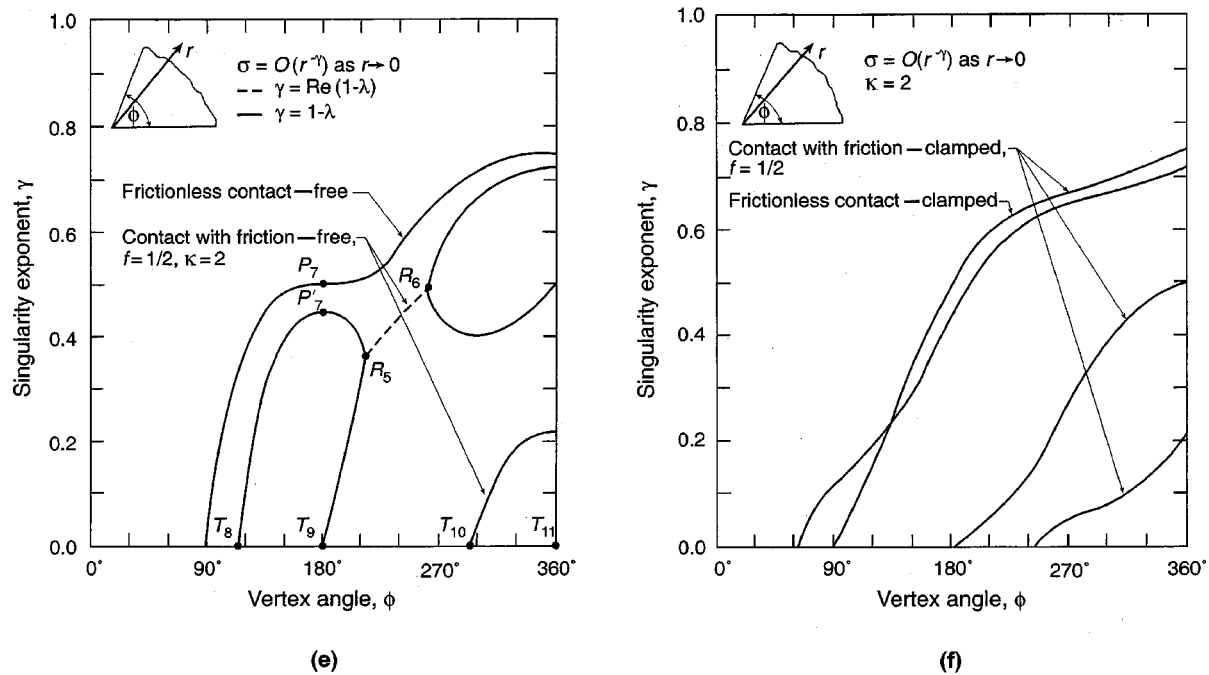


Fig. 2 Continued

in the first of (1.3) with  $\text{Re}(1-\lambda)=1-\xi=\gamma$ ,  $\text{Im}\lambda=\eta$ , and (2.23) still applying to  $\gamma$ . Results for  $\gamma$  satisfying (2.23) are presented in Fig. 2a-f for varying vertex angles.

Included in Fig. 2a are the singularity exponents for the free-free plate, for both symmetric loading from (2.9), and antisymmetric from (2.13). The symmetric curve is given in Fig. 1, Williams [2]. It dominates singular character if loading is symmetric or mixed because the antisymmetric curve realizes weaker singularities with stress-free boundary conditions: Of course, it cannot dominate if loading is purely antisymmetric. The antisymmetric curve may be found in Fig. 9, Rösler [25] or Fig. 3a, Seweryn and Molski [20].

For  $\phi=360^\circ$  with free-free conditions, we have the traditional, mathematically-sharp, stress-free crack with its inverse-square-root singularity for both symmetric and antisymmetric loading ( $P_1$ , Fig. 2a). For  $\phi=270^\circ$ , we have a stress-free  $90^\circ$  reentrant corner with two possible singularities, the stronger being for symmetric loading ( $P_2$  and  $P_3$ , Fig. 2a). For  $\phi < 257.5^\circ$ , no further singularities are found for antisymmetric loading. For  $\phi=180^\circ$ , we have no singularity for symmetric loading. This is because, for this stress-free half-plane geometry, there is no discontinuity in boundary directions or conditions. For  $\phi \leq 180^\circ$ , no further singularities are found for symmetric loading. Further, there are no complex eigenvalues with real parts in the singularity range for the free-free plate; this is shown in Karp and Karal [26].

Given the equivalence of cohesive stress-separation laws with stress-free conditions, the free-free curves of Fig. 2a also apply for these laws. Hence, the removal of some singularities (noted in Part I, Section 2.3) can be confirmed. For a cracked configuration, putting cohesive laws ahead of a sharp crack as well as in back of it effectively gives a free-

free plate of vertex angle  $\phi=180^\circ$ . Thus no singularities. For a  $90^\circ$  reentrant corner under symmetric loading, cohesive laws should be inserted ahead of the corner on the ray bisecting the plate to achieve bounded stiffnesses. This effectively gives a free-free plate with  $\phi=135^\circ$ . Thus no singularities. The same sort of argument applies for antisymmetric loading (see Sinclair, Khatod, and Rummel [27] for further explanation).

Also in Fig. 2a are the singularity exponents for the clamped-clamped plate, for both symmetric loading from (2.10), and antisymmetric from (2.14). These are for a representative value of  $\kappa=2$ , corresponding to Poisson's ratio  $\nu=1/4$  for plane strain, or  $\nu=1/3$  for plane stress. A very similar symmetric curve is given in Fig. 1, Williams [2], for  $\kappa=2^{1/3}$ : Some eigenvalues for antisymmetric response for the same  $\kappa$  are given in Williams [28] from Ricci [29]. The actual symmetric curve for  $\kappa=2$  may be found in Fig. 5a, Seweryn and Molski [20], while the companion antisymmetric curve is given in Fig. 8a, *ibid.* In Williams [2], the singularity associated with symmetric loading under clamped-clamped conditions is claimed to be dominant. This is so if loading is purely symmetric: Otherwise, for these boundary conditions, the singularity associated with antisymmetric loading is dominant.

For clamped-clamped conditions, both symmetric and antisymmetric curves at  $\phi=360^\circ$  have an inverse-square-root singularity. For  $\phi=180^\circ$ , both do not have a singularity for similar reasons for this being so for free-free symmetric response. For  $\phi < 180^\circ$ , no singularities are found for either. No singularities associated with complex eigenvalues are found for either.

Some indication of the influence of Poisson's ratio on

singularities with clamped-clamped conditions is contained in Fig. 2a. This is because free-free with symmetry has the same eigenvalue equation as clamped-clamped with antisymmetry and  $\kappa=1$ —see (2.9) and (2.14). Similarly free-free with antisymmetry is the same as clamped-clamped with symmetry and  $\kappa=1$ —see (2.13) and (2.10). Thus, as  $\kappa$  decreases corresponding to Poisson's ratio increasing, the singularity for antisymmetric clamped-clamped conditions gets stronger, while that for symmetric clamped-clamped gets weaker. The trends thus evident in Fig. 2a are confirmed by singularity exponents for clamped-clamped conditions for  $\kappa = 1\frac{2}{3}$  and 3 in Seweryn and Molski [20].

In Fig. 2b, singularity exponents are plotted for the *frictionless contact-frictionless contact* plate, for both symmetric loading from (2.11), and antisymmetric from (2.15). These two eigenvalue equations are the simplest of all and admit to analytical solution. Thus for symmetric configurations,

$$\gamma = 2 - \frac{2\pi}{\phi} \quad (\pi < \phi < 2\pi) \quad (2.24)$$

while for antisymmetric,

$$\gamma = \frac{\pi}{\phi}, \quad 2 - \frac{3\pi}{\phi} \left( \frac{3\pi}{2} < \phi \leq 2\pi \right) \quad (2.25)$$

Expressions yielding these values of  $\gamma$  are given in equations (36) and (41), Seweryn and Molski [20]. These are the values plotted in Fig. 2b.

The ranges of  $\phi$  in (2.24) and (2.25) bear comment. For symmetric loading, the absence of singular stresses when  $\phi = 180^\circ$  is to be expected for the reasons put forward earlier. Given no singularities are found for  $\phi < 180^\circ$ , the range includes all singularities for this loading. For antisymmetric loading,  $\phi = 270^\circ$  terminates singular response on the lower branch in a similar manner to the free-free antisymmetric case of Fig. 2a. For the upper branch, the same limit on  $\phi$  holds if antisymmetric singularities are not to be stronger than those associated with symmetric loading. The reasons for limiting singularity exponents in this way are as follows. For contact on both plate edges and fields that are purely antisymmetric,  $\sigma_\theta$  must be positive on one edge, negative on the other. Where it is positive would be in violation of our contact stress constraint (2.6). This means that antisymmetric loading needs to act in conjunction with sufficient symmetric loading if compliance with (2.6) is to be achieved. Antisymmetric singularity exponents cannot exceed symmetric if this is to happen. Hence the limit in (2.25). Observe, though, that in the analysis of a given global problem, such compliance with (2.6) whence (2.25) does not have to be the case: It needs to be checked for, and means sought to remedy the situation if it does not occur.<sup>7</sup>

In Fig. 2c, singularity exponents for the *contact with friction-contact with friction* plate are plotted. These are from (2.12) for symmetric configurations, (2.16) for antisymmetric. Values of friction coefficient  $f=1/2$  and of  $\kappa=2$  are taken as representative. The general character of the expo-

nents is similar to that of Fig. 2b for  $f=0$ , including the bounding of singularities for antisymmetric loading by those for symmetric for the same reasons. That is, here too any antisymmetric response must occur in concert with sufficient symmetric participation if compliance with (2.6) is to be achieved.

There are some differences, however. For symmetric configurations and  $f=1/2$ , there are two real branches which merge together at  $\phi=252.5^\circ$  into complex roots with a common real part (shown in Fig. 2c) and equal imaginary parts of opposite sign (not shown). Checking the companion eigenfunction for these real eigenvalues reveals that the upper branch (shown) does have the contact shear opposing motion; the lower branch does not (hence not shown). As previously, though, this removal here does not necessarily mean that fields associated with the lower branch could not be present in a problem. Again, singular stresses cease to be possible for symmetric configurations when  $\phi=180^\circ$ .

For symmetric loading, increasing the coefficient of friction  $f$  tends to reduce singularity exponents, as can be seen by comparing Fig. 2c with Fig. 2b. For antisymmetric loading, results are mixed in this regard. For both types of loading, increasing Poisson's ratio typically increases singularity exponents.

In Fig. 2d, singularity exponents for the *clamped-free* plate are plotted. These exponents are from (2.17). The real parts of all singular branches are shown for the representative value  $\kappa=2$ ; just the dominant singularity for  $\kappa=1$ . A similar curve to the upper branch for  $\kappa=2$  is given in Fig. 1, Williams [2], for  $\kappa=2\frac{1}{13}$ . The real parts of all branches for  $\kappa=2$ , as well as the most singular branch for  $\kappa=1$ , are given in Figs. 12a and 14a, Seweryn and Molski [20], respectively.<sup>8</sup>

For  $\phi=360^\circ$  and clamped-free conditions, there are four possible singularities for  $\kappa=2$ : two for each complex root indicated in Fig. 2d. For  $\phi=180^\circ$  and  $\kappa=2$ , we have an oscillatory singularity as for an adhering, rigid, flat punch ( $P_4$ , Fig. 2d). It is the presence of these *two* roots as complex conjugates that precludes the removal of singular stresses in conforming contact problems when stick-free conditions are assumed. For  $\phi=90^\circ$  we have the singularities of  $P_5$  ( $\nu=1/2$ ,  $\kappa=1$ ) and  $P_6$  ( $\nu=3/8$ ,  $\kappa=3/2$ ) which, for example, apply to the edge of an adhering rubber tire and at the outer surface of an epoxy-steel joint. No singularities are found for  $\phi < 60^\circ$  when  $\kappa=2$ ,  $\phi < 45^\circ$  when  $\kappa=1$ . This trend of a larger range of vertex angles with stress singularities with larger values of Poisson's ratio (smaller  $\kappa$ ) is confirmed by results for other  $\nu$  in Seweryn and Molski [20].

In Fig. 2e, singularity exponents for the *contact-free* plate are plotted. These exponents are from (2.18). The real parts of all singular branches are shown for the chosen representative case of contact with friction ( $f=1/2$  and  $\kappa=2$ ); just the dominant singularity is shown for the frictionless case. The exponents for contact with friction would not appear to be available in the open literature: The values shown in Fig.

<sup>7</sup>This is also the reason for excluding the further antisymmetric singularity exponent  $\gamma = 2 - \pi/\phi$  ( $\pi/2 < \phi < \pi$ ).

<sup>8</sup>The imaginary parts of singular eigenvalues for  $\kappa=2$  and the other singular branches for  $\kappa=1$  are also provided in Seweryn and Molski [20].

2e are confirmed in Klingbeil [30]. The exponents for frictionless contact are given in Fig. 2a, Seweryn and Molski [20].<sup>9</sup>

There need be no restrictions on the branches included in Fig. 2e as a result of contact constraints. This is because the sign of the participation coefficient can always be such that the contact stress condition (2.6) is met, and a rigid body displacement can always be added so as to ensure the frictional shear opposes slip. That is, the local fields associated with the singularity exponents of Fig. 2e can potentially participate in a global problem and all auxiliary contact conditions be met. Whether this actually happens for the particular global configuration of interest needs to be checked.

For  $\phi = 360^\circ$  and contact with friction-free conditions, there are three singular stress fields possible. This is also the case for frictionless contact, although this is not apparent in Fig. 2e because only the most singular branch is included. For  $\phi = 180^\circ$ , the frictionless contact case gives the singularity as for a tire at the edge of a pothole on an icy pavement ( $P_7$ , Fig. 2e). For contact with friction and  $\phi = 180^\circ$ , the singularity that results is as for an adhering tire but with some slip permitted. Under these conditions there is *one* real singularity (at  $P'_7$ , Fig. 2e) compared to the two for an adhering tire with no slip. This enables the stress singularity to be removed for conforming contact when there is contact with friction-free conditions. No singularities are found for  $\phi < 90^\circ$  when  $f = 0$ ,  $\phi < 116.6^\circ$  when  $f = 1/2$ . This is the trend in general, namely, as  $f$  becomes more positive, the range of vertex angles with stress singularities decreases. On the other hand, varying Poisson's ratio while holding  $f$  constant leaves the range of singular vertex angles unchanged.

In Fig. 2f, singularity exponents for the *contact-clamped* plate are plotted. These exponents are from (2.19). All singular branches are shown for the representative case of contact with friction ( $f = 1/2$  and  $\kappa = 2$ ); just the dominant singularity is shown for the representative frictionless case ( $\kappa = 2$ ). The exponents for contact with friction would not appear to be available in the open literature: The values shown in Fig. 2f are confirmed in Smallwood [32]. The exponents for frictionless contact are given in Fig. 5a, Seweryn and Molski [20]. For the same reasons as for Fig. 2e, there need be no restrictions on the branches included in Fig. 2f as a result of contact constraints.

For  $\phi = 360^\circ$  and contact with friction-clamped conditions, there are three singular stress fields possible. The same is true for frictionless contact-clamped conditions, though this is not shown in Fig. 2f. For  $\phi = 180^\circ$  there is but one singularity for a given coefficient of friction. This enables singularities to be removed when transitioning from stick to slip in contact problems. No singularities are found for  $\phi < 90^\circ$  when  $f = 0$ ,  $\phi < 63.4^\circ$  when  $f = 1/2$ . This is the trend in general here, namely, as  $f$  becomes more positive, the range of singular vertex angles increases. Conversely, for constant  $f$ , increasing Poisson's ratio reduces the range of singular vertex angles.

While not strictly a power singularity, we close this section by noting instances of undefined oscillatory stresses as in the last of (1.3). These occur for mixed problems. For the clamped-free plate, their presence is indicated in Fig. 11a, Seweryn and Molski [20], for  $\kappa = 3$ . Solving (2.17) for  $\lambda = 1 + i\eta$  and  $\kappa = 3$  then gives oscillatory stresses when  $\phi = 100.4^\circ, 274.0^\circ$  with  $\eta = 0.13, 0.02$ , respectively. Similarly for the other mixed problems—contact-free and contact-clamped—solving (2.18) and (2.19) for  $\lambda = 1 + i\eta$  leads to oscillatory stresses.

### 2.3 Log singularities with homogeneous boundary conditions

In addition to the singularities revealed for the real and complex  $\gamma$  of Fig. 2, there is the possibility of logarithmic contributions to stress singularities. These may be produced under the homogeneous boundary conditions of Table 1. Then they can take the form of *logarithmic intensification* of stress singularities. That is, stresses which behave as

$$\sigma = O(r^{-\gamma} \ln r) + O(r^{-\gamma}) \text{ as } r \rightarrow 0 \tag{2.26}$$

for  $\gamma > 0$ . For homogeneous boundary conditions and stresses of the form of (2.26), at the outset these stem from real eigenvalues which are repeated roots of the eigenvalue equation. This is a necessary but not sufficient condition for these stresses (see (1.3)).

Repeated roots can be expected to occur where there is a transition from two real roots to roots which are complex conjugates. To see this, suppose  $\lambda$  is an eigenvalue of  $D = 0$  for vertex angle  $\phi$ . Now perturb  $\phi$  by  $\delta\phi$  while continuing to insist  $D = 0$ , and let  $\delta\lambda$  denote the accompanying perturbation in  $\lambda$ . From Taylor's theorem in two variables, we have

$$\begin{aligned} 0 = \frac{\partial D}{\partial \lambda} \delta\lambda + \frac{\partial D}{\partial \phi} \delta\phi + \frac{\partial^2 D}{\partial \lambda^2} \frac{\delta\lambda^2}{2} + \frac{\partial^2 D}{\partial \lambda \partial \phi} \delta\lambda \delta\phi \\ + \frac{\partial^2 D}{\partial \phi^2} \frac{\delta\phi^2}{2} + \dots \text{ as } \delta\phi \rightarrow 0 \end{aligned} \tag{2.27}$$

wherein it is understood that all derivatives are evaluated at  $\lambda$  and  $\phi$ . If  $\lambda$  is a repeated root, then  $\partial D / \partial \lambda = 0$  for  $\lambda, \phi$ . Thus, provided  $\partial D / \partial \phi \neq 0, \partial^2 D / \partial \lambda^2 \neq 0$  at  $\lambda$  and  $\phi$ ,

$$\delta\lambda = \pm \sqrt{-2 \delta\phi \frac{\partial D}{\partial \phi} / \frac{\partial^2 D}{\partial \lambda^2}} + O(\delta\phi) \text{ as } \delta\phi \rightarrow 0 \tag{2.28}$$

As  $\delta\phi$  changes sign in (2.28), we have the anticipated transition from two real roots to roots that are complex conjugates.

This is what occurs at  $R_1$  in Fig. 2d. Further checking of the rank conditions in the second of (1.3) shows that they are satisfied for this repeated root. For  $\gamma > 0$ , these rank conditions are necessary for the possibility of logarithmic intensification of power singularities. In Dempsey [33], such checks are carried out for the dominant singularity in the clamped-free plate and consistently show the possibility of logarithmic intensification of singularities wherever there is a tran-

<sup>9</sup>England [31], Fig. 5, gives values consistent with the exponents given here for  $f = 0$  and  $0 \leq \phi \leq 180^\circ, 270^\circ \leq \phi \leq 360^\circ$ ; the values *ibid* for  $180^\circ < \phi < 270^\circ$  do not apply to the frictionless contact-free plate.

**Table 5. Configurations with logarithmic singularities under homogeneous boundary conditions**

Boundary conditions on $\theta=0, \phi$	Configuration specifications
II-II	$\phi = \phi_*, \kappa = 1$
V-V	$\phi = \pi, 2\pi, \kappa = 1, f \neq 0$
I or VI-II	$\kappa = \cos 2\phi - \phi^{-1} \sin 2\phi, f = -\cot \phi, \phi \neq \pi, 2\pi$
I or VI-V	$\phi = \pi - \phi_*, 2\pi - \phi_*, \kappa = -\phi^{-1} \tan \phi$
II-V	$\kappa = 1 + 2 \cos 2\phi - 2\phi^{-1} \sin 2\phi, f = -\cot \phi, \phi \neq \pi, 2\pi$
	$\phi = \pi/2, 3\pi/2, \kappa = 3, f = -3\phi/2$
	$\phi = \hat{\phi}_\kappa, f = (\kappa - 1)(3 - \kappa)^{-1} \cot \phi, \phi \neq \pi, 2\pi, \kappa \neq 3$

sition from complex to real roots. These transitions occur for any  $\phi > 101.4^\circ$  except  $\phi = 180^\circ$  and  $360^\circ$ , and have  $0 < \gamma < 0.75$ .

It can be expected that logarithmic intensification also occurs for the less singular branch of  $\gamma$  under clamped-free conditions wherever there is a transition from complex to real roots. For  $\kappa = 2$ ,  $R_2$  in Fig. 2d is an example. For logarithmic intensification being possible though, the rank conditions in the second of (1.3) need to be checked for these configurations as well.

On occasion, repeated roots occur without a transition from complex to real values. This can be so if  $\partial D / \partial \phi = 0$  for  $\lambda$  and  $\phi$  in (2.27). Actual examples are  $R_3$  and  $P_4$ , both for  $\kappa = 1$ , in Fig. 2d. This is not obvious from the figure because the less-singular intersecting branch is not shown (see, though, Fig. 14a, Seweryn and Molski [20]). For these points, however, Dempsey [33] has that the rank conditions of (1.3) are not satisfied and, consequently, logarithmic intensification is not possible.

Further configurations wherein logarithmic intensification can be expected are where there are transitions from complex to real eigenvalues for plates in contact with friction. These include  $R_4$  of Fig. 2c, and  $R_5$  and  $R_6$  of Fig. 2e. Again, the rank conditions need to be checked to see if this is really a possibility.

Typically logarithmic intensification of stress singularities can be expected as stress singularities pass from being pure power singularities to oscillatory power singularities. In some sense, the logarithmic intensification can be viewed as a *transition state* between the two, resulting in stresses that are more singular than those with just power singularities, yet arguably less pathological than oscillatory singularities. We consider logarithmic singularities further in this sort of role next when we review their occurrence without power terms.

*Pure logarithmic singularities* have stresses which behave as

$$\sigma = O(\ln r) \text{ as } r \rightarrow 0 \quad (2.29)$$

For the pure logarithmic singularities of (2.29) under the homogeneous boundary conditions of Table 1, we need satisfaction of the penultimate conditions in (1.3). Only then can a log singularity occur. These are the weakest stress singularities possible in elasticity, and consequently the hardest to detect absent an a priori appreciation of their possible participation. Accordingly, their asymptotic identification can be of significant value.

Details of the application of the identification process attending the last of (1.3), for the boundary conditions of Table 1, may be obtained from Sinclair [34]: Results are summarized *ibid.* Every logarithmically singular configuration so identified complied with all of the conditions in the last of (1.3). Moreover, when situations arose during analysis in which some of these requirements were complied with but others not, no logarithmic singularities were found.

Given the importance of being aware of the participation of logarithmic stress singularities, we reiterate the configurations so found here in Table 5. This table gives seven different sets of specifications for configurations with log singularities.

In Table 5,  $\kappa$  is additionally constrained to the range for physically applicable Poisson's ratios. This is broadest for plane strain. Hence

$$1 \leq \kappa \leq 3 \quad (2.30)$$

Further in Table 5, the vertex angles  $\phi_*$ ,  $\phi_\kappa$ , and  $\hat{\phi}_\kappa$  are such that

$$\phi_* = \tan \phi_*, \quad \phi_\kappa = \sin^{-1} \frac{\sqrt{\kappa+1}}{2}$$

$$\kappa \hat{\phi}_\kappa ((\kappa-1)^2 + 4 \cos 2\hat{\phi}_\kappa) = (3\kappa-1) \sin 2\hat{\phi}_\kappa \quad (2.31)$$

wherein the principal value of the arc sine is taken ( $0 \leq \phi_\kappa \leq \pi/2$ ). The first of (2.31) realizes  $\phi_* = 257.5^\circ$ , a value previously noted as that for the termination of power singularities with free-free conditions and antisymmetry (Fig. 2a). For  $\kappa = 1$ , free-free eigenvalues coincide with those for clamped-clamped. Consequently this value for an incompressible solid under clamped-clamped conditions represents a transition from stresses which are singular in themselves to those which are bounded but have unbounded derivatives. We therefore distinguish it as the point  $T_1$  in Fig. 2a. The same is true for all the other logarithmic configurations listed in Table 5: They all represent transitions from power stress singularities to no stress singularities. Further, they typically also represent transitions from real eigenvalues to complex.

Local fields containing logarithmic stress singularities for all the configurations listed in Table 5 can be obtained from Sinclair [34]. For the contact-clamped plate when  $\kappa = 1$ ,  $f = 0$ , and  $\hat{\phi}_\kappa = \phi_*/2$ , fields are also available from Dempsey [21]. All of these fields demonstrate that the fields of (1.1) alone are, in general, incomplete for the plate with homogeneous boundary conditions as in Table 1. In particular, they

**Table 6. Inhomogeneous boundary conditions for in-plane loading**

Identifying Roman numeral	Boundary conditions	Physical description
I'	$\sigma_\theta = -p, \tau_{r\theta} = q$	Uniform tractions
II'	$u_\theta = r\Delta\phi, u_r = r\Delta\phi'$	Pinching with lateral constraint
V'	$u_\theta = r\Delta\phi, \tau_{r\theta} = f\sigma_\theta$	Pinching with friction

demonstrate that the original Williams' eigenfunctions are incomplete for the problems considered in Williams [2].

**2.4 Singularities with inhomogeneous boundary conditions**

All of the preceding singularities for the in-plane loading of an elastic plate occur with homogeneous boundary conditions on its radial edges. Here we consider what additional singular stress fields can be induced by inhomogeneous boundary conditions.

For *applied tractions* which are themselves singular, interior stresses are at least likewise singular. There is also the potential of logarithmic intensification as in (2.26). This can occur if the configuration of interest shares the same singularity as in the applied tractions when under corresponding homogeneous boundary conditions. This would mean log-squared singularities in the event that the applied tractions were logarithmically singular. However, it would not seem that either power or log singularities in applied tractions are likely to be needed in practice.

What is more likely are nonsingular applied tractions. If they are  $ord(r^\gamma)$  as  $r \rightarrow 0$  and  $\gamma > 0$ , then the interior stresses are also nonsingular. This is so even if they get multiplied by  $\ln r$  because  $r^\gamma \ln r = 0$  at  $r = 0$  when  $\gamma > 0$ . Alternatively, if the applied tractions are  $ord(r^0)$  as  $r \rightarrow 0$ , we may see a transition between stresses which are nonsingular for tractions that are  $ord(r^\gamma)$ , to stresses which are singular for tractions that are  $ord(r^{-\gamma})$ . Pure logarithmic singularities are natural candidates for such a transition: We look for further instances of their being induced by uniform tractions in what follows.

For *applied displacements*, stress singularities can also be produced. In the first instance, these stem from prescribed displacements which are not continuously differentiable (as in  $u_\theta \propto \sqrt{r}$ ). Then, singular stresses simply match the singularity in displacement derivatives (see, eg, Browning and Ju

[35]). Again, they can be logarithmically intensified if the singularity coincides with that for homogeneous boundary conditions. If, on the other hand, prescribed displacements are continuously differentiable, generally no stress singularities are produced. An apparent exception occurs when the displacements are linear in  $r$ , the integral of uniform traction conditions in effect.<sup>10</sup> For these conditions, we can similarly expect pure logarithmic singularities.

Given the importance of identifying logarithmically singular configurations, henceforth in this section we consider inhomogeneous boundary conditions as in Table 6. These are the counterparts of those in Table 1 which include uniform tractions or linear displacements.

The boundary conditions of Table 6 merit some explanation. In Conditions I',  $p$  is an applied pressure while  $q$  is a constant shear. In Conditions II',  $\Delta\phi$  can be interpreted as the amount by which the vertex angle of an angular plate is reduced by as a result of pinching contact with a rigid indenter. With this interpretation,  $\Delta\phi$  is positive on a negative  $\theta$ -edge, and vice versa. If such contact occurs with no slip,  $\Delta\phi' = 0$ : If it occurs with slip, we have Conditions V'. The inclusion of the possibility of  $\Delta\phi' \neq 0$  is so as to replicate displacement discontinuities which can occur in boundary conditions in finite element analysis (FEA). Such discontinuities occur in displacement derivatives at nodes when displacement shape functions are used as boundary conditions in submodeling with FEA, a practice implemented in some standard codes (eg, Chapter 14, ANSYS [36] and Section 7.3, ABAQUS [37]; see Sinclair and Epps [38] for further explanation).

Using the conditions in (1.5), instances of logarithmic stress singularities with the inhomogeneous boundary conditions of Table 6 can be identified. Typically by this means, logarithmic singularities in problems have been identified in the literature as follows: Conditions I'–I in Kolosoff [15] and Dempsey [39]; Conditions I'–II in Sinclair [40]; all combinations of other conditions in Sinclair [34] and Sinclair and Epps [38].

The configurations so found are given in Table 7: Therein there are twelve different sets of specifications for configurations with log singularities. In this table,  $\kappa$  continues to be

<sup>10</sup>“Apparent” because displacements which are linear in  $r$  can have discontinuities in their derivatives when  $r \rightarrow 0$  on different  $\theta$ .

**Table 7. Configurations with logarithmic singularities under inhomogeneous boundary conditions**

Boundary conditions on $\theta=0, \phi$	Configuration specifications
I' or VI-I	$\phi = \pi, 2\pi, q \neq 0$ $\phi = \phi_*, p \neq 0$ or $q \neq 0$
II'–II	$\phi = \pi, 2\pi, \Delta\phi \neq 0$ or $\Delta\phi' \neq 0$ $\kappa = 1, \Delta\phi \neq 0$ or $\Delta\phi' \neq 0, \phi \neq \phi_*$
V'–V	$\phi = \pi, 2\pi, \Delta\phi \neq 0, \kappa \neq 1, f \neq 0$ $f = 0, \Delta\phi \neq 0$
VI-VI	$\phi = \phi_*, 2\pi$
I' or VI–II'	$\phi = \phi_\kappa, \pi \pm \phi_\kappa, 2\pi - \phi_\kappa, p \neq 0$ or $q \neq 0$ or $\Delta\phi' \neq 0, \kappa \neq -\phi^{-1} \tan \phi$
I' or VI-V	$\phi = \pi, 2\pi, fp \neq 0$ or $q \neq 0$ $f = -\cot \phi, \phi \neq \pi, 2\pi, fp \neq 0$ or $q \neq 0, \kappa \neq 1 + 2 \cos 2\phi - 2\phi^{-1} \sin 2\phi$
II'–V	$\phi = \pi, 2\pi, \Delta\phi \neq 0$ $\phi = \pi/2, 3\pi/2, \kappa = 3, \Delta\phi \neq 0$ or $f\Delta\phi' \neq 0, f \neq -3\phi/2$ $f = (\kappa - 1)(3 - \kappa)^{-1} \cot \phi, \phi \neq \pi, 2\pi, \phi_\kappa, \Delta\phi \neq 0$ or $\Delta\phi' \neq 0, \kappa \neq 3$

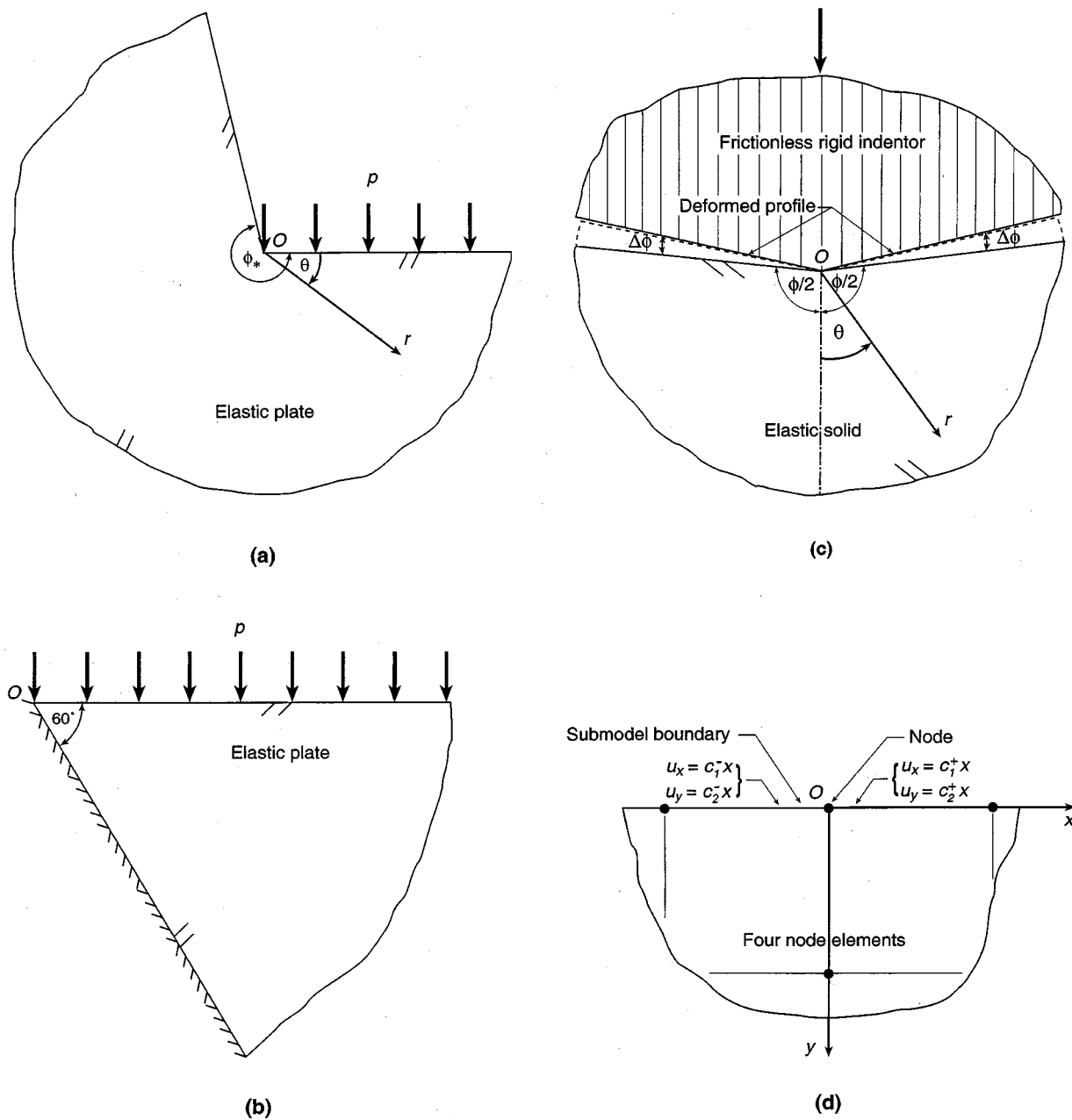


Fig. 3 Examples of configurations with logarithmic stress singularities: a) Levy's problem for a reentrant corner ( $\phi = \phi_*$ ), b) pressure on a clamped acute corner ( $\kappa = 2$ ), c) symmetric indentation by a frictionless rigid sharp plate, d) displacement shape functions as boundary conditions for a submodel in FEA

constrained as in (2.30) while  $\phi_*$ ,  $\phi_\kappa$ , and  $\hat{\phi}_\kappa$  continue to be as in (2.31). By suitably adjoining rigid body rotations, any combination of boundary conditions drawn from Tables 1 and 6 can be realized by the combinations given in Table 7.

A first instance of a logarithmic stress singularity in Table 7 occurs for a step shear on a half-plane ( $\phi = \pi$  and  $q \neq 0$ ). The full stress field is given in Kolosoff [15]. A related instance occurs for a constant shear on one side of a crack ( $\phi = 2\pi$ ). Complete fields are given in Dempsey [39]. In both of these cases, the log singularity must participate if  $q$

$\neq 0$  in the local boundary conditions. This is in contrast to the log singularities of Table 5 whose actual participation depends on far-field conditions.

A further instance of a logarithmic stress singularity for Conditions I'-I in Table 7 occurs in Levy's problem, although such a log field is not included in the original solution in Levy [41]. This problem entails an angular elastic plate of vertex angle  $\phi$  subjected to a uniform pressure  $p$  on one edge while being free of stress on the other (Fig. 3a wherein  $\phi = \phi_*$ ). Levy's traditional solution to the problem may be found in Article 45, Timoshenko and Goodier [42]. By way

of example, the normal stress  $\sigma_\theta$  in Levy's solution, in terms of the polar coordinates  $r$  and  $\theta$  of Fig. 3a, may be expressed by

$$\sigma_\theta = -p \left[ 1 - \frac{\sin \theta \cos(\phi - \theta) - \theta \cos \phi}{\sin \phi - \phi \cos \phi} \right] \quad (2.32)$$

In (2.32), it can be seen that  $\sigma_\theta$  takes on the values of  $-p, 0$  at  $\theta=0, \phi$ , respectively, and that there is no logarithmic singularity in  $\sigma_\theta$ . However, also clear in (2.32) is that the solution breaks down for  $\phi = \phi_*$  of (2.31). This breakdown for the critical vertex angle of  $\phi_*$  is passed by without comment in Levy [41]. It is noted in Fillunger [43], but perhaps is not as widely recognized today as it could be (eg, no mention of its existence is made in Timoshenko and Goodier [42]). Nonetheless, it is serious and must be remedied if any physical sense whatsoever is to be made of elasticity treatments of a loaded plate which is as in Fig. 3a.

Supplementing the fields used to generate (2.32) by those attending (1.2) rectifies the situation. This is done in Dempsey [39]. The resulting  $\sigma_\theta$ , for example, may be expressed by

$$\begin{aligned} \sigma_\theta = -p \left[ 1 - \frac{\theta}{\phi_*} - \frac{\csc \phi_*}{2\phi_*^2} (2(\sin(2\theta - \phi_*) \right. \\ \left. - (2\theta - \phi_*) \cos \phi_*) \ln r + (2\theta - \phi_*) (\cos(2\theta - \phi_*) \right. \\ \left. - \cos \phi_*) \right) \end{aligned} \quad (2.33)$$

for  $\phi = \phi_*$ . Now there is a log singularity for this vertex angle. Complete fields are given in Dempsey [39]. A reasonable transition between (2.32) and (2.33) is achieved in Ting [44].

While it was once understandable to regard the breakdown in the traditional solution to Levy's problem as paradoxical (as in Sternberg and Koiter [45]), armed with the analytical developments of Dempsey [39] and Ting [44], it now would seem to be far less so. Thus here rather than term  $\phi_*$  in Levy's problem a critical angle, we view it as a *transition angle* associated with a logarithmic stress state which is transitional much as in Section 2.3.

All of the foregoing examples occur for vertex angles where  $\lambda=1$  is an eigenvalue. That is, for angles where  $\gamma=0$  in Fig. 2. Such  $\phi$  represent transition angles in the following sense. As the vertex angle  $\phi$  in angular elastic plates increases, there is a companion steady increase in the singular character of stresses near the plate vertex (see Fig. 2). These stresses go from power singularities in their derivatives while being themselves bounded ( $\gamma=0^-$ ), to having power singularities in themselves ( $\gamma=0^+$ ). Transition angles with transitional log singularities demark the two types of behavior.

We identify such transition angles with the letter  $T$  throughout Fig. 2. Hence for the free-free plate of Fig. 2a, we have  $T_1, T_2$ , and  $T_3$  corresponding to  $\phi$  of  $\phi_*, \pi$ , and

$2\pi$ .<sup>11</sup> In addition to a logarithmic stress singularity induced by the pressure  $p$  for  $\phi = \phi_*$  here, we have one for the uniform shear  $q-a$  generalization of Levy's problem in effect. Fields for this log singularity may be found in Dempsey [39].

Another generalization of Levy's problem is included in Table 7. This occurs when the plate edge without applied tractions is clamped rather than free. That is, for Conditions I'-II. Typically there are four transition angles with logarithmic stress singularities for this type of configuration (Table 7, (2.30) and (2.31) for general  $\kappa$ ;  $T_4-T_7$  in Fig. 2d for  $\kappa=2$ ). These angles can be less than  $180^\circ$  (eg, Fig. 3b). Fields for associated log singularities may be obtained from Sinclair [40].

One other generalization of Levy's problem is also included in Table 7. This occurs when the plate edge without applied tractions is in contact. That is, for Conditions I'-V. There is a range of transition angles with logarithmic stress singularities for this type of configuration (Table 7); examples are distinguished as  $T_8-T_{11}$  in Fig. 2e. Again angles can be less than  $180^\circ$ . Fields for associated log singularities may be obtained from Sinclair [34].

Typically, the preceding logarithmic stress singularities induced by uniform tractions can instead be produced by cohesive laws. This is because cohesive law conditions can admit rigid body translations which in turn produce uniform tractions. Thus Conditions VI are generally shown as alternatives to Conditions I' in Table 7. In this role, the conditions given on  $p$  and  $q$  in Table 7 then apply to corresponding uniform tractions within Conditions VI.

Turning to logarithmic stress singularities induced by inhomogeneous displacements, we first consider those attending contact conditions. That is, Conditions V'-V in Table 7. For the case of an elastic angular plate being symmetrically indented by a rigid frictionless plate with a sharp corner (Fig. 3c), the finite rotations of one plate edge with respect to the other produce log singularities. This is so even for small rotations ( $0 < \Delta\phi \ll 1$ ). Local fields can be assembled from those for (1.2). Thus with the  $r$  and  $\theta$  coordinates of Fig. 3c,

$$\begin{Bmatrix} \sigma_r \\ \sigma_\theta \end{Bmatrix} = \frac{4\mu}{1+\kappa} \frac{\Delta\phi}{\phi} \left[ 2 \ln r + \begin{Bmatrix} 1 \\ 3 \end{Bmatrix} \right] \quad (2.34)$$

with  $\tau_{r\theta}=0$ , and

$$u_r = \frac{2r}{1+\kappa} \frac{\Delta\phi}{\phi} [(\kappa-1) \ln r - 1], \quad u_\theta = 2r\theta \frac{\Delta\phi}{\phi} \quad (2.35)$$

Evident in (2.34) is a log singularity which must participate for any  $\Delta\phi \neq 0$ .

Asymptotically the same log singularity as in (2.34) may be extracted from the global problem of indentation with

<sup>11</sup>The case of  $\phi=2\pi$  is not obviously a transition angle in Fig. 2a. This is because it is on a branch with  $\gamma>0$  only when  $\phi>2\pi$ , a range of vertex angles not included in Fig. 2a. This branch can be seen in Fig. 2a, Seweryn and Molski [20], near 'a'' =  $\phi/2 = \pi$  therein.

rotation of a half-space. This problem is solved in Section 48.4, Sneddon [46].<sup>12</sup> Such response can be expected to be the case in other configurations wherein a plate vertex angle gets extended or compressed. That is, that there is an isolated logarithmic stress singularity with a coefficient proportional to the relative amount of rotation and the elastic moduli of the material rotating—see Brock [47] and references therein.

Other configurations with logarithmic stress singularities in response to contact conditions are identified in Table 7. These can also be viewed as transition stress states associated with transition angles (eg,  $T_{12}$  and  $T_{13}$  of Fig. 2c). Fields can be obtained from Sinclair [34].

Logarithmic stress singularities can be induced by inhomogeneous displacements without contact conditions. This occurs for Conditions II'–II in Table 7. For the case of a straight boundary ( $\phi = \pi$ ), these are the spurious log singularities that can be introduced by the use of shape functions as boundary conditions in submodeling in finite element analysis. An example involving four node elements is shown in Fig. 3d. Therein, log singularities at the node at  $O$  occur whenever there is a discontinuity in the derivatives of the boundary displacements  $u$  and  $v$ . That is, whenever the constants are such that  $c'_1 \neq c'_2$  or  $c'_3 \neq c'_4$ . Fields are given in Sinclair and Epps [38]. These spurious singularities when shape functions are prescribed also occur for higher order elements and on any smooth submodel boundary (ibid).

Other configurations with logarithmic stress singularities when Conditions VI and II' occur in concert are identified in Table 7. These, too, are associated with transition angles (eg, when  $\gamma = 0$  in Fig. 2f). Fields can be obtained from Sinclair [34].

In closing this section we observe that most of the log singularities identified in Table 7 stem from compliance with the last of (1.5) for  $n_A = 4$  when  $r_A = 3$ . Consequently, they *do not require* repeated roots of the eigenvalue equation. Indeed, for the most part, repeated roots are specifically excluded in Table 7. Just exactly when this is done in Table 7 can be determined by comparing it with Table 5, every set of specifications in the latter table corresponding to a repeated root. Moreover, when such exclusions are relaxed and repeated roots admitted, typically  $\ln^2 r$  stress singularities are produced, in accordance with the first of (1.5). The only exception is for the second set of specifications for Conditions V–V in Table 5 because the rank requirement is not met.

As an example of a log-squared singularity, we consider symmetric indentation by a rigid sharp plate as in Fig. 3c, but now with lateral motion on the contacting edges completely constrained. That is, Conditions II'–II' with  $\Delta\phi \neq 0$  and  $\Delta\phi' = 0$ . For  $\phi = \phi_*$  of (2.31) and  $\kappa = 1$ ,  $\lambda = 1$  is a repeated root (see Table 5, cf Table 7). The corresponding fields can be assembled from those for (1.1), (1.2), and (1.4). Algebraic details can be obtained from Sinclair [34]. In terms of the  $r$  and  $\theta$  coordinates of Fig. 3c, the resulting fields have:

$$\begin{aligned} \begin{Bmatrix} \sigma_r \\ \sigma_\theta \end{Bmatrix} &= \frac{-2\mu\Delta\phi}{\phi_*^2 \sin \phi_*} \left[ 2 \cos \phi_* (\ln^2 r + 2 \ln r - \theta^2) \right. \\ &\quad \left. \begin{Bmatrix} + \\ - \end{Bmatrix} [2(\cos 2\theta - \cos \phi_*) (\ln r + 1) \right. \\ &\quad \left. - 2\theta \sin 2\theta + \phi_*^2 \cos 2\theta] \right. \\ \tau_{r\theta} &= \frac{2\mu\Delta\phi}{\phi_*^2 \sin \phi_*} \left[ \sin 2\theta (2 \ln r + \phi_*^2 + 2) + 2\theta (\cos 2\theta \right. \\ &\quad \left. - \cos \phi_*) \right] \tag{2.36} \\ u_r &= \frac{r\Delta\phi}{\phi_*^2 \sin \phi_*} \left[ 2(\cos \phi_* - \cos 2\theta) \ln r + 2\theta \sin 2\theta \right. \\ &\quad \left. - \phi_*^2 \cos 2\theta \right] \\ u_\theta &= \frac{r\Delta\phi}{\phi_*^2 \sin \phi_*} \left[ 2(\sin 2\theta - 2\theta \cos \phi_*) \ln r + 2\theta (\cos 2\theta \right. \\ &\quad \left. - \cos \phi_*) + \phi_*^2 \sin 2\theta \right] \end{aligned}$$

for  $\kappa \rightarrow 1$ . Other fields with log-squared singularities may be obtained from [34,40].

### 3 STRESS SINGULARITIES FOR THE IN-PLANE LOADING OF AN ELASTIC PLATE MADE OF MULTIPLE MATERIALS

#### 3.1 Formulation and eigenvalue equations

Here we consider extension of the treatment presented in Section 2 to plates made up of multiple elastic sectors. We first formulate this extended class of problems for homogeneous boundary conditions. Then we outline analytical means that can be used to derive companion eigenvalue equations. We stop short of actually presenting all these equations because of their relative complexity, but do furnish references which contain them subsequently in Section 3.2.

To begin, we continue to use cylindrical polar coordinates  $r$  and  $\theta$  with origin  $O$  to describe the entire angular region of interest  $\mathfrak{R}$ , with its complete vertex angle  $\phi$ . Now, though,  $\mathfrak{R}$  is comprised of  $N$  subregions,  $\mathfrak{R}_i$ ,  $i = 1, 2, \dots, N$ , and  $\phi$  of  $N$  subangles,  $\phi_i$  (Fig. 4). Thus

$$\mathfrak{R} = \bigcup_{i=1}^N \mathfrak{R}_i, \quad \phi = \sum_{i=1}^N \phi_i \tag{3.1}$$

where

$$\begin{aligned} \mathfrak{R}_i &= \{(r, \theta) | 0 < r < \infty, \theta_{i-1} < \theta < \theta_i\} \\ \theta_i &= \sum_{i'=1}^i \phi_{i'} \end{aligned} \tag{3.2}$$

with the understanding  $\theta_0 = 0$ . With these geometric preliminaries in place, we can formulate our class of composite problems as follows.

In general, we seek the planar stress components  $\sigma_r$ ,  $\sigma_\theta$ , and  $\tau_{r\theta}$  and their companion displacements  $u_r$  and  $u_\theta$ , as functions of  $r$  and  $\theta$  throughout  $\mathfrak{R}$ , satisfying: the appropri-

<sup>12</sup>There is a factor of  $a^{-1}$  missing from the stresses given at the end of Section 48.4, where “ $a$ ” is as in Fig. 87 therein.

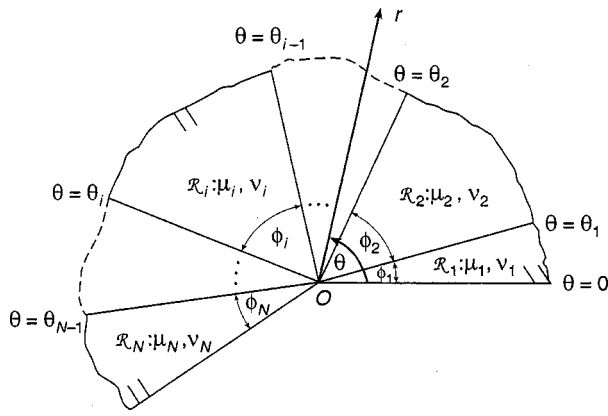


Fig. 4 Geometry and coordinates for the composite angular elastic plate

ate field equations of elasticity; interface conditions on internal plate edges; boundary conditions on external edges if the plate is open ( $\phi < 2\pi$ ), or further interface conditions if it is closed ( $\phi = 2\pi$ ); and regularity requirements at the plate vertex. The field equations hold on  $\mathfrak{R}_i$  ( $i = 1, 2, \dots, N$ ) and are given by (2.2), (2.3), and (2.4) with  $\mu$  and  $\kappa$  in (2.3) being replaced by  $\mu_i$  and  $\kappa_i$ , where  $\mu_i$  is the shear modulus of the material comprising  $\mathfrak{R}_i$  and  $\kappa_i = 3 - 4\nu_i$  for plane strain,  $(3 - \nu_i)/(1 + \nu_i)$  for plane stress, with  $\nu_i$  being Poisson's ratio of this material. The admissible interface conditions are listed in Table 8 and hold on  $\theta = \theta_i$  with  $i = 1, 2, \dots, N - 1$ , if the plate is open,  $i = 0, 1, \dots, N$  if the plate is closed ( $i = 0$  and  $N$  are for but one set of interface conditions). The admissible boundary conditions continue to be as in Table 1 and hold on  $\theta = 0, \phi$  if the plate is open. And the regularity requirements are the same as (2.5) but now hold on  $\mathfrak{R}_i$ ,  $i = 1, 2, \dots, N$ .

The interface conditions of Table 8 merit comment. Conditions A are the traditional conditions usually assumed for a perfectly bonded interface. Conditions B are for contact with friction governed by Amonton's law. As such, to be physically applicable they further require that the normal stress be nowhere tensile on the interface, as in (2.6), and that relative lateral motion on the interface be opposed by shear tractions there. Quite frequently in singularity analysis the special case of frictionless ( $f = 0$ ) contact is treated, so we distinguish the associated conditions by  $B_0$  in Table 8. Conditions A and B are the most common in singularity analysis.

Table 8. Interface conditions for in-plane loading

Identifying letter	Matched quantities	Additional conditions	Physical description
A	$\sigma_\theta, \tau_{r\theta}$ $u_r, u_\theta$		Perfectly bonded
B	$\sigma_\theta, \tau_{r\theta}$ $u_\theta$	$\tau_{r\theta} = f\sigma_\theta$	Contact with friction
$B_0$	$\sigma_\theta, \tau_{r\theta}$ $u_\theta$	$\tau_{r\theta} = 0$	Frictionless contact
C	$\sigma_\theta, \tau_{r\theta}$ $u_r$	$\sigma_\theta = 0$	Separating locking surfaces
D	$\sigma_\theta$ $u_r, u_\theta$	$u_r = 0$	Thin rigid inclusion
E	$\sigma_\theta, \tau_{r\theta}$	$\sigma_\theta = k(u_\theta^+ - u_\theta^-)$ $\tau_{r\theta} = k'(u_r^+ - u_r^-)$	Adhesive stress-separation laws

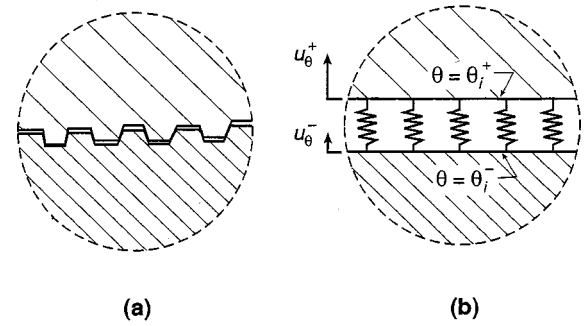


Fig. 5 Sketches of interfaces; a) separating locking surfaces (Conditions C), b) adhesive law action (Conditions E)

Conditions C are from Rao [48]. They do not appear as being particularly physically applicable. They might be interpreted as the conditions for a surface which is rough to the point of locking and thereby prohibiting slip ( $u_r$  matched), yet on the point of separation ( $\sigma_\theta \rightarrow 0$ ). Such an interface is sketched in Fig. 5a.

Conditions D are also from Rao [48]. Essentially they are the same as conditions given in Erdogan and Gupta [49]. They are the composite counterpart of Conditions IV when the latter are interpreted as being for a thin rigid reinforcement. As such, they model a thin inclusion which is relatively stiff compared to its surrounding matrix: It is stiff enough to restrain extension, however it is not so stiff that it restrains bending.

Conditions E are the composite counterparts of cohesive stress-separation laws. Thus  $k$  and  $k'$  are the stiffnesses associated with "springs" resisting normal and lateral separation on an interface. This action for normal separation is sketched in Fig. 5b where

$$u_\theta^+ = \lim_{\theta \rightarrow \theta_i} u_\theta(\theta > \theta_i) \tag{3.3}$$

with  $u_\theta^-$  defined analogously. In the elastic regime, the stiffnesses in these laws should be chosen so that they are consistent with the elastic constitutive laws of the materials comprising the interface. When this is done, the adhesive conditions are the physically appropriate ones for a perfectly bonded interface: Conditions A are just a simplification of them obtained by effectively letting  $k$  and  $k' \rightarrow \infty$  instead of their elastic values.

Conditions E also admit to other interpretations. One is as a model of a flexibly bonded interface in studies of elastic wave interactions in Jones and Whittier [50]. Another is as a model for an interface in a composite which permits some slip in Lene and Leguillon [51] (for this latter interpretation,  $k$  is effectively taken to be infinite, though  $k'$  is finite).

As in Section 2.1, the preceding formulation is absent conditions at infinity and insists on bounded displacements. The basic reasons for these two aspects remain the same. However, we are not aware of a formal extension of the completeness argument for elastic fields with bounded displacements to composite configurations. Absent such, the regularity conditions (2.5) must be viewed as provisional when applied to  $N$ -material plates.

Analysis follows that for single material plates. The conditions for singularities with homogeneous boundary conditions/interface conditions remain as in (1.3). Now, though, the order of the determinant involved is typically increased to

$$n_A = 4N \tag{3.4}$$

Hence the algebra involved in expanding determinants to obtain eigenvalue equations in closed form can be considerably more extensive. While the eigenvalues from the determinant could simply be numerically calculated without algebraic expansion, it is nonetheless useful to obtain a simplified single expression for the eigenvalue equation. Such expressions are more readily used than the raw determinant when the analysis of further specific configurations is required. In addition, typically such expressions facilitate checking by comparison with special cases/other independent algebraic analysis. To assist in obtaining them, some approaches for helping with the algebra entailed are offered in Dempsey and Sinclair [3] and Ying and Katz [52].<sup>13</sup>

Once an eigenvalue equation is obtained for an  $N$ -material problem ( $N \geq 2$ ), verification is important. This is a key concern because of the extent of the algebra involved. As previously mentioned, sometimes such verification is afforded by other independent analysis. Otherwise, in addition to the obvious check of redoing the algebra, one can also perform numerical checks. That is, evaluate the expression for the eigenvalue equation for diverse values of the parameters involved, then compare with a direct calculation of the determinant from its originating matrix. Such comparisons need to take account of any factors removed in simplifying the expansion of the determinant to obtain the eigenvalue equation. They should also be carried out for parameter values which do not, in themselves, realize simplifications of the determinant.

Once checked, eigenvalue equations need to be solved for singular eigenvalues. Generally this requires numerical analysis. Such numerics are straightforward for the most part. The eigenvalues so computed can be verified by back substitution.

At this point, the entire analysis can be further checked by considering *limiting cases*. For bimaterial plates with Conditions A, one check is afforded by setting

$$\mu_1 = \mu_2, \quad \kappa_1 = \kappa_2 \tag{3.5}$$

Then the eigenvalues for the corresponding single material configuration should result.

A second check for bimaterials is to let one of the two materials tend toward being rigid. Consider the fields in (1.1) under the limit  $\mu \rightarrow \infty$ : The displacements go to zero. We therefore set displacements to zero in the interface conditions of Table 8 to recover the corresponding boundary conditions of Table 1 for the one remaining deformable sector. Hence as  $\mu_i \rightarrow \infty$ ,

$$\begin{aligned} A \rightarrow \text{II}, \quad B \rightarrow \text{V}, \quad B_0 \rightarrow \text{III} \\ C \rightarrow \text{IV}, \quad D \rightarrow \text{II}, \quad E \rightarrow \text{VI} \end{aligned} \tag{3.6}$$

for  $\mathfrak{R}_{3-i}$  and  $i = 1$  or  $2$ . Again singular eigenvalues should match single material values.

A third check for bimaterials is to let one of the two materials become limp. Now consider the fields in (1.1) under the limit  $\mu \rightarrow 0$ , but first make the exchanges  $\mu c_1$  for  $c_1, \mu c_2$  for  $c_2$ , and so on to avoid unbounded displacements. Now the stresses go to zero. We therefore set stresses to zero in the interface conditions to recover corresponding boundary conditions. Hence as  $\mu_i \rightarrow 0$ ,

$$\begin{aligned} A \rightarrow \text{I}, \quad B \rightarrow \text{I}, \quad B_0 \rightarrow \text{I} \\ C \rightarrow \text{I}, \quad D \rightarrow \text{IV}, \quad E \rightarrow \text{I} \end{aligned} \tag{3.7}$$

for  $\mathfrak{R}_{3-i}$  and  $i = 1$  or  $2$ . Again, singular eigenvalues should match single material values.

On occasion the eigenvalue equation for a bimaterial is insensitive as to whether  $\mu_1 \rightarrow \infty$  or  $\mu_2 \rightarrow 0$ , or vice versa. This simply means it should recover both of the eigenvalue equations for the corresponding boundary conditions in (3.6) and (3.7) under either limit. For example, the eigenvalue equation for the interface crack can be written as

$$0 = \sin^2 \lambda \pi \left[ 1 - \frac{4 \hat{\mu}_1 \hat{\mu}_2}{(\hat{\mu}_1 + \hat{\mu}_2)^2} \sin^2 \lambda \pi \right] \tag{3.8}$$

where  $\hat{\mu}_1 = \mu_1 + \kappa_1 \mu_2$  and  $\hat{\mu}_2 = \mu_2 + \kappa_2 \mu_1$ . Equation (3.8) is insensitive as to whether  $\mu_1 \rightarrow \infty$  or  $\mu_2 \rightarrow 0$ . From (3.6) and (3.7), these limits correspond to  $A \rightarrow \text{II}$  or  $A \rightarrow \text{I}$ . Thus the interface crack (I-A-I) becomes a half-plane with II-I or I-I. Under either limit, (3.8) recovers the product of the eigenvalue equation for a clamped-free half-plane ((2.17) for  $\phi = \pi$ ) with the eigenvalue equation for the free-free half-plane ((2.9)  $\times$  (2.13) for  $\phi = \pi$ ).

In addition to serving as checks, the limiting cases of (3.5), (3.6), and (3.7) enable a ready first assessment of the singular stresses involved when faced with a new bimaterial configuration which lacks any singularity analysis. It is also possible to extend the application of these types of limits to configurations involving more than two materials.

For the general numerical analysis of eigenvalues for other than special cases, the parameter space to be searched is now increased significantly in dimension over that attending configurations comprised of a single material. This is because it now includes multiple vertex angles as well as multiple pairs of elastic moduli.

For bimaterial plates, dimensional analysis reduces the number of independent elastic moduli from four to three. This number can be further reduced by employing just the two material constants  $\alpha$  and  $\beta$  defined by

$$\begin{Bmatrix} \alpha \\ \beta \end{Bmatrix} = \frac{\mu_2 \begin{pmatrix} + \\ \kappa_1 - \\ - \end{pmatrix} 1 - \mu_1 \begin{pmatrix} + \\ \kappa_2 - \\ - \end{pmatrix} 1}{\mu_2(\kappa_1 + 1) + \mu_1(\kappa_2 + 1)} \tag{3.9}$$

The  $\alpha$  and  $\beta$  of (3.9) are given in Dundurs [53]. This article is a discussion which points out the reduction in the number of independent elastic constants that can be achieved by the

<sup>13</sup>It is also possible to employ symbolic manipulation codes to expand determinants. At present this usually results in lengthy expressions for the determinant. Consequently, such codes typically only provide an alternative to direct numerical treatment of the original determinant.

introduction of  $\alpha$  and  $\beta$  into the butt joint problem treated in Bogy [54]. Equivalent  $\alpha$  and  $\beta$  were given earlier in Zak and Williams [55] to reduce the number of independent elastic constants for the specific problem of a crack terminating perpendicular to a bimaterial interface. Dundurs [56] establishes general criteria for bimaterial configurations under which such reductions can be made.

To demonstrate how the reduction is effected, we consider a perfectly bonded bimaterial with stress-free edges (I-A-I). Absent a difference in materials, this plate's stresses are completely independent of elastic moduli, as is any singularity exponent (see (2.9) and (2.13) for I-I). Consequently, only the traditional matching conditions associated with perfect bonding can introduce any dependence on elastic moduli. Without loss of generality, we take the perfectly bonded interface to occur at  $\theta=0$ . Then, from (1.1), the matching conditions result in the following sparse set of equations:

$$\begin{aligned} c_1^+ + \lambda c_3^+ + c_3^+ &= c_1^- + \lambda c_3^- + c_3^- \\ c_1^+ + \lambda c_3^+ - \kappa_1 c_3^+ &= \frac{\mu_1}{\mu_2} (c_1^- + \lambda c_3^- - \kappa_2 c_3^-) \\ c_2^+ + \lambda c_4^+ - c_4^+ &= c_2^- + \lambda c_4^- - c_4^- \\ c_2^+ + \lambda c_4^+ + \kappa_1 c_4^+ &= \frac{\mu_1}{\mu_2} (c_2^- + \lambda c_4^- + \kappa_2 c_4^-) \end{aligned} \tag{3.10}$$

In (3.10), the constants associated with the material above  $\theta=0$  and moduli  $\mu_1$  and  $\kappa_1$  are distinguished with a plus sign, those with material below and  $\mu_2$  and  $\kappa_2$  with a minus sign. Now subtracting the second of (3.10) from the first gives  $c_3^+$  in terms of  $c_1^-$  and  $c_3^-$  and the two combinations of elastic moduli

$$\frac{\mu_2 - \mu_1}{\mu_2(\kappa_1 + 1)}, \quad \frac{\mu_2 + \kappa_2 \mu_1}{\mu_2(\kappa_1 + 1)} \tag{3.11}$$

Back substituting into the first of (3.10) then gives  $c_1^+$  in terms of  $c_1^-$  and  $c_3^-$  and the same two combinations. And performing the same operations on the third and fourth of (3.10) gives  $c_4^+$  and  $c_2^+$  each in terms of  $c_2^-$  and  $c_4^-$  and the same two combinations. Thus I-A-I stresses and singularity exponents need only depend on the two combinations of elastic moduli given in (3.11). While these two combinations are closer to those used in Zak and Williams [55] than those in Dundurs [53], with some algebra they can be shown to be equivalent to  $\alpha$  and  $\beta$  of (3.9).

Similar analysis establishes that moduli dependence can be reduced to just that on  $\alpha$  and  $\beta$  for bimaterials and with any of the interface conditions A, B (and therefore  $B_0$ ), or C, under any combination of boundary conditions involving I, III, or IV (Table 9). Given the equivalence of cohesive law conditions with stress-free conditions as far as eigenvalue equations are concerned, singular eigenvalues with Conditions VI in bimaterials and with interface conditions A, B, or C can also be expected to depend only on  $\alpha$  and  $\beta$ .

The constants  $\alpha$  and  $\beta$  have seen widespread use for such configurations since Dundurs [56], and have come to be known as *Dundurs parameters*. They admit to physical inter-

pretation to a degree. For plane stress, substituting for  $\mu$  and  $\kappa$  in terms of Young's modulus  $E$  and Poisson's ratio  $\nu$  gives:

$$\alpha = \frac{E_2 - E_1}{E_2 + E_1}, \quad \beta \Big|_{E_2 = E_1} = \frac{\nu_2 - \nu_1}{4} \tag{3.12}$$

Thus,  $\alpha$  is a normalized measure of the mismatch in Young's moduli, while  $\beta$  reflects the difference in Poisson's ratios when there is no difference in Young's moduli. Similar results hold for plane strain if  $E$  is exchanged for  $E/(1-\nu^2)$ .

For bimaterials, the ranges  $0 < \mu_i < \infty$ ,  $0 \leq \nu_i \leq 1/2$ , and  $i = 1, 2$  limit accompanying  $\alpha$  and  $\beta$  to within parallelograms (Dundurs [53]). These are given by

$$\begin{aligned} -1 < \alpha < 1 \\ \frac{\alpha - 1}{4} \leq \beta \leq \frac{\alpha + 1}{4} \dots \text{plane strain} \\ \frac{3\alpha - 1}{8} \leq \beta \leq \frac{3\alpha + 1}{8} \dots \text{plane stress} \end{aligned} \tag{3.13}$$

The parallelogram for plane strain encompasses that for plane stress and accordingly is the one to be searched if all possible singular eigenvalues are to be identified. Often this search can be readily undertaken using an inverse approach. That is, assuming a specific value of singular eigenvalue and then solving for  $\alpha$  and  $\beta$ .

It is also possible to use two sets of  $\alpha$  and  $\beta$  to reduce the number of independent elastic constants from five to four for trimaterial plates: see Koguchi, Inoue, and Yada [57]. Then, too, the introduction of  $\alpha$ s and  $\beta$ s can enable an inverse approach to be adopted.

### 3.2 Power singularities identified in the literature

We now review contributions in the literature that have effected asymptotic assessments of possible stress singularities for  $N$ -material plates under in-plane loading, starting with power singularities. We carry out our review in approximate order of increasing analytical complexity. We begin with bimaterial plates and arguably the simplest of these, those involving "cracks" (Fig. 6): Here "cracks" means mathematical slits which may or may not have the traditional stress-free conditions of fracture mechanics. Next we consider open bimaterial plates (Fig. 7): Altogether, the geometries in Figs. 6 and 7 are the ones which have received the most attention in the literature. Thereafter we conclude the section by reviewing contributions for other bimaterial plates and some trimaterial ones.

There is considerable duplication within the investigations reviewed. We include later references for problems if they represent a means of verification of earlier research, or if they provide further information on the singular stresses involved. We do this irrespective of whether or not we can envisage a situation in which the singular configuration is physically appropriate. We exclude later references otherwise: A significant number of references are thus excluded. In particular, we do not include later references which analyze a global problem whose singular character was previ-

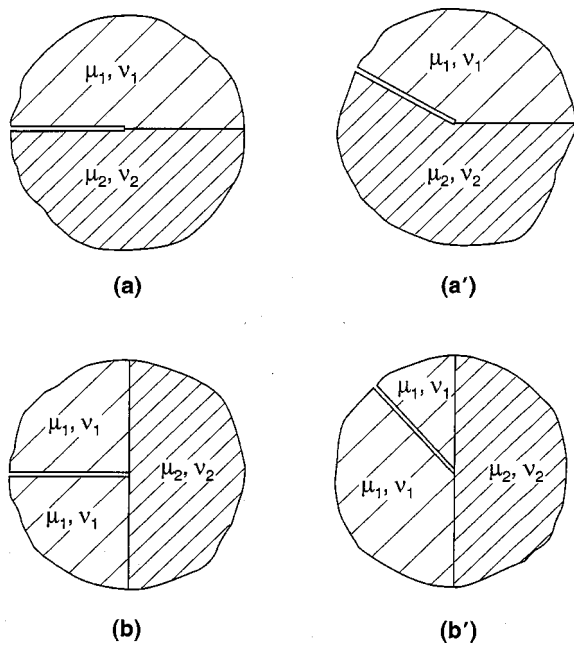


Fig. 6 Bimaterial “crack” geometries analyzed for stress singularities: a) interface crack, a’) interface crack ending at a kink on the interface, b) crack ending orthogonal to an interface, b’) crack ending obliquely to an interface

ously well appreciated—the contribution of this genre of investigation lies in the implications of the global configuration analyzed, rather than singularity identification.

For the *interface crack* of Fig. 6a with stress-free crack flanks, the corresponding boundary and interface conditions

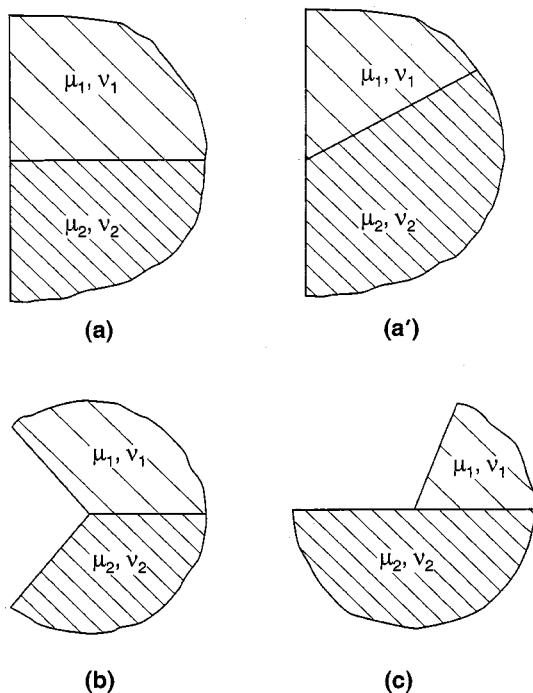


Fig. 7 Open bimaterial plate geometries analyzed for stress singularities: a) butt joint, a’) oblique butt joint, b) two plates of equal vertex angles, c) angular plate on a half-plane

from Tables 1 and 8 are I-A-I. Williams [58] provides both the eigenvalue equation and resulting complex singular eigenvalue in closed form. These results are confirmed in Bogy [59]. The eigenvalue equation is equivalent to that given in (3.8), while the associated singularity exponent is

$$\gamma = \frac{1}{2}, \quad \eta = \frac{1}{2\pi} \ln \frac{\hat{\mu}_1}{\hat{\mu}_2} \tag{3.14}$$

where  $\hat{\mu}_1$  and  $\hat{\mu}_2$  are as in (3.8).

For the interface crack (Fig. 6a) with clamped conditions (II-A-II), Theocaris and Gdoutos [60] give an eigenvalue equation and complex singular eigenvalue in closed form. Ting [61] furnishes a different expression for the imaginary part of the complex singular eigenvalue: This latter result is confirmed in Ballarini [62] and elsewhere.<sup>14</sup> The singularity exponent from Ting [61] for the clamped interface crack is similar to that for stress-free flanks. It has

$$\gamma = \frac{1}{2}, \quad \eta = \frac{1}{2\pi} \ln \frac{\kappa_2 \hat{\mu}_1}{\kappa_1 \hat{\mu}_2} \tag{3.15}$$

Thus the imaginary part differs by at most  $\pm 0.175$  from that in (3.14).

For the interface with one flank free and the other clamped (I-A-II), Theocaris and Gdoutos [60] give an eigenvalue equation. Closed-form expressions for singular eigenvalues are given in Ting [61].

For the interface crack with contact with friction between the crack flanks (B-A), Comninou [63] provides an eigenvalue equation. This equation is confirmed in Dempsey and Sinclair [64]. Singular eigenvalues follow by inspection and are furnished in Comninou [63], as is the companion eigenfunction. The simpler frictionless case (B<sub>0</sub>-A) is treated in the Appendix of Comninou [65].

For the interface crack when there is contact with friction on the interface ahead of a stress-free crack (I-B-I), Gdoutos and Theocaris [22] provides an eigenvalue equation in terms of Dundurs parameters. This equation is confirmed in Comninou [66]. An expression for the resulting singular eigenvalues is given in Gdoutos and Theocaris [22]. The simpler frictionless case (I-B<sub>0</sub>-I) is treated in Dundurs and Lee [67].

Finally, for the interface crack when an inextensible inclusion is inserted into the crack (D-A), Dempsey [21] gives an eigenvalue equation. Closed-form expressions for singular eigenfunctions are given in Wu [68].

We next consider *kinked interface cracks*. Here the geometry for these cracks is taken to be such that the “crack” still lies between the two materials but now terminates at a kink on their interface (Fig. 6a’). This geometry may be viewed as a generalization of that for the previous straight interface crack (Fig. 6a).

For the kinked interface crack (Fig. 6a’) with stress-free flanks (I-A-I), Bogy [59] furnishes the eigenvalue equation in terms of Dundurs parameters. This eigenvalue equation is confirmed in Dempsey and Sinclair [64]. In addition, Bogy [59] provides singular eigenvalues for a variety of kinked

<sup>14</sup>It is also implicit in Erdogan and Gupta [49].

interface cracks. These eigenvalues are numerically determined for the most part. Further numerical eigenvalues are given in Chen and Hasebe [69]. Theocaris and Gdoutos [60] and van Vroonhoven [70] also treat kinked interface cracks with stress-free flanks, but do not use Dundurs parameters.

For the kinked interface crack (Fig. 6a') with clamped conditions either on one flank (I-A-II) or both (II-A-II), Theocaris and Gdoutos [60] gives eigenvalue equations and some singular eigenvalues.

For the kinked interface crack with crack flanks perfectly bonded (A-A), equation (19) of Bogy and Wang [71] is the eigenvalue equation in terms of Dundurs parameters. This equation is confirmed in Dempsey and Sinclair [64] and elsewhere. In addition, Bogy and Wang [71] provides singular eigenvalues for quite a variety of such kinked configurations. Chen and Nisitani [72] provides the associated eigenfunction as well as further eigenvalues. Van Vroonhoven [70], Pageau, Joseph, and Biggers [73], and Chaudhuri, Xie, and Garala [74] also treat the same kinked configuration without using Dundurs parameters.

For the kinked interface crack when there is contact with friction between the crack flanks (B-A), an eigenvalue equation may be found in Dempsey and Sinclair [64] in terms of Dundurs parameters. Corresponding singular eigenvalues for a variety of such configurations are numerically determined in Dempsey [21]. If contact with friction also occurs on the interface ahead of the crack (B-B), an eigenvalue equation may be found in Dempsey and Sinclair [64] in terms of Dundurs parameters.

For the kinked interface crack when Conditions C of Table 8 hold, eigenvalue equations in terms of Dundurs parameters for A-C, B-C, and C-C may be found in Dempsey and Sinclair [64]. Finally, for the kinked interface crack when Conditions D of Table 8 hold, eigenvalue equations for A-D, B-D, C-D, and D-D are given in Dempsey [21].

We now consider "cracks" *terminating at an interface* rather than lying along it. The simplest such configuration is when the crack impinges at a right angle (Fig. 6b), because then the geometry is symmetric enabling symmetric and antisymmetric loading to be analyzed separately. As a consequence, this special case has received attention by a number of investigators in the literature.

For a crack *terminating normal* to an interface (Fig. 6b) and having stress-free flanks (I-A-A-I), Zak and Williams [55] furnishes an eigenvalue equation for loading which is symmetric about the crack. This equation is in terms of parameters which are equivalent to those of Dundurs. It is confirmed in Dempsey and Sinclair [64].<sup>15</sup> Zak and Williams [55] provides singular eigenvalues. Further singular eigenvalues are given in Khrapkov [75] and Bogy [76]. The eigenvalue equation for antisymmetric loading is given in

Dempsey and Sinclair [64]. This equation is the same as for symmetric loading.<sup>16</sup>

For a crack terminating normal to an interface (Fig. 6b) with contact with friction between the flanks (B-A-A), Comninou and Dundurs [77] furnish an eigenvalue equation in terms of Dundurs parameters. Corresponding singular eigenvalues are provided: These are independent of the value of the coefficient of friction.

For a stress-free crack terminating normal to an interface which is itself in contact with friction (I-B-B-I), eigenvalue equations when loading is symmetric or antisymmetric are furnished in Dempsey and Sinclair [64] in terms of Dundurs parameters. These equations are confirmed in Wijeyewickrema, Dundurs, and Keer [78] which in addition provides singular eigenvalues for both modes of loading and a range of values of the coefficient of friction. The simpler case of frictionless contact (I-B<sub>0</sub>-B<sub>0</sub>-I) is treated in Gharpuray, Dundurs, and Keer [79].

Finally, for a stress-free crack terminating normal to an interface on which Conditions C or D hold, eigenvalue equations are available as follows: for I-C-C-I with either symmetric or antisymmetric loading, from Dempsey and Sinclair [64] in terms of Dundurs parameters; for I-D-D-I and either symmetric or antisymmetric loading, from Dempsey [21].

For the more general instance of a crack *terminating obliquely* (Fig. 6b'), several investigations are available. When the crack is free of stress (I-A-A-I), Bogy [76] furnishes the eigenvalue equation in terms of Dundurs parameters, as well as singular eigenvalues for a variety of such configurations. Fenner [80] and Yong-Li [81] compute singular eigenvalues directly from the determinant without algebraic expansion, though Fenner [80] does establish that eigenvalues depend on only two material constants. The eigenvalues in Fenner [80] and Yong-Li [81] include ones which agree closely with corresponding values in Bogy [76] (provided a state of plane stress is assumed in Yong-Li [81]). Wang and Chen [82] treats the same configuration: On occasion, the singular eigenvalues in Wang and Chen [82] agree with corresponding values in Bogy [76], but in some instances there are significant discrepancies between the two.

For a crack terminating obliquely at an interface (Fig. 6b') with flanks in contact with friction (B-A-A), Comninou and Dundurs [77] furnishes an eigenvalue equation in terms of Dundurs parameters. Comninou and Dundurs [77] also provides singular eigenvalues for varying angles of incidence of the crack and different coefficients of friction.

For a stress-free crack terminating obliquely to an interface which is itself in contact with friction (I-B-B-I), Wijeyewickrema, Dundurs and Keer [78] furnishes an eigenvalue equation in terms of Dundurs parameters. When simplified for special instances, this equation agrees with others in the literature. The simpler case of frictionless contact (I-B<sub>0</sub>-B<sub>0</sub>-I) is treated in Gharpuray, Dundurs, and Keer [79].

<sup>15</sup>There would appear to be a typographical error in the equation in Zak and Williams [55]. All that is needed to correct this error is to replace  $\cos \pi$  with  $\cos \lambda \pi$ .

<sup>16</sup>Taken together, the eigenvalue equation for both symmetric and antisymmetric response is given as a simple squared term in Bogy [76]. This equation appears to have an extraneous factor of  $\sin^2 \lambda \pi$ —see (28) and (18) et seq *ibid*. The same factor is present in the eigenvalue equation for when the crack terminates obliquely. It would not appear to lead to errors in eigenvalues reported.

There are some further generalizations for stress-free cracks terminating at an interface (I-A-A-I) which are analyzed in the literature. If the crack flanks in Fig. 6b' are allowed to subtend a finite angle at their tip and thus become a reentrant corner, an analysis may be found in Tan and Meguid [83]. If the interface in Fig. 6b' is allowed to have a kink at the point where the crack terminates, an analysis may be found in Pinsan and Zhuping [84].

We next consider *open bimaterial plates* which do not, for the most part, involve cracks (Fig. 7). We begin with probably the simplest such configuration, the *butt joint* of Fig. 7a. When the outside surfaces are free of stress and the joint is perfectly bonded (I-A-I), Bogy [85] furnishes the eigenvalue equation in terms of Dundurs parameters. This equation is confirmed in Dempsey and Sinclair [64]. Bogy [85] also provides singular eigenvalues: These are consistent with corresponding values in Hein and Erdogan [86]. The ratio of the shear moduli for which a power singularity first starts to appear is given in Kubo, Ohji, and Nakai [87].

For the butt joint (Fig. 7a) with stress-free outside surface and contact with friction on the interface (I-B-I), Theocaris and Gdoutos [88] furnishes the eigenvalue equation in terms of Dundurs parameters. This equation is confirmed in Dempsey and Sinclair [64] (the sign of the friction coefficient has to be changed because the friction condition is applied on a negative  $\theta$ -face in Theocaris and Gdoutos [88], a positive  $\theta$ -face in Dempsey and Sinclair [64]). In addition, Theocaris and Gdoutos [88] provides singular eigenvalues for varying coefficients of friction.

The more general *oblique butt joint* here has the interface meet the outside free surface at an angle other than  $90^\circ$  (Fig. 7a'). When the joint is perfectly bonded (I-A-I), Bogy [59] furnishes the eigenvalue equation in terms of Dundurs parameters. This equation is confirmed in Dempsey and Sinclair [64]. Singular eigenvalues are also provided in Bogy [59] for several angles of incidence of the interface with the outside surface. Further singular eigenvalues are given in Hein and Erdogan [86] and Rao [48]. Geometries for which a power singularity first starts to appear are given in Rao [48], and Kubo, Ohji, and Nakai [87].

For the oblique butt joint (Fig. 7a') when the interface is in contact with friction (I-B-I), Theocaris and Gdoutos [88] furnishes the eigenvalue equation in terms of Dundurs parameters. This equation is confirmed in Dempsey and Sinclair [64] (again, the sign of the friction coefficient has to be changed). In addition, Theocaris and Gdoutos [88] provides singular eigenvalues for several angles of incidence and varying coefficients of friction.

A further open bimaterial geometry investigated in the literature is that of two *plates with equal vertex angles* (Fig. 7b). When the outside edges of the plates are stress free and they are perfectly bonded along their interface (I-A-I), Bogy [59] furnishes the eigenvalue equation. This equation is confirmed in Dempsey and Sinclair [64]. Singular eigenvalues are also provided in Bogy [59] for several plate vertex angles. Further singular eigenvalues are given in Rao [48]. Geometries for which a power singularity first starts to appear are given in Rao [48] and Kubo, Ohji, and Nakai [87].

The stress-free bimaterial plate, with constituent plates with equal vertex angles (Fig. 7b), can have the interface in contact with friction (I-B-I). Theocaris and Gdoutos [88] furnishes the eigenvalue equation in terms of Dundurs parameters under these conditions. This equation is confirmed in Dempsey and Sinclair [64] (again, the sign of the friction coefficient has to be changed). Theocaris and Gdoutos [88] also provides singular eigenvalues for several vertex angles and any value of the coefficient of friction.

The last open bimaterial geometry investigated quite frequently in the literature is that of a *plate sector on a half-plane* (Fig. 7c). When the outside edge of the plate and half-plane surface exterior to it are free of stress, and the two are perfectly bonded along their interface (I-A-I), Bogy [59] furnishes the eigenvalue equation in terms of Dundurs parameters. This eigenvalue equation is confirmed in Gdoutos and Theocaris [22]. Singular eigenvalues when the vertex angle of the plate is  $90^\circ$  are provided in Bogy [59]. Singular eigenvalues for other vertex angles are given in Hein and Erdogan [86] and Gdoutos and Theocaris [22].

For a plate on a half-plane (Fig. 7c) when the plate is in contact with friction (I-B-I), Gdoutos and Theocaris [22] furnishes the eigenvalue equation in terms of Dundurs parameters. This equation is confirmed in Comninou [66]. Singular eigenvalues are provided in Gdoutos and Theocaris [22] for plate angles of  $60^\circ$  and  $90^\circ$  and varying friction coefficients. Singular eigenvalues for some other vertex angles are given in Theocaris and Gdoutos [89]. The simpler case of frictionless contact (I-B<sub>0</sub>-I) is treated in Rao [48] and Dundurs and Lee [67].

There are some other bimaterial plates with asymptotic analysis in the literature. For the perfectly bonded bimaterial plate with stress-free edges (I-A-I) and arbitrary vertex angles, an eigenvalue equation is given in Aksentian [90]. In terms of Dundurs parameters, it is furnished in Bogy [59]. This latter equation is confirmed in Dempsey and Sinclair [64]. If one or both of the edges are clamped instead, respective eigenvalue equations are furnished in Dempsey and Sinclair [64]. These equations are confirmed in Ying and Katz [52].<sup>17</sup> The second configuration is also investigated in Avetisyan and Chobanian [91]. If both edges have rigid thin reinforcements (IV-A-IV), the eigenvalue equation is given in Dempsey and Sinclair [64] in terms of Dundurs parameters, and some eigenvalues are given in Rao [48].

Eigenvalue equations for bimaterial plates with other interface conditions are available as follows. In terms of Dundurs parameters for stress-free bimaterial plates with different interface conditions (I-B-I and I-C-I) and arbitrary vertex angles, eigenvalue equations are given in Dempsey and Sinclair [64]. In terms of Dundurs parameters for further closed bimaterial plates (A-C, B-C, and C-C), eigenvalue equations are also given in Dempsey and Sinclair [64]. Eigenvalue equations involving Conditions II and Conditions B or C are given in Dempsey [21]. Eigenvalue equations involving Conditions D are also given in Dempsey [21].

<sup>17</sup>In addition, these equations appear to be consistent with those given in Aksentian [90] provided  $m_i$  is taken to be Poisson's number rather than Poisson's ratio as stated on p 193. That is, provided  $m_i = 1/\nu_i$ .

Turning to the *trimaterial plate*, the simplest of such configurations occurs when the plates are all comprised of the same material. Picu and Gupta [92] treats a closed plate of this type with frictionless contact on its interfaces ( $B_0$ - $B_0$ - $B_0$ ). Singular eigenvalues are independent of elastic moduli and are given for a range of vertex angles in Picu and Gupta [92]. Other degenerate trimaterial plates wherein there are not three distinct materials include the crack geometries of Figs. 6*b* and 6*b'* reviewed earlier.

When a trimaterial plate is actually comprised of three distinct materials, analysis can be extensive. Nonetheless, there are some true trimaterial plates investigated in the literature. For an open trimaterial plate with bonded interfaces and stress-free/clamped exterior edges (I-A-A-I, I-A-A-II, or II-A-A-II), Ying and Katz [52] derives eigenvalue equations. An eigenvalue equation for the first of these configurations (I-A-A-I) is given in terms of pairs of Dundurs parameters in Koguchi, Inoue, and Yada [57], as are some resulting singular eigenvalues. Further singular eigenvalues from the same equation are presented in Inoue and Koguchi [93]. Additional singular eigenvalues are given in Pageau, Joseph, and Biggers [73], together with some singular eigenvalues for the closed and bonded trimaterial plate (A-A-A). The nature of associated singular eigenfunctions for I-A-A-I is considered in Pageau et al [94].

In closing, we comment on the one remaining set of interface conditions in Table 8, Conditions E. With these adhesive stress-separation laws instead of the classical perfectly-bonded conditions, some reduction in the occurrence of stress singularities is to be expected. This is indicated via limiting cases with single-material plates. However, this is yet to be formally established in general.

### 3.3 Log singularities identified in the literature

Here we review contributions to the literature that have asymptotically established the possibility of logarithmic terms in stress singularities for  $N$ -material plates under in-plane loading. We start with when such singularities can occur with homogeneous boundary conditions, then consider their occurrence with inhomogeneous boundary conditions. We focus on bimaterial plates and follow the same order of geometries as previously in Section 3.2.

Before beginning this review, we recap the requirements for logarithmic participation in bimaterial plates because these continue to be incorrectly stated/applied in the literature. For *homogeneous boundary conditions* as in Table 1, conditions for logarithmic intensification of power singularities are as in the second of (1.3) with  $n_A=8$  for bimaterials. For the case of pure logarithmic singularities, conditions are as in the penultimate of (1.3) with  $n_A=8$ . For *inhomogeneous boundary conditions* as in Table 6, conditions for a log-squared singularity are as in the first of (1.5) for  $n_A=8$ . For the case of pure logarithmic singularities, conditions are as in the last two of (1.5) for  $n_A=8$ . Throughout these conditions for bimaterials, corresponding inequalities for  $\hat{c}$ s and  $\bar{c}$ s are to hold on at least one  $\mathfrak{R}_i$  ( $i=1,2$ ), while equations for  $\bar{c}$ s are to hold on both.

For a pure logarithmic singularity, conditions other than

the preceding continue to be advanced in the literature (eg, Murakami [95] and Wijeyewickrema et al [78]). Typically these have

$$D = \frac{\partial D}{\partial \lambda} = 0 \text{ for } \lambda = 1 \quad (3.16)$$

While appealing in its simplicity, (3.16) is *not sufficient* for a log singularity with *homogeneous* boundary conditions, and it is *not necessary* for a log singularity with *inhomogeneous* boundary conditions. To remove any doubt that this is so, we furnish some demonstrations.

As a first demonstration of (3.16) not being sufficient with homogeneous boundary conditions, we consider the interface crack (Fig. 6*a*) with crack flanks perfectly bonded together. That is, Conditions A hold both ahead of and in back of the “crack” tip. The determinant for this case is given in equation (25), Bogy and Wang [71]. In terms of the eigenvalue  $\lambda$ , this has

$$D = -(1 - \beta^2)^2 \sin^4 \lambda \pi \quad (3.17)$$

Clearly  $D$  of (3.17) satisfies (3.16). The coefficient matrix  $A$  which leads to  $D$  can be assembled from (1.1) on applying Conditions A on  $\theta=0, \pi$ . Checking the rank of this matrix reveals that it drops to four when  $\lambda=1$ . Thus (1.3) requires that the first four derivatives of  $D$  be zero when  $\lambda=1$ . The  $D$  of (3.17) has just its first three derivatives being zero when  $\lambda=1$ . Consequently, no log singularity is possible for this configuration despite the fact that (3.16) is met. This is what one would expect because this configuration has two perfectly bonded half-planes with no discontinuities in either boundary geometry or boundary conditions.

As a second demonstration of (3.16) not being sufficient, we consider the interface crack (Fig. 6*a*), but now with the crack flanks in frictionless contact. The determinant for this configuration is given as equation (54), Comninou [65]. This equation has a multiplicative factor which cannot be zero removed, and otherwise is

$$D = \sin^3 \lambda \pi \cos \lambda \pi \quad (3.18)$$

Clearly  $D$  of (3.18) satisfies (3.16). However, checking the rank of the corresponding coefficient matrix reveals it drops to five when  $\lambda=1$ . Thus (1.3) requires the first three derivatives of  $D$  to be zero when  $\lambda=1$ . The  $D$  of (3.18) has only the first two of its derivatives zero when  $\lambda=1$ . Consequently, no log singularity is possible for this configuration despite the fact that (3.16) is met. This absence of logarithmic stress singularities is consistent with the results in Table 5 for the two limiting cases of (3.6) and (3.7).

As a third and final demonstration of (3.16) not being sufficient, we consider a crack terminating normal to an interface (Fig. 6*b* with I-A-A-I). The determinant in this instance may be obtained from Dempsey and Sinclair [64] as

$$D = \sin^2 \lambda \pi [\alpha + \beta^2 - 2\lambda^2(\alpha - \beta)(1 - \beta) + (1 - \beta^2)\cos \lambda \pi]^2 \quad (3.19)$$

Clearly  $D$  of (3.19) complies with (3.16). This leads Koguchi et al [57] to conclude that log singularities are possible for

any values of  $\alpha$  and  $\beta$ . However, checking the rank of the coefficient matrix reveals that it drops to ten. Because this bimaterial is a degenerate trimaterial ( $n_A = 12$ ), this means that the first two derivatives of  $D$  must be zero at  $\lambda = 1$  for a log singularity in (1.3). The  $D$  of (3.19) has only its first derivative zero at  $\lambda = 1$ . Consequently, no log singularity is possible here. This absence of logarithmic stress singularities is consistent with results in Table 5 for limiting cases.<sup>18</sup>

Demonstrations of (3.16) not being necessary for log singularities with inhomogeneous boundary conditions abound. They can be found in Table 7 as limiting cases.

In the literature, (3.16) is typically used with homogeneous boundary conditions. The configurations identified in this way may admit the possibility of a log singularity, or they may not. The other requirements in (1.3) need to be further checked to decide. Absent such checks, the situation remains ambiguous in this regard and, accordingly, we omit configurations so identified in the review that follows. As a result, to date in the literature the number of bimaterial plates identified as having pure logarithmic singularities is fewer than that for plates comprised of a single material. In fact, one would expect the opposite to be the case given the extra parameters available with bimaterials. This probably means that there are a significant number of bimaterials which do have log singularities that are, as yet, not identified explicitly.

We begin with instances of *logarithmic intensification* of power singularities under *homogeneous boundary conditions*. Quite a variety of such instances are identified in Dempsey [33]. Typically they occur at transitions from complex to real eigenvalues (cf, Section 2.3). For the traditional conditions for perfect bonding on the interface while outer edges are stress free (I-A-I), the following bimaterial geometries are determined as having the possibility of power-logarithmic stress singularities in Dempsey [33]: Figs. 6a' and b', and Figs. 7a', b, and c. Other instances are identified for closed bimaterial plates. These are for perfect bonding (A-A) and the geometry of Fig. 6a', and for frictional contact with perfect bonding (B-A-A) and the geometry of Fig. 6b'. The last is really a degenerate trimaterial.

Turning to *pure logarithmic singularities* with *homogeneous boundary conditions*, there are few instances identified in the literature wherein (1.3) is known to be satisfied for bimaterials. Two such are for two sets of specifications for the oblique butt joint (Fig. 7a') with stress-free conditions (I-A-I) which are given in Chen [96]. Some further instances are given in Dempsey [33] for the following configurations: Fig. 6a' with A-A, and Fig. 7a' with I-A-I. Additional instances may be inferred from Dempsey [33] for the configuration of Fig. 6b' with B-A-A.<sup>19</sup>

<sup>18</sup>For  $D$  of (3.19),  $\lambda = 1$  can be a root of multiplicity 3 for special values of  $\alpha$  and  $\beta$ : Further checking of these special cases reveals that they too do not have log singularities.

<sup>19</sup>The thrust of Dempsey [33] is to gain an appreciation of when power-logarithmic singularities occur. Hence pure log singularities are not explicitly identified and can only be inferred as limits in this paper.

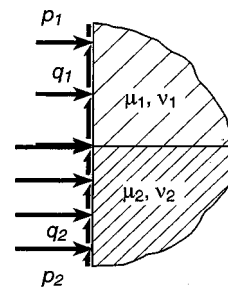


Fig. 8 Butt joint subjected to uniform tractions

Of course there have to be many more instances of pure logarithmic singularities than this for bimaterials. This is apparent from limiting cases. For example, for the kinked crack (Fig. 6a') with stress-free flanks (I-A-I), the limits in (3.6) and (3.7) lead to I-II and I-I, respectively, for a plate of one material. Then Table 5, for I or VI-II, shows there is a log singularity for the first of these limits (the actual vertex angle involved is  $\phi = 101.2^\circ$  when  $\kappa = 2.85$ ). Other configurations with pure logarithmic singularities for limiting cases are: Fig. 6a' with I-A-II, II-A-II, I-B-I, A-A, A-B, A-D, B-B, B-C, B-D, and D-D; Fig. 6b' with I-A-A-I, B-A-A, and I-B-B-I; and Fig. 7a', b, and c with I-A-I and I-B-I.

For *pure logarithmic singularities* with *inhomogeneous boundary conditions*, Bogy [85] provides an example for the butt joint subjected to tractions. Asymptotically at the joint, the configuration is as in Fig. 8 wherein  $p_i$  and  $q_i$  are the constant pressure and uniform shear traction on material  $i$  ( $i = 1, 2$ ). In Bogy [85], a pure log singularity is found to result if

$$\alpha = 0 \text{ or } \alpha = 2\beta \neq \pm 1$$

$$q_1 \neq q_2 \quad (3.20)$$

In addition, a pure log singularity is found to result if

$$\alpha = 2\beta \neq 0$$

$$p_1^2 + p_2^2 \neq 0, \quad p_1(1 + \alpha) \neq p_2(1 - \alpha) \quad (3.21)$$

Complete stress fields corresponding to (3.20) and (3.21) are given in equations (4.6) and (4.7), Bogy [85].

The configurations admitted by (3.21) include ones with continuous tractions across the joint. Here, then, the singularity is associated with the discontinuity in material moduli. Generally this added material discontinuity increases the occurrence of stress singularities over that for a plate made of a single material. However, this does not always have to be so. For the limited cases of  $\alpha = 1$  and  $\beta = \frac{1}{2}$  or  $\alpha = -1$  and  $\beta = -\frac{1}{2}$ , there is no log singularity associated with a step shear. Here, then, the singularity associated with the discontinuity in the applied shear traction is being offset by that associated with the discontinuity in material moduli.

The pure logarithmic singularities associated with (3.20) and (3.21) both occur when  $\lambda=1$  is a repeated root of the eigenvalue equation and (3.16) is indeed satisfied for these instances. So how is this consistent with the conditions in (1.5) for a log singularity with inhomogeneous boundary conditions? For that matter, because any configuration with inhomogeneous boundary conditions can also include the response with corresponding homogeneous boundary conditions, how is it consistent with the conditions of (1.3) for a log singularity with homogeneous boundary conditions?

Answering the second question first, we consider  $\alpha=0$  and  $\alpha=2\beta$  in turn. For  $\alpha=0$ , assembling  $A$  reveals that its rank is seven. Hence the first part of the conditions in (1.3) for a log singularity is actually satisfied. However, assembling associated fields reveals that  $\hat{c}_1, \hat{c}_2,$  and  $\hat{c}_3$  of (1.2) are all zero. Therefore (1.3) has that there is no log singularity for homogeneous boundary conditions when  $\alpha=0$ . For  $\alpha=2\beta$ , the rank of  $A$  drops to six. Then (1.3) requires that, in addition to (3.16) being met,  $\partial^2 D/\partial\lambda^2=0$ . This is not the case for the  $D$  here. Therefore (1.3) has that there is no log singularity for homogeneous boundary conditions when  $\alpha=2\beta$ . Thus there is no pure logarithmic singularity whatsoever for this configuration with homogeneous boundary conditions. The fields given in Bogy [85] in equations (4.6) and (4.7) are consistent with this conclusion.

Answering the first question second, we consider (3.20) and (3.21) in turn. For (3.20), we find that it is an instance of compliance with the second of (1.5). Then since  $r_A$  can equal  $n_A-1$  (for  $\alpha=0$ ), (3.16) can be satisfied too. For (3.21), we find that it is an instance of compliance with the last of (1.5). Then, since  $r_A=n_A-2$ , (3.16) can be satisfied too. The fields given in Bogy [85] are again consistent with these conclusions.

With respect to inhomogeneous boundary conditions, the response of the butt joint is analogous to that of a plate with uniform shear tractions. For this last, as the plate vertex angle varies, regular solutions with  $r^0$  stresses break down. This results in their requiring auxiliary fields for the vertex angle with the breakdown. This in turn leads to a logarithmic stress singularity for this angle. A transition between the two types of solutions can be achieved by suitably supplementing the regular  $r^0$  stresses for inhomogeneous boundary conditions with stresses for corresponding homogeneous boundary conditions. In effect, this is the approach developed in Dempsey [39] and Ting [44]. For the butt joint, the only real difference is that material moduli are varying instead of a vertex angle: Otherwise the same evolution occurs.

Apparently only two further instances of pure logarithmic singularities for bimetals with inhomogeneous boundary conditions are identified in the open literature. These are for the oblique butt joint (Fig. 7a') and may be found in Chen [96]. Of course, there have to be many more instances of log singularities for bimetals with inhomogeneous boundary conditions than the total reported here. Again, this is apparent from limiting cases. For the kinked crack (Fig. 6a') with tractions applied to its flanks (I'-A-I'), the limits in (3.6) and (3.7) lead to I'-II and I'-I, respectively, for a single material plate. Then Table 7 has logarithmic stress singularities for both limiting cases. Other kinked crack configura-

tions with pure log singularities for limiting cases are: I'-IC-I, I'-IC-II, I'-IC-V, II'-IC-II, II'-IC-V, V'-IC-V, where IC denotes interface conditions A, B, C, or D, IC the same set minus C. Similarly, other limiting cases of log singularities can be identified for further geometries in Fig. 6 and Fig. 7.

Finally, for *log-squared singularities with inhomogeneous boundary conditions*, two instances are identified for the oblique butt joint (Fig. 7a') in Chen [96]. Quite a number of other instances can be identified as limiting cases corresponding to (3.6) and (3.7) via Tables 5 and 7 (see the discussion at the end of Section 2.4).

## 4 STRESS SINGULARITIES FOR OUT-OF-PLANE LOADING

### 4.1 Out-of-plane shear of an elastic wedge made of a single material

Here we follow the order of presentation in Section 2 for in-plane loading when we treat out-of-plane shear of single material wedges. Thus we begin by considering a wedge under homogeneous boundary conditions, then we consider inhomogeneous boundary conditions.

The elastic wedge of interest can be framed with cylindrical polar coordinates  $r, \theta,$  and  $z$  with origin  $O$  (Fig. 9). It has indefinite extent in the  $r$  and  $z$  directions while subtending an angle  $\phi$  at its vertex. The only existing displacement entertained is in the  $z$  direction  $u_z$ . This displacement is taken to be independent of  $z$ . Consequently field equations hold on the 2D region  $\mathfrak{R}$  of (2.1). With these geometric preliminaries in place, we can formulate the class of out-of-plane shear problems of initial interest as next.

In general, we seek the out-of-plane shear stresses  $\tau_{rz}$  and  $\tau_{\theta z}$ , and their companion out-of-plane displacement  $u_z$ , as functions of  $r$  and  $\theta$  throughout  $\mathfrak{R}$ , satisfying: the *stress equation of equilibrium* in the absence of body forces,

$$\frac{\partial \tau_{rz}}{\partial r} + \frac{\tau_{rz}}{r} + \frac{1}{r} \frac{\partial \tau_{\theta z}}{\partial \theta} = 0 \tag{4.1}$$

on  $\mathfrak{R}$ ; the *stress-displacement relations* for a linear elastic wedge which is both homogeneous and isotropic,

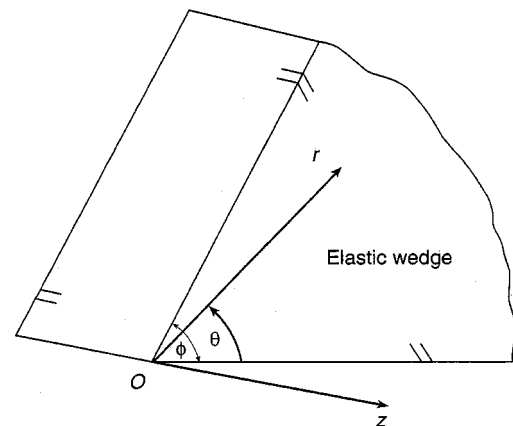


Fig. 9 Geometry and coordinates for the elastic wedge

**Table 9. Boundary conditions for out-of-plane shear**

Identifying Roman numeral	Boundary condition	Physical description
I <sub>s</sub>	$\tau_{\theta z} = 0$	Stress free
II <sub>s</sub>	$u_z = 0$	Clamped
III <sub>s</sub>	$\tau_{\theta z} = k u_z$	Cohesive stress-separation law
I' <sub>s</sub>	$\tau_{\theta z} = q$	Uniform shear
II' <sub>s</sub>	$u_z = r \Delta \phi_s$	Linear displacement

$$\tau_{rz} = \mu \frac{\partial u_z}{\partial r}, \quad \tau_{\theta z} = \frac{\mu}{r} \frac{\partial u_z}{\partial \theta} \tag{4.2}$$

on  $\mathfrak{R}$ , wherein  $\mu$  continues as the shear modulus; any one of the first three admissible *homogeneous boundary conditions* in Table 9 (identified as I<sub>s</sub>, II<sub>s</sub>, and III<sub>s</sub> therein) on the wedge face at  $\theta=0$ , together with another such condition on the wedge face at  $\theta=\phi$ , for  $0 < r < \infty$ ; and the *regularity requirement* at the wedge vertex

$$u_z = O(1) \text{ as } r \rightarrow 0 \tag{4.3}$$

on  $\mathfrak{R}$ . In particular, we are interested in the local behavior of the fields complying with the foregoing in the vicinity of the wedge vertex  $O$ .

Several comments on the preceding are in order. The out-of-plane displacement admitted with its shear stresses is sometimes termed a state of *antiplane shear*. This state is physically representative of the response at cracks and other geometric features under Mode III loading. The displacement  $u_z$  is also physically representative of the *warping* produced when noncircular prismatic bars are subjected to torque. In this role, it complements the  $u_\theta$  displacement component for pure torsion (see, eg, Ch 10, Timoshenko and Goodier [42]).

The homogeneous *boundary conditions* of Table 9 have in-plane counterparts in Table 1 in accordance with: I for I<sub>s</sub>, II for II<sub>s</sub>, and VI for III<sub>s</sub>. It is possible as well to interpret I<sub>s</sub> as the analogue of III, and II<sub>s</sub> as the analogue of IV. If the stiffness  $k$  in III<sub>s</sub> is let to tend to zero, I<sub>s</sub> is recovered, while if it is let to tend to infinity, II<sub>s</sub> is recovered. Otherwise  $k$  is positive on  $\theta=0$ , negative on  $\theta=\phi$ .

As in Section 2.1, there are no *conditions at infinity* or *length scale* present in the formulation. For the reasons advanced in Section 2.1, this is appropriate in an asymptotic treatment. Further, regarding the *regularity requirement* (4.3), we remark that this can be included provided the resulting formulation can be shown to be complete. We consider this completeness issue further once we have corresponding basic fields established. Given completeness, the singular fields admitted by (4.3) have unbounded stresses yet bounded displacements.

Analysis is straightforward and parallels that outlined in Section 1. Indeed, it is simpler than that in Section 1 because the problem at hand is harmonic rather than biharmonic. To see this, substitute (4.2) into (4.1). This shows  $u_z$  to be harmonic. Therefore it admits to separation of variables. This leads to, as our *basic fields for out-of-plane shear*,

$$\begin{aligned} \begin{Bmatrix} \tau_{rz} \\ \tau_{\theta z} \end{Bmatrix} &= \lambda r^{\lambda-1} \begin{Bmatrix} c_1 \\ -c_2 \end{Bmatrix} \sin \lambda \theta + \begin{Bmatrix} c_2 \\ c_1 \end{Bmatrix} \cos \lambda \theta \\ u_z &= \frac{r^\lambda}{\mu} (c_1 \sin \lambda \theta + c_2 \cos \lambda \theta) \end{aligned} \tag{4.4}$$

We are now in a position to discuss further the completeness of fields complying with (4.3). *Given* that  $u_z$  does indeed admit to representation by combinations of functions which are separable in  $r$  and  $\theta$ , the completeness of such functions complying with (4.3) can be argued as follows. At the outset we draw on Sturm-Liouville theory to establish the completeness of the fields in (4.4) for *homogeneous* boundary conditions when  $\lambda$  is real.<sup>20</sup> Then we observe that  $\tau_{rz}$  or  $u_z$  can equally well be represented on a circular arc by series from (4.4) with either  $\lambda$  never negative or  $\lambda$  never positive. As a result, we must have a complete representation just for  $\lambda$  never negative. Hence we must have a complete representation with bounded displacements, provided these displacements are separable.

*Eigenvalue equations* are obtained on introducing the fields of (4.4) into pairs of homogeneous boundary conditions drawn from Table 9. This leads to, for *nonmixed problems* (I<sub>s</sub> or III<sub>s</sub>-I<sub>s</sub> or III<sub>s</sub>, II<sub>s</sub>-II<sub>s</sub>),

$$\sin \lambda \phi = 0 \tag{4.5}$$

and for *mixed problems* (I<sub>s</sub> or III<sub>s</sub>-II<sub>s</sub>),

$$\cos \lambda \phi = 0 \tag{4.6}$$

Equation (4.5) for I<sub>s</sub>-I<sub>s</sub> has an associated torsion problem which is analyzed in Saint-Venant [98]. This problem is antisymmetric about the wedge bisector so that only the antisymmetric contribution to (4.5) is involved (viz,  $\cos \lambda \phi / 2 = 0$ ). However, this is the part of (4.5) which leads to singular eigenvalues. Moreover, given that the torsion problem I<sub>s</sub>-I<sub>s</sub> can be solved via the warping displacement (Neumann problem) or via a stress function (Poisson's equation with Dirichlet conditions), this equation also holds for II<sub>s</sub>-II<sub>s</sub>. Equation (4.6) for I<sub>s</sub>-II<sub>s</sub> can also be viewed as for a torsion problem if a vertex angle of  $2\phi$  is taken. Equation (4.6) for I<sub>s</sub>-II<sub>s</sub> is explicitly obtained as a limiting case for a bimaterial wedge in Aksentian [90]. The equivalence of III<sub>s</sub> with I<sub>s</sub> as far as both eigenvalue equations are concerned is argued in Sinclair [99].

In accordance with (4.3), the range of eigenvalues for admissible power singularities of the form of (4.4) is as previously (ie,  $0 < \lambda < 1$ ). Such singular eigenvalues can be determined in closed form for the elementary transcendental equations represented by (4.5) and (4.6). Reintroducing the singularity exponent  $\gamma = 1 - \lambda$ , we thus have the following admissible power singularities: for nonmixed problems,

$$\gamma = 1 - \frac{\pi}{\phi} \quad (\pi < \phi \leq 2\pi) \tag{4.7}$$

and for mixed problems,

$$\gamma = 1 - \frac{\pi}{2\phi} \quad \left( \frac{\pi}{2} < \phi \leq 2\pi \right)$$

<sup>20</sup>See, eg, Ch V, Courant and Hilbert [97].

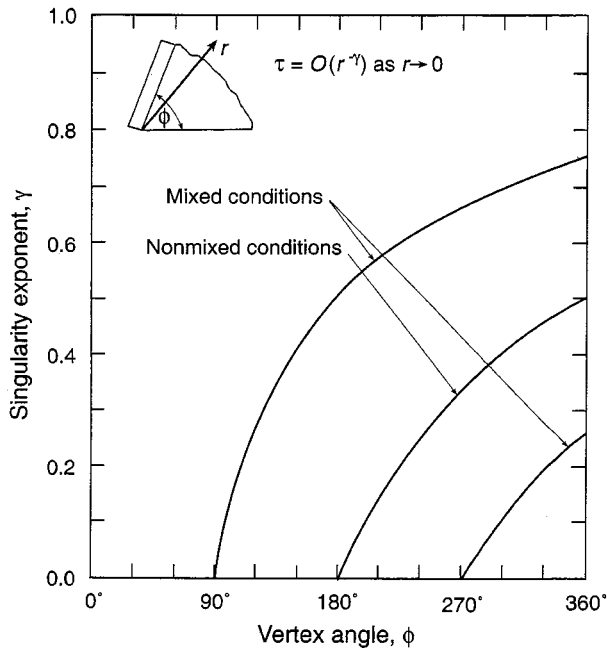


Fig. 10 Singularity exponents in out-of-plane shear for varying wedge angles

$$\gamma = 1 - \frac{3\pi}{2\phi} \left( \frac{3\pi}{2} < \phi \leq 2\pi \right) \tag{4.8}$$

The singularity exponents of (4.7) and (4.8) are plotted in Fig. 10 wherein  $\tau$  denotes either shear.

For nonmixed problems, stress singularities are only associated with reentrant corners. For prismatic bars under torsion, this is recognized in Section 710, Thomson and Tait [100], and in Saint-Venant [101]. For  $\phi = 360^\circ$  with free-free conditions, the nonmixed curve of Fig. 10 recovers the inverse-square-root singularity of a traditional stress-free crack under Mode III loading. The associated eigenfunction is given in Irwin and Kies [102]. For  $\phi = 270^\circ$ , the nonmixed curve produces the singularity as for a keyway in a shaft transmitting torque. For other vertex angles, the curve for nonmixed problems in Fig. 10 is similar in character to the upper curves in Fig. 2a which are for corresponding nonmixed problems with in-plane loading.

For mixed problems, a broader range of vertex angles leads to stress singularities (Fig. 10). This is similar to the corresponding situation with in-plane loading (Fig. 2a cf 2d). Furthermore, the general character of the mixed curves with out-of-plane shear (Fig. 10) is quite similar to those for  $\gamma = 2$  with in-plane loading (Fig. 2d).

In light of the preceding discussion regarding completeness, it would seem to be unlikely for there to be anything other than real power singularities for out-of-plane shear of a wedge under homogeneous boundary conditions. This expectation is in fact met by the eigenvalue equations (4.5) and (4.6). Separating real and imaginary parts in these equations reveals that there are no complex eigenvalues. In addition, differentiating these equations with respect to  $\lambda$  reveals there

Table 10. Single material configurations in out-of-plane shear with logarithmic singularities

Boundary conditions on $\theta=0, \phi$	Configuration specifications
$I'_s$ or $III_s - I_s$	$\phi = \pi, 2\pi, q \neq 0$
$II'_s - II_s$	$\phi = \pi, 2\pi, \Delta\phi_s \neq 0$
$III_s - III_s$	$\phi = 2\pi$
$I'_s$ or $III_s - II'_s$	$\phi = \pi/2, 3\pi/2, q \neq 0, \Delta\phi_s \neq 0$

are no repeated roots. Hence (1.3) (with  $n_A = 2$  therein) has that there are no singularities other than those of Fig. 10 with homogeneous boundary conditions.

This need not be the case for *inhomogeneous boundary conditions*. For uniform tractions/linear displacements, logarithmic stress singularities are possible.<sup>21</sup> The specific inhomogeneous boundary conditions considered to this end are included in Table 9, distinguished by primes. Herein  $q$  continues as a constant shear traction for  $I'_s$ , while  $\Delta\phi_s$  is the out-of-plane angle rotated through by  $II'_s$ . For these conditions, use of the basic fields of (4.4) leads to systems which, in general, cannot be solved when  $\lambda = 1$  is an eigenvalue. Thus we need auxiliary fields. These follow from (4.4) on differentiating with respect to  $\lambda$ . For the stress component  $\tau_{rz}$  this leads to, as an example of our *auxiliary fields for out-of-plane shear*,

$$\tau_{rz} = r^{\lambda-1} [(1 + \lambda \ln r)(\hat{c}_1 \sin \lambda \theta + \hat{c}_2 \cos \lambda \theta) + \lambda \theta (\hat{c}_1 \cos \lambda \theta - \hat{c}_2 \sin \lambda \theta)] \tag{4.9}$$

In (4.9), carets atop constants continue to indicate they do not have to be the same as in (4.4). Using the full fields associated with (4.9), in conjunction with those of (4.4), then enables solution. Hence a log singularity for  $\lambda = 1$  (see (4.9)). This occurs when the last of (1.5) holds for  $n_A = 2$ . Now, though, the conditions on the constants within auxiliary fields can be dispensed with. This is because a logarithmic stress singularity attends any nontrivial  $c$  in the auxiliary fields for out-of-plane shear (see (4.9)). Configurations that do comply with the foregoing requirements and thereby do have log singularities are given in Table 10.<sup>22</sup>

In Table 10, the logarithmic stress singularity on a half-plane with  $I'_s - I_s$  or  $II'_s - II$  can be anticipated from the asymptotic analysis in Wasow [103]. For  $I'_s - I_s$  and both  $\phi = \pi$  and  $\phi = 2\pi$ , these log singularities are fully developed in Ting [104], together with a reasonable transition for varying vertex angles through  $\pi$  and  $2\pi$  effected by means of the approach of Ting [44]. For other configurations in Table 10, a similar analysis may be found in Sinclair [105]. For the most part,  $III_s$  is equivalent to  $I'_s$  in Table 10 because it can produce a uniform shear in response to a rigid body transla-

<sup>21</sup>As in Section 2.4, it is possible for nonsingular inhomogeneous displacements to produce other than logarithmic singularities, eg,  $u_z \propto \sqrt{r}$ . Further, if these singularities coincide with ones for corresponding homogeneous boundary conditions, they could possibly be logarithmically intensified.

<sup>22</sup>The full fields for Eq. (4.9) do give rise to a logarithmic displacement field associated with homogeneous boundary conditions. This occurs for  $\lambda = 0, c_1 = 0$ , and  $c_2 = F/\phi$  and is for a line-load of strength  $F$  in out-of-plane shear. The corresponding  $\tau_{\theta z}$  is zero, so that stress-free conditions are obeyed by this stress field for any vertex angle  $\phi$ . However, the associated logarithmic displacement field is not in compliance with (4.3), so that our original statement concerning the absence of logarithmic terms with homogeneous boundary conditions still holds.

**Table 11. Interface conditions for out-of-plane shear**

Identifying letter	Matched quantities	Additional conditions	Physical description
$A_s$	$\tau_{\theta z}, u_z$		Perfectly bonded
$B_s$	$\tau_{\theta z}$	$\tau_{\theta z}=0$	Frictionless contact
$D_s$	$u_z$	$u_z=0$	Thin rigid inclusion
$E_s$	$\tau_{\theta z}$	$\tau_{\theta z}=k(u_z^+ - u_z^-)$	Adhesive stress-separation law

tion. Under these circumstances, the requirements placed on  $q$  for  $I'_s$  apply to the uniform shear within  $III_s$ .

## 4.2 Out-of-plane shear of an elastic wedge made of multiple materials

In this section we consider extension of the treatment in the preceding section to wedges made of multiple materials. We first formulate this extended class of problems. Thereafter we review contributions to the literature which identify attendant stress singularities under homogeneous boundary conditions. We then discuss the further singularities possible with inhomogeneous boundary conditions.

To begin, we continue to use cylindrical polar coordinates,  $r$ ,  $\theta$ , and  $z$  with origin  $O$  to describe the entire wedge of interest with its complete vertex angle  $\phi$ . Now, though, the wedge is comprised of  $N$  prismatic subwedges with vertex angles  $\phi_i$ ,  $i=1,2,\dots,N$ . Each of these subwedges is of indefinite extent in both the  $r$  and  $z$  directions. We also continue to entertain displacement in the  $z$  direction alone, with this displacement being independent of  $z$ . Consequently, field equations hold on the 2D region  $\mathfrak{R}$  of (3.1) (Fig. 4). With these geometric preliminaries in place, we can formulate the class of out-of-plane shear problems of initial interest as next.

In general, we seek the out-of-plane shear stresses  $\tau_{rz}$  and  $\tau_{\theta z}$  and their companion out-of-plane displacement  $u_z$  as functions of  $r$  and  $\theta$  throughout  $\mathfrak{R}$ , satisfying: the appropriate *field equations* of elasticity; *interface conditions* on internal wedge faces; *boundary conditions* on external faces if the wedge is open ( $\phi < 2\pi$ ), or further interface conditions if it is closed ( $\phi = 2\pi$ ); and a *regularity requirement* at the wedge vertex. The field equations hold on  $\mathfrak{R}_i$  of (3.2),  $i=1,2,\dots,N$ , and are given by (4.1) and (4.2), with  $\mu$  in the latter being replaced by  $\mu_i$ , the shear modulus of the material comprising  $\mathfrak{R}_i$ . The admissible interface conditions are listed in Table 11 and hold on  $\theta = \theta_i$  of (3.2), with  $i=1,2,\dots,N-1$  if the wedge is open,  $i=0,1,\dots,N$  if the wedge is closed ( $i=0$  and  $N$  are for but one set of interface conditions). The admissible boundary conditions continue to be as in Table 9 and hold on  $\theta=0, \phi$  if the wedge is open. And the regularity requirement is the same as (4.3), but now holds on  $\mathfrak{R}_i$ ,  $i=1,2,\dots,N$ .

The interface conditions of Table 11 have in-plane counterparts in Table 8 as follows: A for  $A_s$ ,  $B_0$  for  $B_s$ , D for  $D_s$ , and E for  $E_s$ . There is no counterpart to Conditions C of Table 8 in out-of-plane shear. In Conditions  $E_s$ ,  $k$  is the stiffness in the adhesive stress-separation law and  $u_z^+$  and  $u_z^-$  are defined analogously to  $u_\theta^+$  of (3.3). In reality, Conditions  $A_s$  for perfect bonding are just a simplification of Conditions  $E_s$  obtained on letting  $k$  tend to infinity.

As in Section 4.1, the preceding formulation is absent conditions at infinity and insists on bounded displacements. The basic reasons for these two aspects remain the same. The limited completeness argument advanced in Section 4.1 can be extended to composite configurations with interface conditions  $A_s$ ,  $B_s$ , or  $D_s$ : for these conditions, composite configurations are merely equivalent to multiple regular Sturm-Liouville problems.

Conditions  $A_s$  have received by far the most attention in the literature. Accordingly, we focus attention on these traditional conditions for a perfectly bonded interface next. We comment briefly on the nature of results for other interface conditions at the end of the section.

We begin our review of perfectly bonded wedges made of multiple materials by considering *bimaterials*. Analysis for this class of composite wedge is straightforward and compact. This is because the order of the coefficient matrices involved is only four (cf 8 for most in-plane bimaterials), and eigenvalue equations depend on a single material parameter. Here

$$\bar{\mu} = \mu_1 / \mu_2 \quad (4.10)$$

serves as this single material constant.

*Eigenvalue equations* for bimaterial wedges in out-of-plane shear are available in the literature as follows. For the open bimaterial wedge and Conditions  $I_s - A_s - I_s$ ,  $\Pi_s - A_s - \Pi_s$ , and  $I_s - A_s - \Pi_s$  eigenvalue equations are obtained in Aksentian [90]. The first two of these equations are confirmed both in Rao [48] and in Sinclair [99]. The last eigenvalue equation for  $I_s - A_s - \Pi_s$  is confirmed both in Sinclair [99] and in Ma and Hour [106]. For a crack terminating at an interface (Fig. 6b') and Conditions  $I_s - A_s - A_s - I_s$ , an eigenvalue equation is given in Fenner [80]. For the closed bimaterial wedge and Conditions  $A_s - A_s$ , an eigenvalue equation is given in Sinclair [99]. This eigenvalue equation is confirmed in Pageau *et al* [73].

*Eigenvalues* for the dominant power singularity for  $I_s - A_s - I_s$  are given in a compact graphical form in Rao [48] for any values of  $\phi_1$  and  $\phi_2$ , but for a somewhat limited range of  $\bar{\mu}$ . Eigenvalues for a more extensive range of  $\bar{\mu}$  but limited values of  $\phi_1$  and  $\phi_2$  are given in Sinclair [99]: The  $\phi_1$  and  $\phi_2$  treated therein correspond to the geometries in Fig. 6a, a', and Fig. 7. Secondary power singularities are also given in Sinclair [99].

There is a certain duality between  $I_s - A_s - I_s$  and  $\Pi_s - A_s - \Pi_s$  which enables singular eigenvalues for the latter to be directly obtained from eigenvalues for the former. Specifically this is done by entering graphs of eigenvalues for  $I_s - A_s - I_s$  with the true  $\bar{\mu}$  replaced by  $1/\bar{\mu}$  (see Sinclair [99] for further explanation). For both types of configuration, the discontinuity of an abrupt change in shear modulus attending Conditions  $A_s$  means it is no longer necessary to have a reentrant corner for singular stresses to be possible.

Singular eigenvalues for  $I_s - A_s - \Pi_s$  and geometries as in Fig. 6a, a', and Fig. 7 are given in Sinclair [99]. Some further eigenvalues for  $I_s - A_s - \Pi_s$  are provided in Ma and

**Table 12. Bimaterial configurations in out-of-plane shear with logarithmic singularities**

Boundary conditions on $\theta=0, \phi$	Configuration specifications
$I'_s$ or $III_s-I'_s$ or $III_s$	$\phi_1 = \phi_2 = \pi, q_1 \neq q_2$ $\phi_1 = \phi_2 = \pi/2, q_1 \neq -\bar{\mu}q_2$ $\phi_1 = \pi/2, \phi_2 = 3\pi/2, q_1 \neq \bar{\mu}q_2$
$II'_s-II'_s$	$\bar{\mu} = -\cot \phi_1 \tan \phi_2, q_1 \cos \phi_2 \neq q_2 \cos \phi_1$ $\phi_1 = \phi_2 = \pi, \Delta \phi_1 \neq \Delta \phi_2$ $\phi_1 = \phi_2 = \pi/2, \mu_1 \Delta \phi_1 \neq -\mu_2 \Delta \phi_2$ $\phi_1 = \pi/2, \phi_2 = 3\pi/2, \mu_1 \Delta \phi_1 \neq \mu_2 \Delta \phi_2$ $\bar{\mu} = -\tan \phi_1 \cot \phi_2, \bar{\mu} \Delta \phi_1 \sin \phi_2 \neq -\Delta \phi_2 \sin \phi_1$
$I'_s$ or $III_s-II'_s$	$\phi_1 = \pi, \phi_2 = \pi/2, q_1 \neq \mu_2 \Delta \phi_2$ $\phi_1 = \pi/2, \phi_2 = \pi, q_1 \neq \mu_1 \Delta \phi_2$ $\bar{\mu} = \cot \phi_1 \cot \phi_2, q_1 \sin \phi_2 \neq -\mu_2 \Delta \phi_2 \cos \phi_1$

Hour [106], which also furnishes associated eigenfunctions for all three types of configuration  $I_s-A_s-I_s$ ,  $II_s-A_s-II_s$ , and  $I_s-A_s-II_s$ .

Singular eigenvalues for the crack terminating at an interface with  $I_s-A_s-A_s-I_s$  are given in Fenner [80] for a wide range of  $\bar{\mu}$  and all angles of incidence.

Singular eigenvalues for  $A_s-A_s$  are given in Sinclair [99]. Some further eigenvalues for  $A_s-A_s$  are provided in Pageau et al [73], together with the associated eigenfunction.

In view of the discussion of completeness, it would seem to be unlikely for there to be anything other than real power singularities for out-of-plane shear of a bimaterial wedge under homogeneous boundary conditions. That this is the case is confirmed in Sinclair [99]. Further, there is no logarithmic participation under homogeneous boundary conditions  $I_s$  and  $II_s$  (ibid).

Again, this absence of other singularities need not be the case for *inhomogeneous boundary conditions*. For the uniform traction/linear displacement conditions of Table 9, logarithmic stress singularities are possible. Following basically the same steps as in Section 4.1, Sinclair [107] identifies instances of such log singularities. These we present in Table 12.

In Table 12 it is understood that  $\phi_1$  and  $\phi_2$  are required to be such that positive shear moduli are involved with

$$0 < \bar{\mu} < \infty \tag{4.11}$$

Further in Table 12,  $q_1$  is  $q$  and  $\Delta \phi_1$  is  $\Delta \phi_s$  on  $\mathfrak{R}_1$ , while  $q_2$  is  $q$  and  $\Delta \phi_2$  is  $\Delta \phi_s$  on  $\mathfrak{R}_2$ . As previously, Conditions  $III_s$

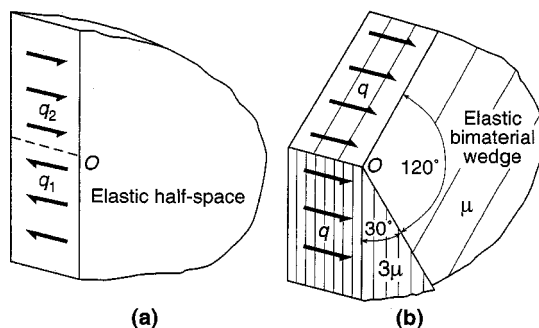


Fig. 11 Examples of wedges with logarithmic stress singularities: a) half-space with discontinuous shear traction, b) bimaterial wedge with continuous shear traction

can act like  $I'_s$  by virtue of uniform shears being induced in response to a rigid body translation. In this role, restrictions on  $q_1$  and  $q_2$  in Table 12 then apply to the uniform shears so induced.

By way of examples of the logarithmic stress singularities of Table 12, Fig. 11 illustrates  $I'_s-A_s-I'_s$  for a half-space and for a bimaterial wedge with vertex angles of  $30^\circ$  and  $120^\circ$ . For the first (Fig. 11a), Table 12 has  $\bar{\mu}=1$  and  $q_1 \neq -q_2$  when  $\phi_1 + \phi_2 = \pi$ . Hence there is no material discontinuity. Here, then, the discontinuity in the shear traction by itself has an associated log singularity (this is the configuration analyzed in Ting [104]). For the second (Fig. 11b), Table 12 has  $\bar{\mu}=3$  and  $q_1 \neq -\sqrt{3}'q_2$  when  $\phi_1=30^\circ$  and  $\phi_2=120^\circ$ . Hence we can take  $q_1=-q$  and  $q_2=q$  so that there is no discontinuity in the shear traction. Here, then, the discontinuity in material moduli by itself has an associated log singularity. Notice, too, that there need not be a reentrant corner present for a log singularity with either of these discontinuities.

There are a few analyses of *trimaterial wedges* in out-of-plane shear available in the literature. The simplest degenerate trimaterial treated is a stress-free crack in one material terminating normal to an interface with a second material ( $I_s-A_s-A_s-I_s$  and a cross section as in Fig. 6b). Singular eigenvalues are determined in closed form in Barnett [108]. These eigenvalues are confirmed in Fenner [80]. When the crack is other than perpendicular to the interface ( $I_s-A_s-A_s-I_s$  and Fig. 6b'), the eigenvalue equation for this degenerate trimaterial is given in Sendekyj [109]. This equation is confirmed in Fenner [80] which also furnishes some singular eigenvalues. True trimaterial wedges with cross sections as in Fig. 6b and either stress-free crack flanks ( $I_s-A_s-A_s-I_s$ ) or bonded ones ( $A_s-A_s-A_s$ ) are analyzed in Pageau et al [110]. This reference provides eigenvalue equations, singular eigenvalues, and accompanying eigenfunctions. A further true trimaterial wedge with each constituent single-material wedge having a vertex angle of  $90^\circ$  and with outside stress-free faces ( $I_s-A_s-A_s-I_s$ ) is analyzed in Keer and Freeman [111]. This reference provides the eigenvalue equation.

In closing, we comment on the other interface conditions in Table 11. We observe that Conditions  $B_s$  and  $D_s$  act like the boundary conditions  $I_s$  and  $II_s$  of Table 9. Consequently, bimaterials with these interface conditions simply have the same singular character as two single-material wedges. For Conditions  $E_s$ , some reduction in singular stresses over that for  $A_s$  is to be expected. This is indicated via limiting cases with single-material wedges. However, this is yet to be formally established in general.

### 4.3 Out-of-plane bending: Classical theory

Here we consider the singularities that can occur in the out-of-plane bending of an elastic plate when treated within classical fourth-order theory. We follow the same order of presentation as previously. Thus we first treat plates made of a single material under homogeneous boundary conditions, then inhomogeneous conditions, then plates made of multiple materials under these two types of conditions in turn.

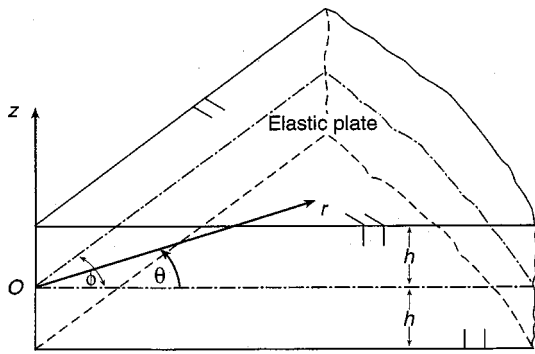


Fig. 12 Geometry and coordinates for the angular elastic plate in bending

The angular elastic plate to be bent can be framed with cylindrical polar coordinates  $r, \theta$ , and  $z$  with origin  $O$  at the vertex of the mid-plane of the plate (Fig. 12). It has indefinite extent in the  $r$  direction, thickness  $2h$  in the  $z$  direction, and subtends an angle  $\phi$  at its vertex. The displacement of primary concern is that in the  $z$  direction  $u_z$ . This displacement has associated moment resultants  $M_r, M_\theta$ , and  $M_{r\theta}$  shown acting in a positive sense in Fig. 13a, and shear resultants  $Q_r$  and  $Q_\theta$  shown likewise in Fig. 13b. All of these field quantities are taken to be independent of  $z$ . Consequently, field equations hold on the 2D region  $\mathfrak{R}$  of (2.1) and (3.1) for single-material and multiple-material plates, respectively. With these preliminaries in place, we can formulate the out-of-plane bending problems of initial interest as next.

In general, we seek the out-of-plane displacement  $u_z$ , and its associated resultants  $M_r, M_\theta, M_{r\theta}, Q_r$ , and  $Q_\theta$ , as functions of  $r$  and  $\theta$  throughout  $\mathfrak{R}$  of (2.1), satisfying: the *equations of equilibrium* in the absence of body forces and loading on the plate faces at  $z = \pm h$ ,

$$\begin{aligned} \frac{\partial}{\partial r}(rQ_r) + \frac{\partial Q_\theta}{\partial \theta} &= 0 \\ \frac{\partial M_r}{\partial r} - \frac{1}{r} \frac{\partial M_{r\theta}}{\partial \theta} + \frac{M_r - M_\theta}{r} - Q_r &= 0 \\ \frac{1}{r} \frac{\partial M_\theta}{\partial \theta} - \frac{\partial M_{r\theta}}{\partial r} - \frac{2M_{r\theta}}{r} - Q_\theta &= 0 \end{aligned} \tag{4.12}$$

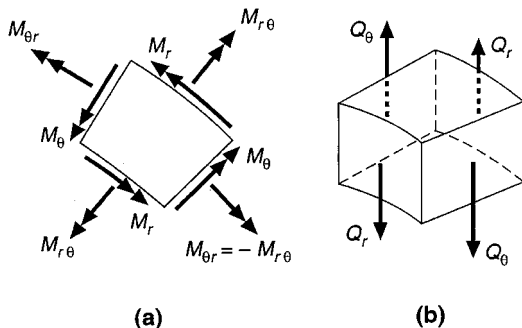


Fig. 13 Stress resultants on plate elements: a) positive moment resultants (element viewed from  $z = h$  face), b) positive shear resultants

Table 13. Boundary conditions for out-of-plane bending with classical theory

Identifying Roman numeral	Boundary conditions	Physical description
$I_b$	$M_\theta = 0, Q_\theta - \frac{\partial M_{r\theta}}{\partial r} = 0$	Stress free
$II_b$	$u_z = 0, \frac{\partial u_z}{\partial \theta} = 0$	Clamped
$III_b$	$\frac{\partial u_z}{\partial \theta} = 0, Q_\theta = 0$	Symmetry
$IV_b$	$u_z = 0, M_\theta = 0$	Simply supported
$V_b$	$M_\theta = k_r \frac{\partial^2}{\partial r^2} \left( \frac{1}{r} \frac{\partial u_z}{\partial \theta} \right),$ $Q_\theta - \frac{\partial M_{r\theta}}{\partial r} = k_b \frac{\partial^3 u_z}{\partial r^3}$	Elastically restrained
$I'_b$	$M_\theta = M_0 + M'_0 r,$ $Q_\theta - \frac{\partial M_{r\theta}}{\partial r} = V_0$	Applied moment/shear
$II'_b$	$u_z = u_0 r^3, \frac{\partial u_z}{\partial \theta} = u'_0 r^3$	Applied displacement/rotation
$IV'_b$	$M_\theta = \hat{M}_0 + \hat{M}'_0 r, u_z = \hat{u}_0 r^3$	Applied moment/displacement

on  $\mathfrak{R}$ ; the *resultant-displacement relations* for a linear elastic plate which is both homogeneous and isotropic,

$$\begin{aligned} \begin{Bmatrix} M_r \\ M_\theta \end{Bmatrix} &= -\mu_b \begin{Bmatrix} \nu \\ 1 \end{Bmatrix} \nabla^2 u_z \begin{Bmatrix} + \\ - \end{Bmatrix} (1-\nu) \frac{\partial^2 u_z}{\partial r^2} \\ M_{r\theta} &= \mu_b (1-\nu) \frac{\partial}{\partial r} \left( \frac{1}{r} \frac{\partial u_z}{\partial \theta} \right) \\ \begin{Bmatrix} Q_r \\ Q_\theta \end{Bmatrix} &= -\mu_b \begin{Bmatrix} \frac{\partial}{\partial r} \\ \frac{1}{r} \frac{\partial}{\partial \theta} \end{Bmatrix} (\nabla^2 u_z) \end{aligned} \tag{4.13}$$

on  $\mathfrak{R}$ , wherein  $\mu_b = 4\mu h^3/3(1-\nu)$  is the flexural rigidity and  $\nabla^2$  the Laplacian operator in  $r$  and  $\theta$  coordinates; any one of the first five sets of admissible *boundary conditions* in Table 13 (identified as  $I_b - V_b$  therein) on the plate edge at  $\theta = 0$ , together with another such set on the edge at  $\theta = \phi$  or the bisector at  $\theta = \phi/2$  as appropriate, for  $0 < r < \infty$ ; and the *regularity requirement* at the plate vertex,

$$u_z = O(r) \text{ as } r \rightarrow 0 \tag{4.14}$$

on  $\mathfrak{R}$ . In particular, we are interested in the local behavior of the fields complying with the foregoing in the vicinity of the plate vertex,  $O$ .

Several comments on the preceding formulation are in order. When the plate has *lateral loading* on a *face*, the right-hand side of the first of (4.12) is no longer zero. Provided this lateral loading is continuous or, if singular, has integrable singularities, it in itself does not produce singularities in any of the resultants.

The resultants are related to the *stresses* in the plate by

$$\begin{Bmatrix} M_r \\ M_\theta \\ M_{r\theta} \end{Bmatrix} = \int_{-h}^h \begin{Bmatrix} \sigma_r \\ \sigma_\theta \\ -\tau_{r\theta} \end{Bmatrix} z dz, \quad \begin{Bmatrix} Q_r \\ Q_\theta \end{Bmatrix} = \int_{-h}^h \begin{Bmatrix} \tau_{rz} \\ \tau_{\theta z} \end{Bmatrix} dz \tag{4.15}$$

These relations are consistent with the sign conventions shown in Fig. 13. Assuming  $\sigma_r$ ,  $\sigma_\theta$ , and  $\tau_{r\theta}$  to be linear in  $z$ , it is possible to invert the first of (4.15). Likewise, assuming  $\tau_{rz}$  and  $\tau_{\theta z}$  to be parabolic in  $z$  and zero at  $z = \pm h$ , it is possible to invert the second of (4.15). It follows that any singularity in the moment resultants  $M_r$ ,  $M_\theta$ , and  $M_{r\theta}$  gives rise to the same singularity in the stresses  $\sigma_r$ ,  $\sigma_\theta$ , and  $\tau_{r\theta}$ , respectively, while any singularity in the shear resultants  $Q_r$  and  $Q_\theta$  gives rise to the same singularity in the shear stresses  $\tau_{rz}$  and  $\tau_{\theta z}$ , respectively.

Turning to the boundary conditions of Table 13, the historical introduction in Love [112] credits Kirchhoff [113] as being first to advance Conditions  $I_b$  for a free edge. While it would be physically natural to insist that all three resultants be zero on a free edge, the fourth-order classical theory can only admit two conditions per edge. Conditions  $I_b$  are the two that arise out of a variational development of the theory. Conditions  $II_b$  are the counterparts of built-in end conditions in beam theory. Conditions  $I_b$  and  $II_b$ , respectively, are physically closest to Conditions I and II of Table 1 for in-plane loading.

As previously, when the same conditions apply on both plate edges it is advantageous to distinguish between symmetric and antisymmetric response. Symmetric response about the plate bisector implies that  $u_z$  is an even function of  $\theta$  about  $\theta = \phi/2$ . Conditions  $III_b$  ensure that this is so. Conditions  $IV_b$  physically correspond to a simply supported or hinged edge: If applied on the plate bisector, however, they take on the role of antisymmetry conditions by ensuring  $u_z$  is an odd function of  $\theta$  about  $\theta = \phi/2$ .

Conditions  $V_b$  are for a plate attached to an elastic bar in torsion and bending. Hence  $k_t$  is the bar's torsional stiffness,  $k_b$  its bending stiffness. With the present resultants,  $k_t$  is positive on a positive  $\theta$  edge and vice versa, while  $k_b$  is negative on a positive  $\theta$  edge and vice versa. These conditions are physically closest to Conditions VI of Table 1 for in-plane loading.<sup>23</sup>

As earlier, there are no *conditions at infinity* or in-plane *length scale* present in the formulation. For the reasons advanced in Section 2.1, this is appropriate in an asymptotic treatment. Further, regarding the *regularity requirement* (4.14), we remark that this can be included provided the resulting formulation can be shown to be complete. Given the analogy between the extensional case and bending set out subsequently in this section, completeness would seem likely, although it is not formally established. Given completeness, the singular fields admitted by (4.14) have bounded displacements.

Analysis proceeds on using the second and third of (4.12) to eliminate  $Q_r$  and  $Q_\theta$  from the first, then substituting for the moment resultants from (4.13). This establishes that  $u_z$  is

biharmonic. Hence we can simply use the biharmonic Airy stress function used to generate (1.1) (from Williams [2]) as the displacement in bending (as in Williams [115]). Thus we obtain, as our *basic displacement solution for classical bending theory*,

$$u_z = r^{\lambda+1} \Lambda(\lambda, \theta) \tag{4.16}$$

$$\Lambda(\lambda, \theta) = c_1 \cos(\lambda + 1)\theta + c_2 \sin(\lambda + 1)\theta + c_3 \cos(\lambda - 1)\theta + c_4 \sin(\lambda - 1)\theta$$

where  $c_i (i=1-4)$  continue as constants. Stress resultants follow from (4.13). Now we can apply the homogeneous boundary conditions of Table 13. These boundary conditions then turn out to have mathematically analogous conditions in Table 1 for in-plane extension. This enables us here simply to use the eigenvalue equations for in-plane extension given in Section 2.1 for out-of-plane bending with classical theory.

To explain the *mathematical analogy* further, the simplest bending boundary conditions to consider are for a clamped or built-in edge. Applying Conditions  $II_b$  of Table 13 on  $\theta = \phi$  to  $u_z$  of (4.16) implies

$$\Lambda = 0, \quad \frac{\partial \Lambda}{\partial \theta} = 0, \quad \text{at } \theta = \phi \tag{4.17}$$

These requirements on  $\Lambda$  are the same as would result from a stress-free edge for a plate in extension (see (1.1) on replacing  $(\lambda + 1)c_3$  and  $(\lambda + 1)c_4$  therein with  $c_3$  and  $c_4$ ). It follows that clamped conditions under bending are mathematically analogous to stress-free conditions in extension as far as eigenvalue equations are concerned.

Similarly, other mathematical analogies can be developed. For example, a free edge under bending is analogous to a clamped edge with extension. This last analogy only holds, however, when  $\kappa$  in extension conditions is replaced by  $\kappa_b = (3 + \nu)/(1 - \nu)$ . All told, the following mathematical analogies hold between the bending boundary conditions of Table 13 and the extensional boundary conditions of Table 1:

$$I_b \rightarrow II(\lambda - 1) \text{ with } \kappa \rightarrow \kappa_b, \quad II_b \text{ or } V_b \rightarrow I \tag{4.18}$$

$$III_b \rightarrow III, \quad IV_b \rightarrow IV$$

Without the  $(\lambda - 1)$  factor, the first of (4.18) is developed in a general context in Southwell [116], which also observes that the second for  $II_b$  was well known circa 1950. The factor  $(\lambda - 1)$  is not significant when considering power singularities, but could play a role in identifying log singularities when  $\lambda = 1$ . The analogy for  $III_b$  follows directly from comparing conditions as done for (4.17), while the analogy for  $IV_b$  is noted in Rao [48]. The equivalence of  $V_b$  and  $II_b$  follows from an adaptation of the argument in Sinclair [99] for boundary conditions which have terms with a different  $r$ -dependence within a single condition. While the equivalence of elastically restrained conditions with built in holds for any  $\lambda$ , similar arguments show elastically restrained conditions to be equivalent to stress-free conditions for the special case of  $\lambda = 1$ , and to symmetry conditions for the special

<sup>23</sup>A development of the conditions for an elastically restrained plate in rectangular coordinates may be found in Art 22, Timoshenko and Woinowsky-Krieger [114].

case of  $\lambda=2$ . This last can lead to log singularities with elastically restrained conditions, something we investigate subsequently.

From (4.18), then, we have the following eigenvalue equations for general  $\lambda$ , and free ( $I_b$ ), built-in ( $\Pi_b$ ), simply supported ( $IV_b$ ), and elastically restrained ( $V_b$ ) conditions, directly from Tables 2–4 of Section 2.1:

$I_b-I_b$	(2.10) $(\lambda-1)$ with $\kappa \rightarrow \kappa_b$ for symmetric response	(4.19)
	(2.14) $(\lambda-1)$ with $\kappa \rightarrow \kappa_b$ for antisymmetric response	
$\Pi_b$ or $V_b-\Pi_b$ or $V_b$	(2.9) for symmetric response	
	(2.13) for antisymmetric response	
$I_b-\Pi_b$ or $V_b$	(2.17) $(\lambda-1)$ with $\kappa \rightarrow \kappa_b$	
$I_b-IV_b$	(2.14) $(\lambda-1)$ with $\kappa \rightarrow \kappa_b, \phi \rightarrow 2\phi$	
$\Pi_b$ or $V_b-IV_b$	(2.13) with $\phi \rightarrow 2\phi$	

For simply supported conditions on both plate edges, the corresponding eigenvalue is merely indicated at the end of Section 2.1. This is because the corresponding extensional configuration is not that physically significant and consequently has received little attention. Here, with bending, it is physically important, so we give its symmetric and antisymmetric equations explicitly:

$$IV_b-IV_b \quad \cos \lambda \phi + \cos \phi = 0 \quad \text{for symmetric response}$$

$$\cos \lambda \phi - \cos \phi = 0 \quad \text{for antisymmetric.} \tag{4.20}$$

The equations in (4.20) are consistent with (4.18) and the combined eigenvalue equation indicated at the end of Section 2.1.

For the most part, the eigenvalue equations of (4.19) and (4.20) are basically available in the literature. Dixon [117] gives an equation for  $\Pi_b-\Pi_b$  and a  $90^\circ$  corner. Carrier and Shaw [118] gives an equation for  $I_b-I_b$  and antisymmetric response. These equations are confirmed in Williams [115], which also gives equations for all combinations of  $I_b, \Pi_b,$  and  $IV_b$ . When conditions are nonmixed, symmetric and antisymmetric equations are not distinguished in Williams [115] but are both included in a single equation. Combined in this way, corresponding equations in (4.19) and (4.20) are either exactly the same as, or equivalent to, the equations in Williams [115].<sup>24</sup>

From (4.13) and (4.16),

$$M = O(r^{\lambda-1}), \quad Q = O((c_3^2 + c_4^2)r^{\lambda-2}), \quad \text{as } r \rightarrow 0 \tag{4.21}$$

on  $\mathfrak{R}$ , where  $M$  is any moment resultant,  $Q$  either shear resultant. Thus provided  $u_z$  is not purely harmonic (ie, provided  $c_3 \neq 0$  or  $c_4 \neq 0$ ), the general range of eigenvalues for power singularities is

$$0 \leq \lambda < 2 \tag{4.22}$$

Singular eigenvalues in this range comply with the regularity requirement (4.14).

Singular eigenvalues within the range (4.22) are determined in the literature as follows. For all possible combina-

tions of the boundary conditions  $I_b, \Pi_b,$  and  $IV_b$  and vertex angles not exceeding  $180^\circ$ , Williams [115] furnishes the real parts of dominant singular eigenvalues. Typically these are determined numerically.

For  $IV_b-IV_b$ , singular eigenvalues can be determined analytically from (4.20). Thus for symmetric configurations,

$$\lambda = (2n-1) \frac{\pi}{\phi} - 1 \quad ((2n-1) < \phi < n\pi, n=1,2)$$

$$\lambda = 1 \pm \frac{\pi}{\phi} \quad (\pi < \phi \leq 2\pi) \tag{4.23}$$

while for antisymmetric,

$$\lambda = \frac{2\pi}{\phi} - 1 \quad (\pi < \phi \leq 2\pi) \tag{4.24}$$

For the minus sign in the second of (4.23), the range of  $\phi$  can be extended to include  $\pi$ . Some of the limits on the ranges for  $\phi$  in (4.23) and (4.24) are because the shear resultants are identically zero for these eigenvalues and thus there are no singularities when  $1 < \lambda < 2$ .<sup>25</sup> The dominant singularity for  $\phi \leq \pi$  comes from the first of (4.23) with  $n=1$ . This eigenvalue is plotted in Williams [115].

For  $\Pi_b-\Pi_b$  and any vertex angle, the real parts of singular eigenvalues for both symmetric and antisymmetric response are given in Morley [119]. For  $\phi=270^\circ$  with  $I_b-I_b, \Pi_b-\Pi_b,$  and  $IV_b-IV_b$ , singular eigenvalues are given in Hrubec and Hrabok [120], including real and imaginary parts when eigenvalues are complex. For all possible combinations of boundary conditions  $I_b, \Pi_b,$  and  $IV_b$  and vertex angles between  $180^\circ$  and  $360^\circ$ , Leissa, McGee, and Huang [121] furnishes the real parts of dominant singular eigenvalues. For  $I_b-I_b$  when  $\nu=0, 1/3, 1/2, \Pi_b-\Pi_b,$  and  $I_b-\Pi_b$  when  $\nu=0$ , singular eigenvalues may be obtained from Seweryn and Molski [20], on using the analogies in (4.19). In Seweryn and Molski [20], symmetric and antisymmetric responses are distinguished and provided separately, both real and imaginary parts of complex eigenvalues are furnished, and singular eigenvalues other than just the dominant ones are given. For  $I_b-\Pi_b$  and  $\phi=90^\circ$ , complex singular eigenvalues are tabulated in Gregory, Chonghua, and Wan [122] for  $\nu=0, 1/4, 1/3, 1/2$ .

The singular eigenfunctions for a cracked plate under bending within fourth-order classical theory are derived in Williams [123]. Under symmetric loading one might expect the tension side of the plate to have the same stress distribution as for a Mode 1 crack in extension (developed in Williams [124] and Irwin [125]). While both have inverse-square-root stress singularities and tensile normal stresses acting transverse to the crack and directly ahead of the crack tip, classical bending theory predicts a compressive normal stress acting parallel to the crack and ahead of it. This is in marked contrast to the extensional case which has the normal stress parallel to the crack being tensile and equal in magnitude to the transverse component. Given the key role played by boundary conditions in influencing the character of stress

<sup>24</sup>None of the  $(\lambda-1)$  factors in (4.19) are present in equations in the literature. Possibly this is because the basic fields attending (4.16) are nonsingular for  $\lambda=1$ . Auxiliary fields are singular however.

<sup>25</sup>The Kirchhoff shear,  $Q_\theta - \partial M_{r,\theta} / \partial r$ , would however be singular for wider ranges of  $\phi$  with  $1 < \lambda < 2$ .

singularities, the arguably less physical result of classical bending theory may be because the crack flanks are not truly stress free with fourth-order theory.

Turning to *stress singularities involving logarithmic terms*, at the outset these stem from auxiliary bending fields generated by differentiating (4.16) with respect to  $\lambda$ . The ensuing development is outlined in Sinclair [126]. As for the extensional case, *logarithmic intensification* of power singularities can be expected to occur when eigenvalues transition from complex to real. Such instances have yet to be fully checked out in the literature. Rather than logarithmic intensification, here we concentrate on *pure logarithmic* singularities.

There are two eigenvalues which result in what might be termed pure logarithmic singularities. First for  $\lambda = 1$ , pure log singularities are possible in moment resultants. Typically, these are accompanied by  $1/r$  singularities in shear resultants. That is, we have

$$M = O(\ln r), \quad Q = O((\hat{c}_3^2 + \hat{c}_4^2)/r), \quad \text{as } r \rightarrow 0 \quad (4.25)$$

on  $\Re$  when  $\lambda = 1$ , where  $\hat{c}_3$  and  $\hat{c}_4$  are constants in auxiliary fields corresponding to  $c_3$  and  $c_4$  in the basic fields attending (4.16). Even when  $\hat{c}_3 = \hat{c}_4 = 0$  and the shear resultants vanish, the Kirchhoff shear has a  $1/r$  singularity. Thus these singularities are associated with some form of concentrated shear loading.

Second for  $\lambda = 2$ , pure log singularities are possible in shear resultants. That is, we have

$$M = o(1), \quad Q = O((\hat{c}_3^2 + \hat{c}_4^2) \ln r), \quad \text{as } r \rightarrow 0 \quad (4.26)$$

on  $\Re$  when  $\lambda = 2$ . These are the weakest singularities possible and consequently the least readily detected with numerical methods. Accordingly their asymptotic identification can be of significant value.

Conditions for singularities as in (4.25) with homogeneous boundary conditions are as in the next to last of (1.3) with  $n_A = 4$ . Conditions with inhomogeneous boundary conditions are as in the last two of (1.5) with  $n_A = 4$ . Examples of corresponding boundary conditions are those associated with the constants  $M_0$  and  $\hat{M}_0$  in  $I'_b$  and  $IV'_b$  of Table 13, respectively, with the other constants in these conditions being set to zero.

Conditions for singularities as in (4.26) with homogeneous boundary conditions are as in the next to last of (1.3) with  $n_A = 4$  except that now  $\lambda = 2$ . Conditions with inhomogeneous boundary conditions are as in the last of (1.5) with  $n_A = 4$ , but now with  $\lambda = 2$  instead of 1. Corresponding boundary conditions are those associated with the constants  $M'_0, V_0, u_0, u'_0, \hat{M}'_0$ , and  $\hat{u}_0$  in  $I'_b, II'_b$ , and  $IV'_b$ , with  $M_0$  and  $\hat{M}_0$  being set to zero (see Sinclair [126]).

As a first example of a singularity as in (4.25), we have the out-of-plane line load on the edge of a half-plane plate. This has

$$M = \text{ord}(\ln r), \quad Q_r = \text{ord}(1/r), \quad Q_\theta = 0, \quad \text{as } r \rightarrow 0 \quad (4.27)$$

on  $\Re(\phi = \pi)$ . Full fields may be obtained from Article 49, Nadai [127]. A second example is the half-plane plate again but now under a step moment on its edge (Fig. 14a). This has

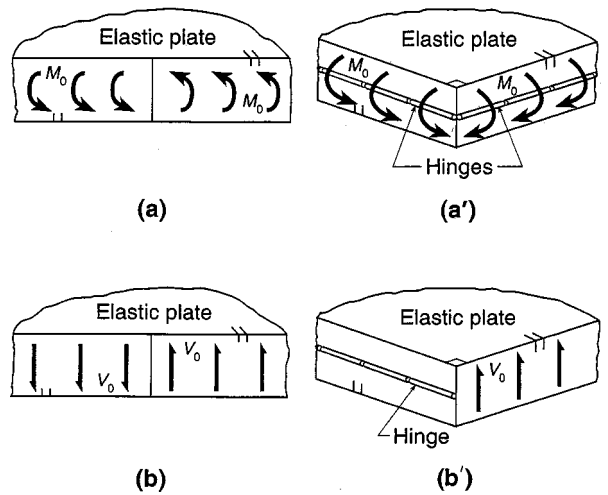


Fig. 14 Examples of configurations with logarithmic stress singularities: a), a') plates with applied moments and log singularities in  $\sigma_r, \sigma_\theta$ , and  $\tau_{r\theta}$ ; b), b') plates with applied shears and log singularities in  $\tau_{rz}$  and  $\tau_{\theta z}$ .

fields as in (4.27) but with the roles of  $Q_r$  and  $Q_\theta$  reversed. A third example is the hinged quarter-plane plate under applied moments (Fig. 14a'). This has

$$M = \text{ord}(\ln r), \quad Q_r = Q_\theta = 0, \quad \text{as } r \rightarrow 0 \quad (4.28)$$

on  $\Re(\phi = \pi/2)$ . The Kirchhoff shear, though, still behaves like  $1/r$  as  $r \rightarrow 0$ .

The presence of  $1/r$  terms make it unlikely that any of the foregoing could pass undetected in a stress analysis. This is not the case for singularities as in (4.26). Accordingly, we list all configurations known to have singularities of this form in Table 14 (from Sinclair [126]). For elastically restrained conditions, some of these stem from their equivalence with symmetry conditions for the special case of  $\lambda = 2$ .

In Table 14,  $\phi_b$  is such that

$$4\kappa_b \sin^2 \phi_b = (\kappa_b + 1)(2 \pm \sqrt{4 - \kappa_b}) \quad (4.29)$$

If in addition to (4.29),  $\kappa_b = -\tan \phi_b / \phi_b \cos 2\phi_b$ , by definition, then  $\kappa = \hat{\kappa}_b, \phi_b = \hat{\phi}_b$ . Two examples of singularities as in (4.26) are shown in Figs. 14b and b'. The first is for a half-plane plate with a step shear and thus quite analogous to the extensional case. The second is for a quarter-plane plate, hinged on one edge with shear on the other. This example is perhaps less obvious than the first, although it is really equivalent to it. Even less obvious in Table 14 is  $I'_b - I_b$  for the half-plane when  $M_\theta = M'_0 r$ : Here the moment resultant actually varies continuously along the plate edge, though its derivative does not.

Turning to plates made of multiple materials under bending, there are relatively few instances of singularity identification compared to the extensional case. However, Fenner [80] shows that perfectly bonded conditions in bending with fourth-order theory are effectively equivalent to perfectly bonded conditions in extension as far as eigenvalue equa-

**Table 14. Configurations with logarithmic singularities in shear resultants**

Boundary conditions on $\theta=0, \phi$	Configuration specifications ( $m=1,2$ )
$I'_b - I_b$	$\phi = \pi$ or $2\pi$ , $M'_0 \neq 0$ or $V_0 \neq 0$ $\kappa_b = \pm \sec \phi$ , and $M'_0(\kappa_b + 2)f\left(\tan \frac{\phi}{2}\right)^{\pm 1} \neq \pm V_0(2 - \kappa_b)$
$II'_b - II_b$ or $V_b$ $IV'_b - IV_b$ $I_b - II_b$ or $V_b$ $I'_b - II'_b$	$\phi = \pi$ or $2\pi$ , $u_0 \neq 0$ or $u'_0 \neq 0$ $\phi = \pi$ or $2\pi$ , $M'_0 \neq 6\hat{u}_0(1 - \nu)\mu_b$ $\phi = \hat{\phi}_b$ , $\kappa_b = \hat{\kappa}_b$ $\phi = \phi_b$ , $\kappa_b \neq \hat{\kappa}_b$ and $(M'_0 - 6u_0(1 - \nu)\mu_b \cos 3\phi)(3 \sin 3\phi - (\kappa_b + 2)\sin \phi) \neq (V_0 + 2u'_0(1 - \nu)\mu_b \cos 3\phi)(3 \cos 3\phi + (\kappa_b - 2)\cos \phi)$
$I'_b - IV'_b$	$\phi = (2m - 1)\frac{\pi}{2}$ , and $24\hat{u}_0(1 - \nu)\mu_b \neq \hat{M}'_0(\kappa_b + 5) - (-)^m V_0(\kappa_b + 1)$
$I'_b - V'_b$	$\phi = m\pi$ , $M'_0 \neq (-)^m \hat{M}'_0$ $\phi = \pi$ or $2\pi$ , $V_0 \neq 0$ $\phi = \pi/2$ or $3\pi/2$ , $M'_0 \neq 0$ $\kappa_b = \sec 2\phi$ , $M'_0(\kappa_b + 2)\tan \phi \neq V_0(2 - \kappa_b)$
$II'_b - IV'_b$	$\phi = (2m - 1)\frac{\pi}{2}$ , and $2\hat{M}'_0 \neq (1 - \nu)\mu_b(3(3 - \kappa_b)\hat{u}_0 - (-)^m(\kappa_b + 1)u'_0)$
$II'_b - V_b$	$\phi = m\pi$ , $\hat{u}_0 \neq (-)^m u_0$ $\phi = \pi/2$ or $3\pi/2$ , $u_0 \neq 0$
$IV'_b - V_b$	$\phi = \pi$ or $2\pi$ , $u'_0 \neq 0$ $\phi = \pi/2$ or $3\pi/2$ , $\hat{M}'_0 \neq 6\hat{u}_0\mu_b(1 - \nu)$

tions are concerned. Herein perfect bonding in bending matches  $u_z$ ,  $\partial u_z / \partial \theta$ ,  $M_\theta$ , and  $Q_\theta - \partial M_{r\theta} / \partial r$ . Then the equivalence holds provided

$$\kappa \rightarrow \kappa_b, \quad \mu_1 / \mu_2 \rightarrow \mu_2 / \mu_1 \tag{4.30}$$

where  $\mu_1$  and  $\mu_2$  are the shear moduli for material on either side of the interface. Thus using the analogies in (4.19), eigenvalue equations for perfectly bonded interfaces can be obtained from extensional counterparts (Section 3).

There are two instances of bimaterial plates under bending explicitly treated in the literature. The first concerns a crack meeting an interface (Figs. 6*b* and *b'*). Fenner [80] determines singular eigenvalues for any angle of incidence and a range of ratios. The singular eigenfunctions for the crack parallel to the interface may be obtained from Sih and Rice [128]. The second concerns a bonded bimaterial plate. Huang [129] computes singular eigenvalues for a variety of geometries and a range of moduli ratios.

**4.4 Out-of-plane bending: Higher-order theory**

In this section we consider the singularities that can occur in the out-of-plane bending of an elastic plate when treated within sixth-order theory. The particular theory considered is due to Reissner [130]. This is the sixth-order theory that has received most attention when it comes to singularity identification. We do comment briefly, though, on a similar theory in Hencky [131].

The angular elastic plate to be bent continues to be as in Fig. 12. As for classical theory, the out-of-plane displacement of the plate is  $u_z$ , its moment resultants are  $M_r$ ,  $M_\theta$ , and  $M_{r\theta}$ , and its shear resultants are  $Q_r$  and  $Q_\theta$  (positive resultants shown Fig. 13). In addition, the plate has rotations  $\omega_r$  and  $\omega_\theta$ . All of these field quantities are taken to be in-

dependent of  $z$  so that field equations continue to apply on  $\mathfrak{R}$  of (2.1). With these preliminaries in place, we can formulate the class of out-of-plane bending problems of interest as next.

In general, we seek the out-of-plane displacement  $u_z$ , its rotations  $\omega_r$  and  $\omega_\theta$ , and its associated resultants  $M_r$ ,  $M_\theta$ ,  $M_{r\theta}$ ,  $Q_r$ , and  $Q_\theta$  as functions of  $r$  and  $\theta$  throughout  $\mathfrak{R}$ , satisfying: the *equations of equilibrium* in the absence of body forces and loading on the plate faces, (4.12) on  $\mathfrak{R}$ ; the *resultant-displacement/rotation relations* for a linear elastic plate which is both homogeneous and isotropic,

$$\begin{aligned} \begin{Bmatrix} M_r \\ M_\theta \end{Bmatrix} &= -\mu_b \begin{Bmatrix} \nu \\ 1 \end{Bmatrix} \nabla^2 u_z \begin{Bmatrix} + \\ - \end{Bmatrix} (1 - \nu) \frac{\partial^2 u_z}{\partial r^2} \begin{Bmatrix} + \\ - \end{Bmatrix} \frac{4h^2}{5} \frac{\partial Q_r}{\partial r} \\ M_{r\theta} &= \mu_b (1 - \nu) \frac{\partial}{\partial r} \left( \frac{1}{r} \frac{\partial u_z}{\partial \theta} \right) - \frac{2h^2}{5} \left( \frac{1}{r} \frac{\partial Q_r}{\partial \theta} + r \frac{\partial}{\partial r} \left( \frac{Q_\theta}{r} \right) \right) \end{aligned} \tag{4.31}$$

$$\begin{Bmatrix} Q_r \\ Q_\theta \end{Bmatrix} = \frac{5\mu_b(1 - \nu)}{4h^2} \begin{Bmatrix} \omega_r + \frac{\partial u_z}{\partial r} \\ \omega_\theta + \frac{1}{r} \frac{\partial u_z}{\partial \theta} \end{Bmatrix}$$

**Table 15. Boundary conditions for out-of-plane bending with Reissner’s theory**

Identifying Roman numeral	Boundary conditions	Physical description
$I_B$	$M_\theta = 0, Q_r = 0, Q_\theta = 0$	Stress free
$II_B$	$u_z = 0, \omega_r = 0, \omega_\theta = 0$	Clamped
$III_B$	$\omega_\theta = 0, M_{r\theta} = 0, Q_\theta = 0$	Symmetry
$IV_B$	$u_z = 0, \omega_r = 0, M_\theta = 0$	Simply supported

on  $\mathfrak{R}$ , wherein  $\mu_b$  remains as the flexural rigidity; any one of the sets of *boundary conditions*  $I_B$ ,  $II_B$ , or  $IV_B$  in Table 15 on the plate edge at  $\theta=0$ , together with another such set on the edge at  $\theta=\phi$ , or one of Conditions  $III_B$  and  $IV_B$  on the plate bisector at  $\theta=\phi/2$  as appropriate, for  $0 < r < \infty$ ; and the *regularity requirement* at the plate vertex,

$$u_z = o(1), \quad \omega_r = O(1), \quad \omega_\theta = O(1), \quad \text{as } r \rightarrow 0 \quad (4.32)$$

on  $\mathfrak{R}$ . In particular, we are interested in the local behavior of the fields complying with the foregoing in the vicinity of the plate vertex  $O$ .

Several comments on the preceding formulation are in order. First, as with classical theory, the presence of lateral loading has no effect on the nature of any singularities provided the loading is integrable. Second, the resultants continue to be related to stresses as in (4.15) so that singularities in resultants lead to singularities in corresponding stress components. Third, the boundary conditions now prescribe three quantities per edge (cf, Table 13): Accordingly, they enable the physically natural conditions attending a stress-free edge to be enforced. Fourth, when the same boundary conditions apply on both plate edges, Conditions  $III_B$  and  $IV_B$  enable one to distinguish between symmetric and anti-symmetric response—in this role, Conditions  $IV_B$  are equivalent to antisymmetry conditions. Fifth, there are no conditions at infinity nor should there be in this asymptotic formulation. Sixth and last, the regularity requirement is consistent with classical theory and therefore analogous to earlier such requirements: However, absent a formal proof of completeness for Reissner’s theory, it is provisional at this time.

The theory in Hencky [131] has the same equations of equilibrium and boundary conditions as Reissner’s theory. Differences occur in the resultant-displacement/rotation relations. In the absence of loading on the plate faces, these differences are confined to the numerical coefficients of  $h^2$  terms in (4.31). Moreover, these differences are consistent throughout (4.31). As a result, Reissner’s theory can be transformed into that of Hencky simply by making the transformation  $h \rightarrow \sqrt{5/6}h$  in (4.31) wherever  $h$  occurs explicitly (ie, there is no change to  $\mu_b$ ). It follows that we can expect the singularities in Hencky’s theory to stem from the same eigenvalue equations as for Reissner’s theory once this transformation is implemented.

Analysis proceeds on introducing a stress function  $\chi$  so that the first of (4.12) is satisfied. Thus

$$Q_r = \frac{1}{r} \frac{\partial \chi}{\partial \theta}, \quad Q_\theta = - \frac{\partial \chi}{\partial r} \quad (4.33)$$

on  $\mathfrak{R}$ . Substituting (4.31) and (4.33) into the last of (4.12) then gives

$$\frac{\partial}{\partial r} \left( \chi - \frac{2h^2}{5} \nabla^2 \chi \right) = \frac{\mu_b}{r} \frac{\partial}{\partial \theta} (\nabla^2 u_z) \quad (4.34)$$

$$\frac{1}{r} \frac{\partial}{\partial \theta} \left( \chi - \frac{2h^2}{5} \nabla^2 \chi \right) = - \mu_b \frac{\partial}{\partial r} (\nabla^2 u_z)$$

on  $\mathfrak{R}$ . In solving (4.34), we need solutions with six constants sharing a common power of  $r$  in order to meet the six boundary conditions, three to an edge, which hold for all  $r$ . To this end, Burton and Sinclair [132] use a series approach with

$$u_z = r^{\lambda+1} \Lambda(\lambda, \theta) + O(r^{\lambda+3}) \quad (4.35)$$

$$\chi = r^{\lambda+1} \hat{\Lambda}(\lambda, \theta) + O(r^{\lambda+3})$$

on  $\mathfrak{R}$ . Hence  $\Lambda$  is as in (4.16),  $\hat{\Lambda}$  likewise with  $c_i$  ( $i=1-4$ ) exchanged for  $\hat{c}_i$ . Then relating the dominant term on the left-hand side of (4.34) as  $r \rightarrow 0$ , the  $\nabla^2 \chi$  term, to that of the right-hand side relates  $\hat{c}_3$  and  $\hat{c}_4$  to  $c_3$  and  $c_4$ . This leaves six free constants as desired ( $c_1-c_4$ ,  $\hat{c}_1$ , and  $\hat{c}_2$ ). The resulting fields for the dominant terms as  $r \rightarrow 0$  are given in [132].

What is overlooked in Burton and Sinclair [132] is the possibility of  $\chi$  terms on the left-hand side of (4.34) interacting with the right when  $\chi$  is purely harmonic. This omission is corrected in Yen and Zhou [133], the resulting additional field being given in [133].

Substituting the fields in Burton and Sinclair [132] into the various combinations of boundary conditions available from Table 15 leads to associated *eigenvalue equations*. With the exception of the equation for  $IV_B-IV_B$ , these equations are confirmed in Yen and Zhou [133]. This confirmation occurs because the additional solution available in Yen and Zhou [133] does not actively participate other than for a plate simply supported on both edges. These confirmed equations then are the same as extensional counterparts provided  $\kappa$  takes on its value for plane stress ( $\kappa = (3-\nu)/(1+\nu)$ ). Accordingly, drawing on results from Tables 2–4 of Section 2.1, we have:<sup>26</sup>

$I_B-I_B$	(2.9) for symmetric response	(4.36)
	(2.13) for antisymmetric response	
$II_B-II_B$	(2.10) for symmetric response	
	(2.14) for antisymmetric response	
$I_B-II_B$	(2.17)	
$I_B-IV_B$	(2.13) with $\phi \rightarrow 2\phi$	
$II_B-IV_B$	(2.14) with $\phi \rightarrow 2\phi$	

For  $IV_B-IV_B$ , the additional field of Yen and Zhou [133] is active and the eigenvalue equation in Burton and Sinclair [132] has an additional factor. Accordingly we have:

$$IV_B-IV_B \quad (\cos \lambda \phi \pm \cos \phi) \cos(\lambda-1) \frac{\phi}{2} = 0 \quad (4.37)$$

The plus sign in (4.37) is associated with symmetric response, the minus sign with antisymmetric. The eigenvalue equations in (4.36) and (4.37) are independent of  $h$ . Consequently, the singular eigenvalues in Hencky’s theory are the *same* as those in Reissner’s theory.

For (4.35) from (4.31) and (4.33),

$$M = O(r^{\lambda-1}), Q = O(r^\lambda) \quad (4.38)$$

$$\omega = O(r^\lambda), u_z = O(r^{\lambda+1}), \text{ as } r \rightarrow 0$$

<sup>26</sup>There is a typographical error in the second eigenvalue equation in Table 1 of Burton and Sinclair [132]. The correct result is given in (4.36).

on  $\mathfrak{R}$ , where  $\omega$  is either rotation component. From (4.32), admissible *power singularities* in moment resultants then occur for

$$0 \leq \operatorname{Re} \lambda < 1 \quad (4.39)$$

For the additional solution of Yen and Zhou [133],

$$M = O(r^{\lambda-3}), \quad Q = O(r^{\lambda-2}) \quad (4.40)$$

$$\omega = O(r^{\lambda-2}), \quad u_z = O(r^{\lambda+1}), \quad \text{as } r \rightarrow 0$$

on  $\mathfrak{R}$ . Admissible power singularities in moment resultants occur for

$$2 \leq \operatorname{Re} \lambda < 3 \quad (4.41)$$

Observe that, with either (4.38) and (4.39) or (4.40) and (4.41),  $M$  is singular while  $Q$  is not, in contrast to classical theory where  $Q$  is typically more singular than  $M$ . *Singular eigenvalues* as in (4.39) for (4.38) can be obtained directly from their extensional counterparts (see Section 2.2).

For simple supported conditions, singular eigenvalues as in (4.39) for (4.38) from the first factor in (4.37) are included in (4.23) and (4.24). Singular eigenvalues as in (4.41) for (4.40) from the second factor in (4.37) are:

$$\lambda = \frac{\pi}{\phi} + 1 \quad (\pi/2 < \phi \leq \pi) \quad (4.42)$$

$$\lambda = \frac{3\pi}{\phi} + 1 \quad (3\pi/2 < \phi \leq 2\pi)$$

These eigenvalues are given in Yen and Zhou [133].

There is a further singular field for simply supported conditions not included in [132,133]. This has

$$M = O(r^{\pi/\phi}), \quad Q = O(r^{\pi/\phi-1}) \quad (4.43)$$

$$\omega = O(r^{\pi/\phi+1}), \quad u_z = O(r^{\pi/\phi}), \quad \text{as } r \rightarrow 0$$

on  $\mathfrak{R}$ . Thus for  $\phi > \pi$ , this field has  $Q$  singular,  $M$  not, in contrast to the results in [132,133]. This singularity is identified in Huang, McGee, and Leissa [134].

Turning to companion eigenfunctions for Reissner's theory, for the fields associated with (4.39), both the  $r$ -dependence and the individual functions of  $\theta$  in eigenfunctions can be shown to be the same as extensional counterparts (see Williams [2] and Burton and Sinclair [132]). Thus all that is needed for eigenfunctions to coincide completely to within a multiplicative factor is that the weighting of the individual functions of  $\theta$  be the same in bending as in extension.

That this in fact can occur is demonstrated for the case of a crack in a plate of vanishing thickness in Knowles and Wang [135]. For a plate of finite thickness, it is demonstrated for a crack in Hartranft and Sih [136] and Wang [137]. Hence the tensile side of the plate in bending behaves as if it is a crack in a plate in extension, a physically reasonable result in contrast to that of classical theory.

On the compression side of the plate, the eigenfunction for the crack in Reissner's theory leads to interpenetration or overlapping of the crack's flanks. While this is not physically possible, it is nonetheless possible in an elastic analysis

within Reissner's theory (it is also possible with classical theory). In some instances, overlapping displacements may be negated by the addition of an in-plane tension of sufficient magnitude. Otherwise, more physically appropriate results can only be obtained by entertaining contact of the flanks and tracking this contact as loading proceeds. Such an analysis is really 3D, as well as being geometrically nonlinear: As such, it is outside the scope of this section.

For *logarithmic* terms under *homogeneous* boundary conditions, conditions like (1.3) are indicated in Burton and Sinclair [132] for fields stemming from (4.35). No actual instances of these singularities are identified in Burton and Sinclair [132]. Logarithmic terms can be generated for simply-supported conditions and the additional fields of Yen and Zhou [133], although it remains to be determined what additional conditions these logarithmic fields must meet in order to participate.

There is also the possibility of logarithmic singularities being induced by *inhomogeneous* boundary conditions. This type of response can be expected to include configurations that correspond to instances of log stress singularities under inhomogeneous boundary conditions for plates in extension (Section 2.4). Some support of this expectation being fulfilled can be found in Hartranft [138]. There a log singularity is identified in  $M_r$  in response to a step in  $M_{r\theta}$  on a plate edge ( $\phi = \pi$ ), whereas no log singularity is found for a step in  $M_\theta$ . Thus this situation is analogous to the in-plane case wherein a step in shear on a half-plane plate produces a log singularity (Table 7, Section 2.4), while a step in normal stress does not. A further log singularity in  $Q_r$  in response to a step in  $Q_\theta$  on a plate edge is identified in Hartranft [138]. While this configuration has no counterpart in extension, it is analogous to the antiplane shear case wherein a step in shear on a half-space wedge produces a log singularity (Table 10, Section 4.1).

For plates made of multiple materials treated within Reissner's theory, the only singularity identifications that would appear to be available in the literature are those in Huang [129]. These are for closed bimaterial plates and simply supported bimaterial plates.

## 5 STRESS SINGULARITIES FOR OTHER ELASTIC CONFIGURATIONS

### 5.1 Axisymmetric configurations

A representative axisymmetric configuration is sketched in Fig. 15. This depicts a right circular cylinder with a conical cap bonded into a half-space which in general is comprised of a material with distinct elastic moduli from the cylinder. The end of the cylinder above the half-space is subjected to an applied torque  $T$  and an axial force  $F$ . Stress singularities can be expected at the vertex of the cone  $P_s$ , and at points where the perimeter of the cylinder is bonded to the half-space (eg,  $P'_s$ ). For each location, we wish to consider the singularities that may be induced by either the torque  $T$  or the force  $F$ . Thus we have four configurations: the inner core

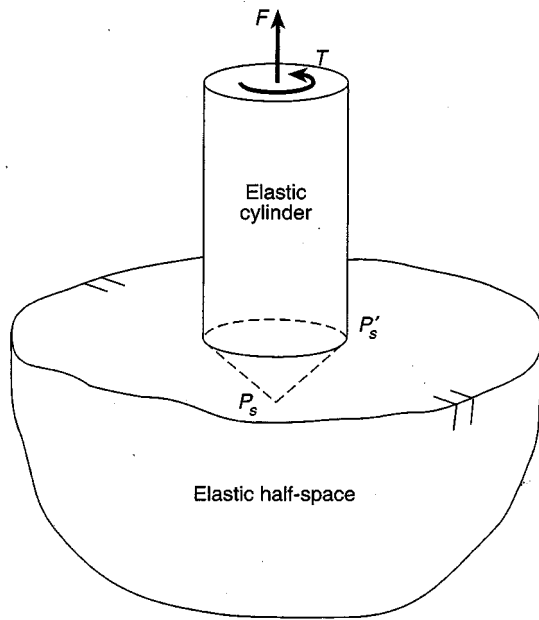


Fig. 15 Singular axisymmetric configurations

vertex with torsion or with axial loading, and the outer cylinder boundary with torsion or with axial loading. We treat each of these in turn in what follows.

For a cone vertex under torsion, spherical polar coordinates  $\rho, \psi,$  and  $\theta$  enable the asymptotic problem to be readily formulated (Fig. 16). These coordinates share a common origin  $O$  with the rectangular Cartesian coordinates  $x, y,$  and  $z,$  and are related to them by:

$$x = \rho \sin \psi \cos \theta, \quad y = \rho \sin \psi \sin \theta, \quad z = \rho \cos \psi \quad (5.1)$$

for  $0 \leq \rho < \infty, 0 \leq \psi \leq \pi,$  and  $0 \leq \theta < 2\pi.$  Under pure torsion, the only displacement is that in the  $\theta$  direction,  $u_\theta,$  which is a function of  $\rho$  and  $\psi$  alone. Hence the open region of interest  $\mathfrak{R}$  is

$$\mathfrak{R} = \{(\rho, \psi) | 0 < \rho < \infty, 0 < \psi < \phi/2\} \quad (5.2)$$

where  $\phi$  is now the vertex angle of the cone. With these geometric preliminaries in place, we can formulate our inner torsion problems as next.

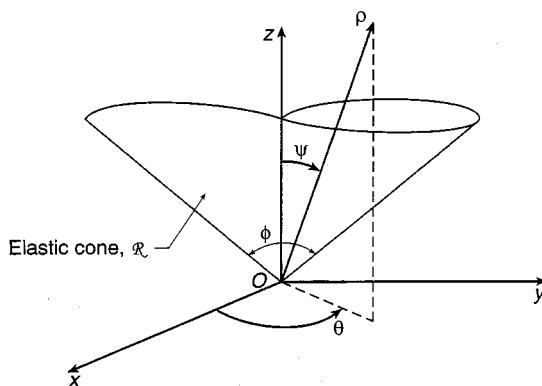


Fig. 16 Spherical polar coordinates for a cone vertex

In general, we seek the axisymmetric shear stresses  $\tau_{\rho\theta}$  and  $\tau_{\theta\psi}$  and their companion displacement  $u_\theta,$  as functions of  $\rho$  and  $\psi$  throughout  $\mathfrak{R},$  satisfying: the stress equation of equilibrium absent body force,

$$\rho \frac{\partial \tau_{\rho\theta}}{\partial \rho} + \frac{\partial \tau_{\theta\psi}}{\partial \psi} + 3\tau_{\rho\theta} + 2\tau_{\theta\psi} \cot \psi = 0 \quad (5.3)$$

on  $\mathfrak{R};$  the stress-displacement relations for a linear elastic cone which is both homogeneous and isotropic,

$$\tau_{\rho\theta} = \mu \left( \frac{\partial u_\theta}{\partial \rho} - \frac{u_\theta}{\rho} \right), \quad \tau_{\theta\psi} = \frac{\mu}{\rho} \left( \frac{\partial u_\theta}{\partial \psi} - u_\theta \cot \psi \right) \quad (5.4)$$

on  $\mathfrak{R},$  wherein  $\mu$  continues as the shear modulus; the boundary condition for either a clamped or a stress-free cone surface,

$$u_\theta = 0 \quad \text{or} \quad \tau_{\theta\psi} = 0 \quad \text{at} \quad \psi = \phi/2 \quad (5.5)$$

for  $0 < \rho < \infty;$  and the regularity requirement at the cone vertex,

$$u_\theta = O(1) \quad \text{as} \quad \rho \rightarrow 0 \quad (5.6)$$

on  $\mathfrak{R}.$  In particular, we are interested in the local behavior of the fields complying with the foregoing in the vicinity of the cone vertex  $O.$

To solve the preceding problems, first substitute (5.4) into (5.3). Then seeking a separable solution for  $u_\theta$  of the form  $\rho^\lambda f(\psi)$  leads to Legendre's associated differential equation. Hence, for bounded  $u_\theta$  when  $\psi = 0,$

$$u_\theta = c_\lambda \rho^\lambda P_\lambda^1(\cos \psi) \quad (5.7)$$

Here  $c_\lambda$  is a constant coefficient, and  $P_\lambda^1$  is an associated Legendre function of the first kind of degree  $\lambda$  and order one.<sup>27</sup> The eigenvalue equations attending (5.4), (5.5), and (5.7) are developed and solved numerically in Bažant and Keer [140]. No roots are found in the range  $0 < \lambda < 1$  irrespective of cone vertex angle  $\phi.$  Consequently, no power singularities are found for the cone vertex under torsion.

For a cone vertex under axial loading, the same spherical polar coordinates are appropriate (Fig. 16). Now there are two displacements,  $u_\rho$  and  $u_\psi.$  However, both are still only functions of  $\rho$  and  $\psi,$  so that the region of interest remains  $\mathfrak{R}$  of (5.2). On this region we can formulate our inner axial problems as next.

In general, we seek the axisymmetric stress components  $\sigma_\rho, \sigma_\psi, \sigma_\theta,$  and  $\tau_{\rho\psi},$  and their companion displacements  $u_\rho$  and  $u_\psi,$  as functions of  $\rho$  and  $\psi$  throughout  $\mathfrak{R},$  satisfying: the stress equations of equilibrium absent body forces,

$$\rho \frac{\partial \sigma_\rho}{\partial \rho} + \frac{\partial \tau_{\rho\psi}}{\partial \psi} + 2\sigma_\rho - \sigma_\psi - \sigma_\theta + \tau_{\rho\psi} \cot \psi = 0 \quad (5.8)$$

$$\frac{\partial \sigma_\psi}{\partial \psi} + \rho \frac{\partial \tau_{\rho\psi}}{\partial \rho} + 3\tau_{\rho\psi} + (\sigma_\psi - \sigma_\theta) \cot \psi = 0$$

on  $\mathfrak{R};$  the stress-displacement relations for a linear elastic cone which is both homogeneous and isotropic,

<sup>27</sup>The function  $P_\lambda^1$  is as defined in Ch 8, Abramowitz and Stegun [139].

$$\begin{aligned} \sigma_\rho &= 2\mu \left[ \frac{\nu\Theta}{1-2\nu} + \frac{\partial u_\rho}{\partial \rho} \right] \\ \sigma_\psi &= 2\mu \left[ \frac{\nu\Theta}{1-2\nu} + \frac{1}{\rho} \left( \frac{\partial u_\psi}{\partial \psi} + u_\rho \right) \right] \\ \sigma_\theta &= 2\mu \left[ \frac{\nu\Theta}{1-2\nu} + \frac{1}{\rho} (u_\rho + u_\psi \cot \psi) \right] \\ \tau_{\rho\psi} &= \mu \left[ \frac{1}{\rho} \frac{\partial u_\rho}{\partial \psi} + \frac{\partial u_\psi}{\partial \rho} - \frac{u_\psi}{\rho} \right] \end{aligned} \tag{5.9}$$

with

$$\Theta = \frac{\partial u_\rho}{\partial \rho} + \frac{2u_\rho}{\rho} + \frac{1}{\rho} \frac{\partial u_\psi}{\partial \psi} + \frac{u_\psi}{\rho} \cot \psi \tag{5.10}$$

on  $\mathfrak{R}$ , wherein  $\Theta$  continues as the dilatation,  $\nu$  as Poisson's ratio; the *boundary conditions* for either a clamped or stress-free cone surface,

$$u_\rho = u_\psi = 0 \text{ at } \psi = \phi/2 \tag{5.11}$$

or

$$\sigma_\psi = \tau_{\rho\psi} = 0 \text{ at } \psi = \phi/2 \tag{5.12}$$

for  $0 < \rho < \infty$ ; and the *regularity requirements* at the cone vertex,

$$u_\rho = O(1), \quad u_\psi = O(1), \text{ as } \rho \rightarrow 0 \tag{5.13}$$

on  $\mathfrak{R}$ . In particular, we are interested in the local behavior of the fields complying with the foregoing in the vicinity of the cone vertex  $O$ .

Thompson and Little [141] uses Papkovitch-Neuber potentials to develop solutions for the preceding field equations, and also derives the eigenvalue equation for (5.12). Using the same solutions, Bažant and Keer [140] derives the eigenvalue equation for (5.11), and solves both eigenvalue equations numerically. Power singularities are found for both clamped and stress-free conditions for reentrant cone vertices (ie,  $\pi < \phi \leq 2\pi$ ). The singularity exponents involved are all real and depend on the value of Poisson's ratio. Singularity exponents are given for  $\nu$  ranging from 0–0.499 in increments of 0.1 in Bažant and Keer [140]. Exponents for  $\nu = 0.3$  are confirmed in Beagles and Sändig [142].

Further singularities for a cone vertex under axial loading occur when the cone is *rigid* and *indents* an elastic half-space (cf, Fig. 15 near  $P_s$ ). Herein the boundary conditions in the contact region are

$$u_\psi = u_0 - \rho \cot \phi/2, \quad \tau_{\rho\psi} = f\sigma_\psi, \text{ at } \psi = \pi/2 \tag{5.14}$$

where  $u_0$  is the penetration of the cone vertex and  $f$  continues as the coefficient of friction. The frictionless case of this configuration is analyzed in Love [143] and leads to a logarithmic stress singularity at the cone vertex. The friction case also has a log singularity (Hanson [144]).

*Bimaterial* cone vertices (as at  $P_s$  in Fig. 15) are analyzed in Keer and Parihar [145]. Perfect bonding on the interface is assumed (ie,  $\sigma_\psi$ ,  $\tau_{\rho\psi}$ ,  $u_\rho$ , and  $u_\psi$  are matched at  $\psi = \phi/2$ ). Power singularities are identified for varying elastic moduli and cone vertex angles. In contrast to the single material

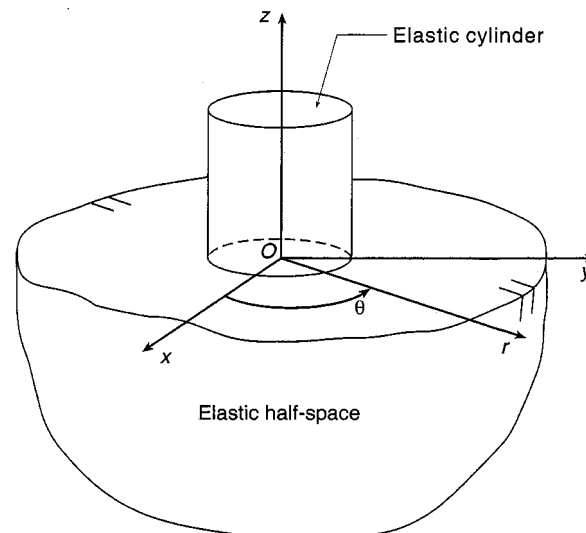


Fig. 17 Cylindrical polar coordinates for a cylindrical boundary

cone, some of the singularity exponents involved are complex. However, the magnitude of the singularity exponent, or of its real part if complex, is bounded from above by that for clamped conditions in Bažant and Keer [140].

By way of an example of a *cylindrical boundary under torsion*, we reconsider the configuration in Fig. 15, but now with the cylinder and half-space comprised of a single elastic material. For this and like configurations, cylindrical polar coordinates,  $r$ ,  $\theta$ , and  $z$  enable ready formulation (Fig. 17). These coordinates share a common origin  $O$  with the rectangular Cartesian coordinates  $x$ ,  $y$ , and  $z$  and are related to them by

$$x = r \cos \theta, \quad y = r \sin \theta, \quad z = z \tag{5.15}$$

for  $0 \leq r < \infty$ ,  $0 \leq \theta < 2\pi$ , and  $-\infty < z < \infty$ . Under pure torsion, the only displacement is that in the  $\theta$  direction,  $u_\theta$ , which is a function of  $r$  and  $z$  alone. Hence the open region of interest  $\mathfrak{R}$  becomes

$$\mathfrak{R} = \{(r, z) | 0 \leq r < R, 0 \leq z < \infty \text{ or } 0 \leq r < \infty, -\infty < z < 0\} \tag{5.16}$$

where  $R$  is the radius of the cylinder. On this region we can formulate our sample *outer torsion problem* as next.

In general, we seek the axisymmetric shear stresses  $\tau_{r\theta}$  and  $\tau_{\theta z}$ , and their companion displacement  $u_\theta$ , as functions of  $r$  and  $z$  throughout  $\mathfrak{R}$ , satisfying: the *stress equation of equilibrium* absent body force,

$$\frac{\partial \tau_{r\theta}}{\partial r} + \frac{2\tau_{r\theta}}{r} + \frac{\partial \tau_{\theta z}}{\partial z} = 0 \tag{5.17}$$

on  $\mathfrak{R}$ ; the *stress-displacement relations* for a linear elastic cylinder and half-space which are also homogeneous and isotropic,

$$\tau_{r\theta} = \mu \left( \frac{\partial u_\theta}{\partial r} - \frac{u_\theta}{r} \right), \quad \tau_{\theta z} = \mu \frac{\partial u_\theta}{\partial z} \tag{5.18}$$

on  $\mathfrak{R}$ ; the stress-free *boundary conditions*,

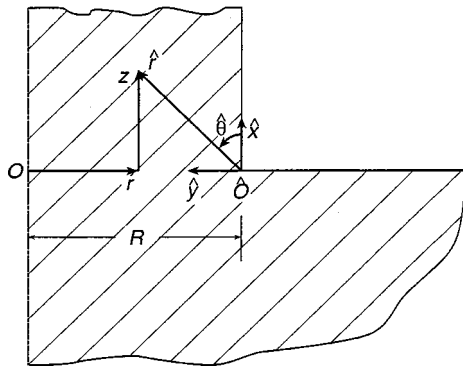


Fig. 18 Section through the cylinder and the half-space with local coordinates at the reentrant corner

$$\tau_{r\theta} = 0 \text{ at } r = R \text{ (} 0 < z < \infty \text{)} \tag{5.19}$$

$$\tau_{\theta z} = 0 \text{ at } z = 0 \text{ (} R < r < \infty \text{)}$$

and the *regularity requirement* at the reentrant corner,

$$u_\theta = O(1) \text{ as } \sqrt{(R-r)^2 + z^2} \rightarrow 0 \tag{5.20}$$

on  $\mathfrak{R}$ . In particular, we are interested in the local behavior of the fields complying with the foregoing in the vicinity of the reentrant corner at  $r = R$  and  $z = 0$ .

One expects that in the local vicinity of greatest interest, a state of *out-of-plane* or *antiplane shear* dominates response. If this is so, we can simply draw on the singularities identified for antiplane shear (Sections 4.1 and 4.2) to identify the singularities possible in outer torsion problems.

To show that antiplane shear indeed characterizes response for the case of our sample problem, as well as for any other outer torsion problem, we proceed as follows. Without loss of generality we consider a section through the configuration of Fig. 17 on the  $y$  axis for  $y \geq 0$ . For this section we introduce local cylindrical polar coordinates  $\hat{r}$ ,  $\hat{\theta}$ , and  $\hat{z}$  with origin  $\hat{O}$  at the reentrant corner (Fig. 18). These are related to rectangular Cartesian coordinates  $\hat{x}$ ,  $\hat{y}$ , and  $\hat{z}$  sharing the same origin  $\hat{O}$  as in (5.15) with carets: Consistent with a right-handed system,  $\hat{z}$  is positive out of the plane of Fig. 18. Then the original coordinate system is related to the new local system in the plane of Fig. 18 by:

$$r = R - \hat{r} \sin \hat{\theta}, \quad z = \hat{r} \cos \hat{\theta} \tag{5.21}$$

For the shear stresses of the local coordinate system,  $\tau_{\hat{r}\hat{z}}$  and  $\tau_{\hat{\theta}\hat{z}}$ , equilibrium of a pair of appropriately oriented triangles leads to

$$\tau_{\hat{r}\hat{z}} = \tau_{r\theta} \sin \hat{\theta} - \tau_{\theta z} \cos \hat{\theta} \tag{5.22}$$

$$\tau_{\hat{\theta}\hat{z}} = \tau_{r\theta} \cos \hat{\theta} + \tau_{\theta z} \sin \hat{\theta}$$

Now we wish to substitute (5.18) into (5.22) to determine the stress-displacement relations in the local coordinate system. In order for the results to be in terms of the local quantities, we make the exchange  $u_\theta = -u_{\hat{z}}$  and invoke the chain rule to obtain

$$\frac{\partial}{\partial r} = -\sin \hat{\theta} \frac{\partial}{\partial \hat{r}} - \frac{\cos \hat{\theta}}{\hat{r}} \frac{\partial}{\partial \hat{\theta}} \tag{5.23}$$

$$\frac{\partial}{\partial z} = \cos \hat{\theta} \frac{\partial}{\partial \hat{r}} - \frac{\sin \hat{\theta}}{\hat{r}} \frac{\partial}{\partial \hat{\theta}}$$

Then (5.18), (5.22), and (5.23) give

$$\tau_{\hat{r}\hat{z}} = \mu \frac{\partial u_{\hat{z}}}{\partial \hat{r}} + O(R^{-1}) \text{ as } R \rightarrow \infty \tag{5.24}$$

$$\tau_{\hat{\theta}\hat{z}} = \frac{\mu}{\hat{r}} \frac{\partial u_{\hat{z}}}{\partial \hat{\theta}} + O(R^{-1}) \text{ as } R \rightarrow \infty$$

In (5.24), the limit  $R \rightarrow \infty$  corresponds to approaching the corner at  $\hat{O}$ . Thus under this limit we have the same stress-displacement relations as for antiplane shear (cf, (4.2) of Section 4.1).

Turning to the stress equation of equilibrium, we invert (5.22) to obtain  $\tau_{r\theta}$  and  $\tau_{\theta z}$  in terms of  $\tau_{\hat{r}\hat{z}}$  and  $\tau_{\hat{\theta}\hat{z}}$ , then substitute into (5.17). This gives, using (5.23),

$$\frac{\partial \tau_{\hat{r}\hat{z}}}{\partial \hat{r}} + \frac{\tau_{\hat{r}\hat{z}}}{\hat{r}} + \frac{1}{\hat{r}} \frac{\partial \tau_{\hat{\theta}\hat{z}}}{\partial \hat{\theta}} + O(R^{-1}) = 0 \text{ as } R \rightarrow \infty \tag{5.25}$$

Again, we have the same equation as for antiplane shear (cf, (4.1) of Section 4.1). Further, the boundary conditions for our sample problem simply are

$$\tau_{\hat{\theta}\hat{z}} = 0 \text{ at } \hat{\theta} = 0, \quad 3\pi/2 \tag{5.26}$$

for  $0 < \hat{r} < \infty$ . Thus we have in (5.24)–(5.26) an antiplane shear problem belonging to the class formulated in Section 4.1. Consequently, from (4.7),

$$\tau = O(\hat{r}^{-1/3}) \text{ as } \hat{r} \rightarrow 0 \tag{5.27}$$

where  $\tau$  is either shear stress.

There is nothing special about our sample problem. Any other feature on the cylindrical boundary can have its boundary conditions transformed so that locally they match those of Table 9, Section 4.1. Further, when multiple materials are involved, interface conditions can be matched with those of Table 11, Section 4.2. It follows that all of the singularities identified in Sections 4.1 and 4.2, including log singularities, apply to corresponding outer torsion problems.

Demonstrations of this correspondence are available in the literature. Early examples are the penny-shaped crack under torsion in Section 5.4, Neuber [17], and torsion of a rigid disk on a half-space in Reissner and Sagoci [146]. Both have inverse-square-root singularities as would be predicted from (4.7) with  $\phi = 2\pi$  and from (4.8) with  $\phi = \pi$ , respectively. For a general V-notch in a pipe under torsion, Tsuji et al [147] obtains singularities as in (4.7). This paper also

treats a bimaterial corner and finds the same stress singularities as for antiplane shear. Other examples of outer torsion problems with bimetals leading to the same singularities as for antiplane shear may be found in Freeman and Keer [148], Westmann [149], and Keer and Freeman [150]. A tri-material example is given in Keer and Freeman [111]. Still further examples exist in the literature: The preceding is not an extensive list but merely intended to reflect the variety of configurations displaying the correspondence.

By way of example of a *cylindrical boundary under axial loading*, we continue to use our sample geometry of a single material version of Fig. 15, but now under an axial load instead of a torque. The cylindrical polar coordinates,  $r$ ,  $\theta$ , and  $z$  of (5.15), Fig. 17, then continue to be appropriate. Now, though, we have the two displacements,  $u_r$  and  $u_z$ . However, spatial dependence continues to be just on  $r$  and  $z$  so that  $\mathfrak{R}$  of (5.16) continues to be the region of interest. On this region we can formulate our sample *outer axial problem* as next.

In general, we seek the axisymmetric stress components  $\sigma_r$ ,  $\sigma_\theta$ ,  $\sigma_z$ , and  $\tau_{rz}$ , and their companion displacements  $u_r$  and  $u_z$ , as functions of  $r$  and  $z$  throughout  $\mathfrak{R}$ , satisfying: the *stress equations of equilibrium* absent body forces,

$$\frac{\partial \sigma_r}{\partial r} + \frac{\partial \tau_{rz}}{\partial z} + \frac{\sigma_r - \sigma_\theta}{r} = 0 \tag{5.28}$$

$$\frac{\partial \sigma_z}{\partial z} + \frac{\partial \tau_{rz}}{\partial r} + \frac{\tau_{rz}}{r} = 0$$

on  $\mathfrak{R}$ ; the *stress-displacement relations* for a linear elastic cylinder and half-space which are also homogeneous and isotropic,

$$\sigma_r = 2\mu \left( \frac{\nu \Theta}{1-2\nu} + \frac{\partial u_r}{\partial r} \right), \quad \sigma_\theta = 2\mu \left( \frac{\nu \Theta}{1-2\nu} + \frac{u_r}{r} \right) \tag{5.29}$$

$$\sigma_z = 2\mu \left( \frac{\nu \Theta}{1-2\nu} + \frac{\partial u_z}{\partial z} \right), \quad \tau_{rz} = \mu \left( \frac{\partial u_r}{\partial z} + \frac{\partial u_z}{\partial r} \right)$$

with dilatation

$$\Theta = \frac{\partial u_r}{\partial r} + \frac{u_r}{r} + \frac{\partial u_z}{\partial z} \tag{5.30}$$

on  $\mathfrak{R}$ ; the stress-free *boundary conditions*,

$$\sigma_r = \tau_{rz} = 0 \quad \text{at } r=R \quad (0 < z < \infty) \tag{5.31}$$

$$\sigma_z = \tau_{rz} = 0 \quad \text{at } z=0 \quad (R < r < \infty)$$

and the *regularity requirements* at the reentrant corner

$$u_r = O(1), \quad u_z = O(1), \quad \text{as } \sqrt{(R-r)^2 + z^2} \rightarrow 0 \tag{5.32}$$

on  $\mathfrak{R}$ . In particular, we are interested in the local behavior of the fields complying with the foregoing in the vicinity of the reentrant corner at  $r=R$  and  $z=0$ .

One expects that, in the local vicinity of greatest interest, a state of *plane strain* dominates response. This is because, for a section such as that on the  $y$  axis, plane strain has  $\partial/\partial\theta$  being a null operator, in common with axisymmetry ( $\theta$  as in Fig. 17). If, in fact, such a correspondence holds, we can

simply draw on the singularities identified in Sections 2 and 3 to identify the singularities possible in outer axial problems.

That indeed this correspondence occurs is argued in Barton [151] and Zak [152]. The approach is similar to that presented here for the simpler torsion problem—simpler because fewer field quantities are involved. While Zak [152] explicitly treats stress-free and clamped boundary conditions, the correspondence is equally applicable to the other boundary conditions in Tables 1 and 6 of Section 2, and to the interface conditions in Table 8 of Section 3. The end result is that not just our sample problem but all outer axial problems have corresponding plane strain configurations which characterize their stress singularities. Conversely, it follows that all of the singularities identified in Sections 2 and 3, including those involving logarithmic terms, apply to corresponding outer axial problems.

Demonstrations of this correspondence are available in the literature. Early examples are the penny-shaped crack under transverse tension in Sneddon [153], and the rigid, right circular cylinder, with a flat lubricated end, pressed into a half-space in Harding and Sneddon [154]. Both have inverse-square-root singularities as is predicted by corresponding plane strain configurations. A further example of a clamped-free right-angled corner is given in Benthem and Minderhoud [155], and shares the same singularity as that of (2.17) in Section 2.1. An example for a bonded bimaterial cylinder is given in Agarwal [156], and leads to essentially the same eigenvalue equation for singularities as given in Bogy [85] for the corresponding plane strain configuration. Again, the references listed here are merely intended to reflect some of the variety of configurations displaying the correspondence.

### 5.2 Three-dimensional geometries with continuous vertex paths

In this section, we continue to be interested in angular regions, but now these regions are 3D rather than 2D. We distinguish three classes of such geometries. These classes

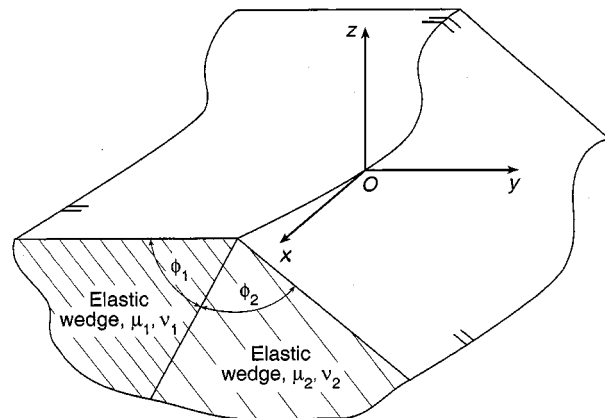


Fig. 19 Bimaterial elastic wedge with vertex locus a smooth curve

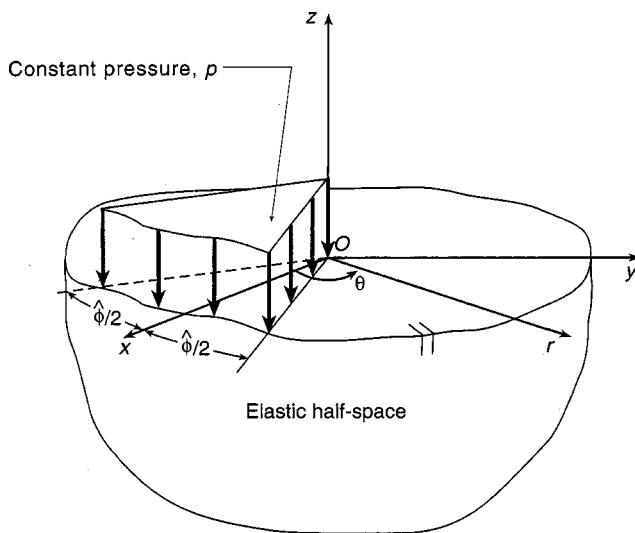


Fig. 20 Constant pressure on a surface sector of an elastic half-space

are arranged in order of decreasing continuity. As one might expect, consequently they are in order of decreasing tractability.

The three classes of 3D geometries are as follows:

- i) Geometries wherein the vertex involved traces out a path with a continuously turning tangent. An example is the bimaterial wedge in Fig. 19: Here the vertex has an angle of  $\phi_1 + \phi_2$  and its path follows a smooth curve.
- ii) Geometries wherein the vertex involved traces out a path that is continuous but has a discontinuity in its direction. An example is the half-space with a loaded surface sector in Fig. 20: Here the “vertex” has an angle of  $\pi$  and its path turns abruptly through  $2\pi - \hat{\phi}$  at  $O$ .

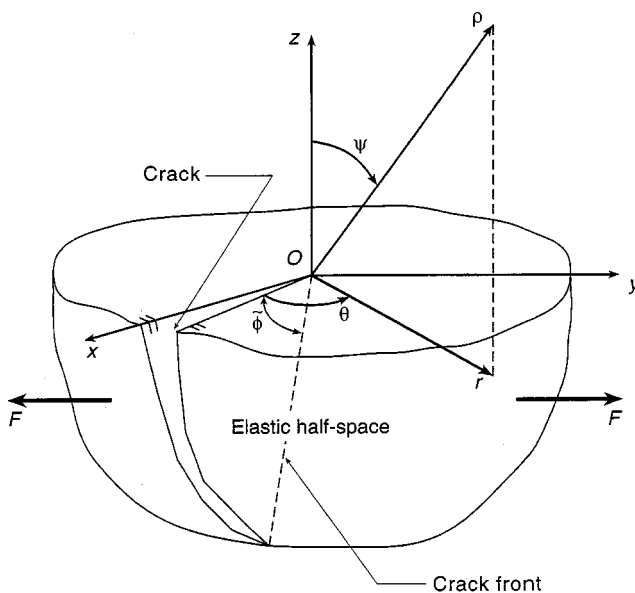


Fig. 21 Elastic half-space with a crack terminating at its surface

- iii) Geometries wherein the vertex involved traces out a discontinuous path. An example is the crack intersecting a free surface in Fig. 21: Here the vertex has an angle of  $2\pi$  and its path ceases abruptly at  $O$ .

We review singularities identified for each of these classes in turn. We begin with the first two in this section, then review the third in a separate following section because of the extensive number of contributions for this class.

In undertaking these reviews, we do admit some contributions entailing a significant amount of numerical analysis. Previously, in two dimensions, analysis was almost entirely analytical: Numerical analysis was essentially confined to the calculation of eigenvalues from equations derived, a numerical process that need have no errors effectively, as may be verified by back substitution. Here we entertain numerical methods that do entail numerical approximations. We do this because of the greater intractability of 3D geometries to purely analytical approaches. We still focus, though, on local singularity identification rather than on global analysis of singular problems.

For the *first class of 3D geometries*, the key general result is established in Aksentian [90]. For the geometry of Fig. 19, Aksentian [90] proves the asymptotic equivalence of 3D response at the vertex to the combination of plane strain response (in the  $yz$  plane in Fig. 19) and out-of-plane shear response (in the  $x$  direction in Fig. 19).<sup>28</sup> Thus, when the vertex in a 3D configuration has a path with a continuously turning tangent, all the plane strain singularities identified in Sections 2 and 3 can participate, together with all the antiplane shear singularities identified in Sections 4.1 and 4.2. Although eigenvalue equations are only explicitly derived for stress-free and clamped boundary conditions and perfectly bonded interface conditions in Aksentian [90], the applicability of the equivalence for other boundary and interface conditions follows immediately from the asymptotic governing equations, (1.5)–(1.7), [90], provided footnote 17 of Section 3.2 is observed.

An example of this equivalence between 2D and 3D singularities occurs for the 3D problem of a flat elliptical crack under transverse tension. This shares the same inverse-square-root singularity of a crack in plane strain (Sadowsky and Sternberg [158] and Green and Sneddon [159]). When this elliptical crack is loaded in shear as well, the inverse-square-root singularity of a crack in antiplane shear also participates (Kassir and Sih [160]). Another example is the contact of an elastic half-space by a flat, frictionless, rigid punch of elliptical cross section. Again, the inverse-square-root singularity of plane strain is present (Galín [161] and Green and Sneddon [159]). When a torsional shear is applied in addition, the inverse-square-root singularity of antiplane shear is added (Mindlin [162]).

<sup>28</sup>For the case of a single material ( $\phi_2=0$ ) and a crack ( $\phi_1=2\pi$ ), the same result is given in Hartranft and Sih [157]. There, however, the result is assumed rather than proven.

As an initial instance of the *second class of 3D geometries*, we consider an elastic half-space loaded with a pressure  $p$  on a surface sector which subtends an angle  $\hat{\phi}$  (Fig. 20). Hence in this problem, in general, stresses and displacements are sought throughout the half-space satisfying: the 3D field equations of elasticity,<sup>29</sup> and the boundary conditions, on  $z=0$ ,

$$\sigma_z = \begin{cases} -p & \text{for } -\hat{\phi}/2 < \theta < \hat{\phi}/2 \\ 0 & \text{for other } \theta, \end{cases} \quad (5.33)$$

$$\tau_{yz} = \tau_{zx} = 0 \quad \text{for } -\pi < \theta \leq \pi$$

all for  $0 < r < \infty$  (see Fig. 20 for coordinates).

In particular, in the surface at  $z=0$ , the stress components in rectangular coordinates are given by

$$\begin{cases} \sigma_x \\ \sigma_y \end{cases} = \begin{cases} - \\ + \end{cases} \frac{p(1-2\nu)}{2\pi} \sin \hat{\phi} \ln r \quad \text{as } r \rightarrow 0 \quad (5.34)$$

with  $\tau_{xy} = 0$ , where  $\nu$  is Poisson's ratio of the half-space. For  $\hat{\phi} = \pi/2$ , this state of pure shear with a log singularity is consistent with results derived in Love [164]. For general  $\hat{\phi}$ , the log singularity of (5.34) is identified in Turteltaub and Wheeler [165].

Notice that when  $\hat{\phi} = 2\pi$ , no singularity occurs in (5.34). This is as it should be when the half-space surface is loaded throughout with a constant pressure. Further, when  $\hat{\phi} = \pi$ , no singularity occurs. This is consistent with the 2D problem of a step normal pressure on a half-space in plane strain which has no singularity (Michell [166]). It is also consistent with the teaching of Aksentian [90] since then the configuration in Fig. 20 is a member of the first class of 3D geometries.

The means of singularity identification in Turteltaub and Wheeler [165] is via asymptotics on line integral representations and is quite analytically sophisticated. With further application, no doubt it could produce results for other normal loadings. Too, it can treat shear tractions on the half-space surface (see later). Here, instead, we next develop a more limited approach. While this approach cannot treat shear tractions, it is simple for normal loadings.

A potential representation of the stresses within an elastic half-space free of surface shear tractions is given in Section 5.7, Green and Zerna [167]. This representation can be expressed in terms of a single harmonic function  $\Psi = \Psi(r, \theta, z)$ , with  $r$ ,  $\theta$ , and  $z$  as in Fig. 20. Assuming  $\Psi$  admits to a Taylor's series expansion in  $z$ , the nonzero stresses in the surface  $z=0$  then are given by:

$$\begin{cases} \sigma_r \\ \sigma_\theta \end{cases} = \begin{bmatrix} 2\nu \\ 1 \end{bmatrix} \nabla^2 \Psi \begin{cases} + \\ - \end{cases} (1-2\nu) \frac{\partial^2 \Psi}{\partial r^2} \quad (5.35)$$

$$\sigma_z = \nabla^2 \Psi, \quad \tau_{r\theta} = \frac{1-2\nu}{r} \frac{\partial}{\partial r} \left( \frac{1}{r} \frac{\partial \Psi}{\partial r} \right)$$

In (5.35),  $\nabla^2$  is the Laplacian in  $r$  and  $\theta$  coordinates. Further, because  $\Psi$  is harmonic in  $r$ ,  $\theta$ , and  $z$ ,  $\nabla^2 \Psi = -\partial^2 \Psi / \partial z^2$ , a

result used in (5.35). Now with a view to representing a constant normal pressure over a sector, we take

$$\Psi = r^2 \left[ \sum_{n=0}^{\infty} (a_n \cos n\theta) + \hat{a}_2 \ln r \cos 2\theta \right] \quad (5.36)$$

The  $r$ -dependence in (5.36) realizes a  $\sigma_z$  from (5.35) which is independent of  $r$ , as desired. By suitably selecting the Fourier coefficients  $a_n$  in the summation in (5.36), it would appear to be possible to represent a step pressure on the sector with  $-\hat{\phi}/2 < \theta < \hat{\phi}/2$ . However, when just the terms in the summation in (5.36) are substituted into (5.35), the  $\sigma_z$  so produced lacks a contribution from  $a_2$ . Needed, therefore, is the  $\hat{a}_2$  term in (5.36). With this addition, a complete representation for a constant pressure on the sector results. Also with this addition, the log singularity terms of (5.34) result (on transforming  $\sigma_r$ ,  $\sigma_\theta$ , and  $\tau_{r\theta}$  into their counterparts in rectangular coordinates).

One consequence of the foregoing development is that any pressure distribution which is constant in  $r$  and even in  $\theta$  on a sector in Fig. 20 has a log singularity associated with it ( $\hat{\phi} = \pi, 2\pi$ ). Thus, for example, if in (5.33)

$$\sigma_z = \begin{cases} -p \cos \frac{\pi\theta}{\hat{\phi}} & \text{for } -\hat{\phi}/2 \leq \theta \leq \hat{\phi}/2 \\ \hat{\phi} & \\ 0 & \text{for other } \theta \end{cases} \quad (5.37)$$

there is an associated log singularity. This pressure distribution has no jumps at  $\theta = \pm \hat{\phi}/2$ , but still has a jump as  $r \rightarrow 0$  for  $-\hat{\phi}/2 < \theta < \hat{\phi}/2$ . A similar development leads to a log singularity if the pressure distribution is odd in  $\theta$  on the surface sector, provided there is still a jump in the distribution as  $r \rightarrow 0$  ( $\hat{\phi} \neq \pi, 2\pi$ ). On the other hand, if in (5.33)

$$\sigma_z = \begin{cases} -pr & \text{for } -\hat{\phi}/2 \leq \theta < \hat{\phi}/2 \\ 0 & \text{for other } \theta \end{cases} \quad (5.38)$$

there is no log singularity ( $r^3$  is now the factor outside the brackets in (5.36), and an  $\hat{a}_3$  term is required instead of  $\hat{a}_2$ ). This pressure distribution does have jumps at  $\theta = \pm \hat{\phi}/2$ , but none as  $r \rightarrow 0$ . Clearly, then, log singularities like that of (5.34) are associated with jumps in  $r$  rather than  $\theta$ . Away from  $O$ , this outcome is consistent with Aksentian [90] and the absence of singularities with pressure jumps in two dimensions.

If the sector in Fig. 20 is loaded via uniform shear tractions rather than pressures, log singularities result along the edges of the sector. For  $\hat{\phi} = \pi/2$ , these log singularities are contained in results in Smith and Alavi [168], Shah and Kobayashi [169], and Liao and Atluri [170]. For general  $\hat{\phi}$ , they are identified in Turteltaub and Wheeler [165]. For the component of the shear traction normal to the sector boundary, the log singularities are as for plane strain (Kolossoff [15]). For the component parallel, as for antiplane shear (Ting [104]). Again, therefore, away from  $O$  a realization of the equivalence in Aksentian [90].

<sup>29</sup>A convenient compendium of the 3D field equations of elasticity in all three coordinate systems eventually used in this section is provided in Ch 2, Hughes and Gaylord [163].

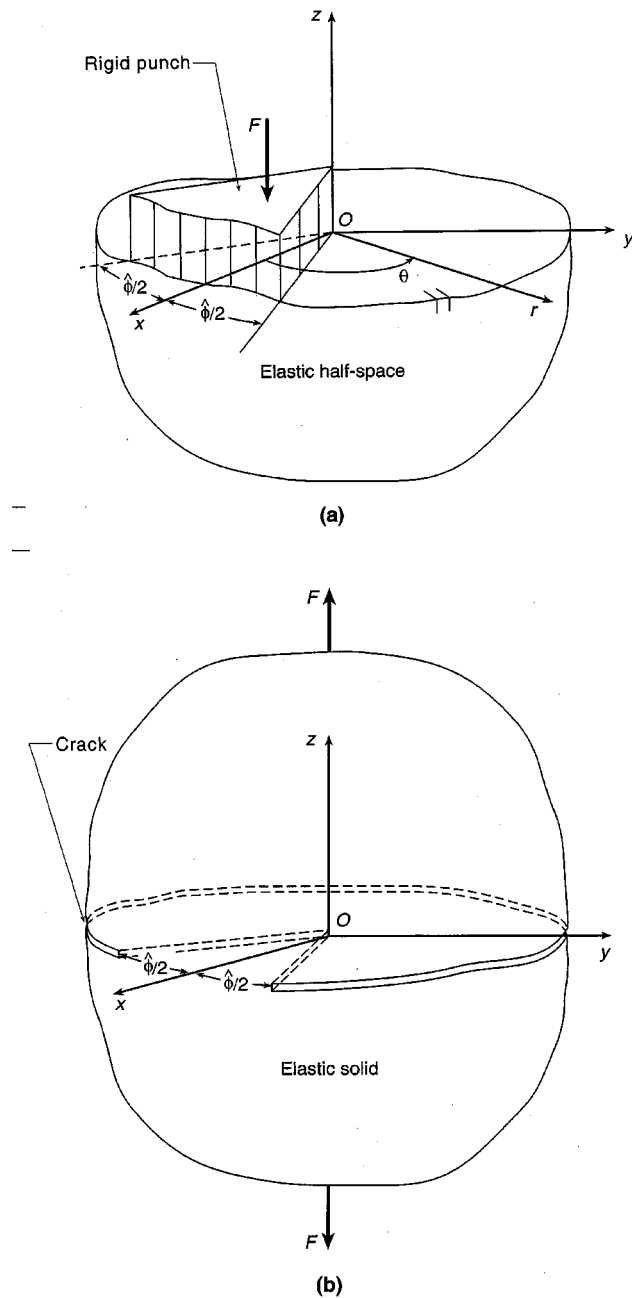


Fig. 22 a) Rigid punch with a wedge-shaped flat base pressed into an elastic half-space, b) dual crack problem

Another instance of the second class of 3D geometries involves the elastic half-space again, but this time under a flat rigid punch on the surface sector (Fig. 22a). The punch is frictionless or lubricated, and indents the half-space by an amount  $u_0$ . Hence in this problem, in general, stresses and displacements are sought throughout the half-space satisfying: the 3D field equations of elasticity, and the boundary conditions, on  $z=0$ ,

$$\begin{aligned}
 u_z &= -u_0 \text{ for } -\hat{\phi}/2 < \theta < \hat{\phi}/2 \\
 \sigma_z &= 0 \text{ for } \hat{\phi}/2 < |\theta| \leq \pi \\
 \tau_{yz} &= \tau_{zx} = 0 \text{ for } -\pi < \theta \leq \pi
 \end{aligned}
 \tag{5.39}$$

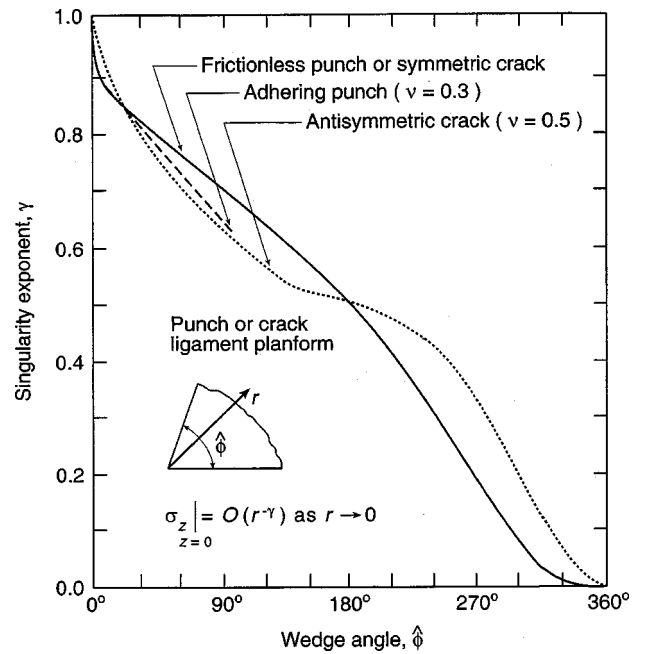


Fig. 23 Singularity exponents for varying wedge angles

all for  $0 < r < \infty$  (see Fig. 22a for coordinates). The homogeneous part ( $u_0=0$ ) of this punch problem has a dual or equivalent crack problem. The latter has a full elastic space with a crack on the  $xy$  plane when  $\hat{\phi}/2 < |\theta| \leq \pi$ , a crack ligament in the same plane when  $|\theta| < \hat{\phi}/2$  (Fig. 22b). Under symmetric loading  $F$ , this crack configuration can be treated as a half-space with boundary conditions as in (5.39) with  $u_0=0$ .

For either configuration, the potential representation given in Green and Zerna [167] reduces analysis of the singularities present to the determination of those attending a single harmonic function  $\Psi$ , with  $\Psi=0$  within the surface sector,  $\partial\Psi/\partial z=0$  without. This is a relatively simple 3D problem. Consequently, and also because of the multiple physical interpretations harmonic functions admit to, this problem has been the subject of quite a number of investigations. In chronological order, these include: Galin [171], Rvachev [172], Noble [173], Aleksandrov and Babeshko [174], Bažant [175], Walden [176], Morrison and Lewis [177], Brothers [178], Keer and Parihar [179], Ioakimidis [180], Takakuda [181], Xu and Kundu [182], and Glushkov, Glushkova, and Lapina [183]. The means of analysis in these references vary from primarily numerical to largely analytical. There is generally good agreement as to the stress singularities unearthed with these means between [173], [175–181], and [183].

The analysis that stands out in its efforts to verify singularity exponents is Morrison and Lewis [177]. Therein, in addition to comparing with a full set of earlier analyses, two independent approaches are employed to check results. These two agree to typically within 0.1%. Furthermore, subsequent analyses in Brothers [178], Keer and Parihar [179], and Takakuda [181] all display excellent agreement with

singularity exponents calculated in Morrison and Lewis [177] (to within 1%). Accordingly these are the results summarized here.

Singularity exponents  $\gamma$  for varying wedge angles  $\hat{\phi}$  are presented in Fig. 23. There  $\gamma$  is as in

$$\sigma_z|_{z=0} = O(r^{-\gamma}) \text{ as } r \rightarrow 0 \tag{5.40}$$

for  $-\hat{\phi}/2 < \theta < \hat{\phi}/2$ . For  $\hat{\phi} = 2\pi$  there is no singularity ( $\gamma = 0$ ). This is as it should be when the punch indents the entire half-space surface. For  $\hat{\phi} = \pi$ ,  $\gamma = 1/2$ . This, in conjunction with the  $\theta$ -dependence in  $\sigma_z$  on  $z=0$ , realizes inverse-square-root singularities as the edges of the punch are approached. That is, for example,

$$\sigma_z|_{z=0} = O\left(1 / \sqrt{r\left(\frac{\hat{\phi}}{2} - \theta\right)}\right) \text{ as } \theta \rightarrow \frac{\hat{\phi}}{2} \tag{5.41}$$

These inverse-square-root singularities on the edges of the punch are also present for all wedge angles  $\hat{\phi} \neq 2\pi$ . Away from  $O$ , they represent a further demonstration of the equivalence with plane strain response of Aksentian [90].

Of course, the dual crack problem has the same singularity exponents as shown for the frictionless punch in Fig. 23. In contrast to the 2D situation, however, its antisymmetric counterpart does not necessarily share the same exponents. This antisymmetric crack problem can also be treated as a half-space problem. Then the boundary conditions are, on  $z = 0$ ,

$$\begin{aligned} u_x = u_y = 0 & \text{ for } -\hat{\phi}/2 < \theta < \hat{\phi}/2 \\ \sigma_z = 0 & \text{ for } -\pi < \theta \leq \pi \\ \tau_{yz} = \tau_{xz} = 0 & \text{ for } \hat{\phi}/2 < |\theta| \leq \pi \end{aligned} \tag{5.42}$$

all for  $0 < r < \infty$ . Associated singularity exponents are calculated in Parihar and Keer [184]. These exponents depend on Poisson's ratio. For  $\nu = 0$ , they are the same as for the symmetric crack. For  $\nu \neq 0$ , they differ. Exponents for  $\nu = 0.5$  differ most and are plotted in Fig. 23 with a dotted curve. Exponents for  $\nu = 0.3$  are also given in Parihar and Keer [184].

A further configuration involving the wedge-shaped punch takes the punch to adhere to the half-space rather than to allow frictionless slip. Then the boundary conditions become, on  $z = 0$ ,

$$\begin{aligned} u_z = -u_0, u_x = u_y = 0, & \text{ for } -\hat{\phi}/2 < \theta < \hat{\phi}/2 \\ \sigma_z = \tau_{yz} = \tau_{zx} = 0 & \text{ for } \hat{\phi}/2 < |\theta| \leq \pi \end{aligned} \tag{5.43}$$

all for  $0 < r < \infty$ . This punch problem also has a dual crack problem. The latter is for an interface crack with one material being rigid.

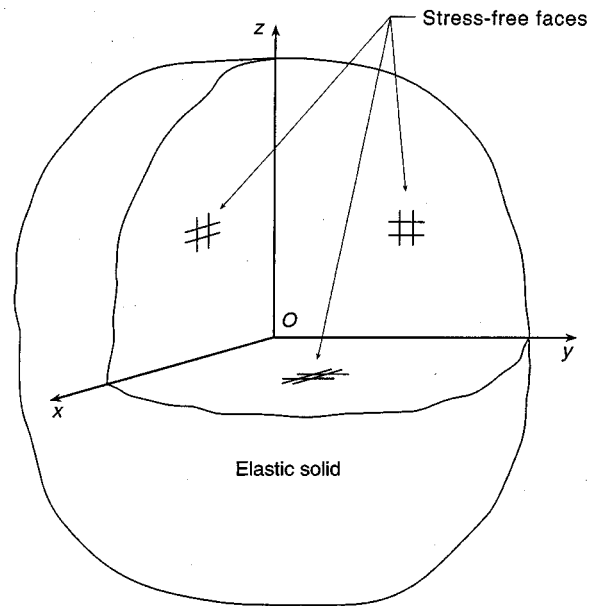


Fig. 24 Three-dimensional reentrant corner

The adhering punch problem is less tractable than the frictionless case, and leads to complex singularity exponents. The real part of such exponents is included in Fig. 23 as a broken line. For  $0 < \hat{\phi} \leq 45^\circ$ , these results are from Parihar and Keer [185]: for  $\hat{\phi} = 90^\circ$ , from Brothers [178]. These exponents are for  $\nu = 0.3$ . For  $\nu = 0.5$ , results for the adhering punch are the same as for the frictionless case. For other  $\nu$ , see Parihar and Keer [185], which also gives the imaginary parts of exponents. While the magnitude of the real part is less than the singularity exponent for the frictionless case in the range  $0 < \hat{\phi} \leq 90^\circ$  in Fig. 23, the oscillatory nature attending these complex exponents makes these singularities arguably more pathological. Again, at the edges of the punch ( $\theta \rightarrow \pm \hat{\phi}/2$ ), plane strain response occurs. That is, inverse-square-root singularities with oscillatory multipliers as in Abramov [186].

Our final instance of the second class of 3D geometries involves an elastic solid with a 3D reentrant corner. When this corner has faces which are perpendicular to one another, the configuration is tantamount to removing an octant from a full elastic space (Fig. 24; sometimes termed the Fichera vertex). This geometry can be viewed as a wedge with a vertex with an angle of  $3\pi/2$  and which follows a path which turns abruptly through  $\pi/2$  at  $O$ . Hence it qualifies for our second class. When the corner is stress free, the boundary conditions are:

$$\begin{aligned} \sigma_x = \tau_{xy} = \tau_{zx} = 0 & \text{ at } x=0 \text{ for } y>0 \text{ and } z>0 \\ \sigma_y = \tau_{yz} = \tau_{xy} = 0 & \text{ at } y=0 \text{ for } x>0 \text{ and } z>0 \\ \sigma_z = \tau_{zx} = \tau_{yz} = 0 & \text{ at } z=0 \text{ for } x>0 \text{ and } y>0 \end{aligned} \tag{5.44}$$

where the coordinate system used is as in Fig. 24. The dominant singularities that can be present at  $O$  for this stress-free corner are estimated in Abdel-Messieh and Thatcher [187],

Schmitz, Volk, and Wendland [188], and Glushkov, Glushkova, and Lapina [183]. There is good agreement between the first and third sources of numerical values of singularity exponents. For  $\nu$  ranging from 0.2 to 0.5, dominant singularity exponents from both sources exceed 0.58. This is stronger than the corresponding 2D reentrant corner (dominant  $\gamma = 0.46$ ). Two-dimensional plane strain and antiplane shear singularities can be expected to be possible away from  $O$  (from Aksentian [90]).

### 5.3 Three-dimensional geometries with crack-surface intersections

As an initial instance of the *third class of 3D geometries*, we consider an elastic half-space loaded transversely to a crack within it, with the crack intersecting the half-space's free surface (Fig. 21). We begin with when the crack front intersects this surface at right angles ( $\bar{\phi} = \pi/2$  in Fig. 21). Under Mode I loading, symmetry enables attention to be confined just a quarter-space ( $y > 0, z < 0$  in Fig. 21). Hence in this problem, in general, stresses and displacements are sought throughout the quarter-space satisfying: the *3D field equations of elasticity; stress-free crack conditions* on the crack flank,

$$\sigma_y = \tau_{yz} = \tau_{xy} = 0 \quad \text{on } y = 0 \quad (5.45)$$

for  $x > 0$  and  $z < 0$ ; *symmetry conditions* ahead of the crack,

$$v = 0, \quad \tau_{yz} = \tau_{xy} = 0, \quad \text{on } y = 0 \quad (5.46)$$

for  $x < 0$  and  $z < 0$ ; and *free-surface conditions* on the quarter-space surface,

$$\sigma_z = \tau_{zx} = \tau_{yz} = 0 \quad \text{on } z = 0 \quad (5.47)$$

for all  $x$  and for  $y > 0$  (see Fig. 21 for the rectangular coordinate system used). As this particular 3D configuration is going to merit extensive discussion, hereafter we simply term it *the 3D crack problem*.

Over the years, there have been numerous contributions to the literature which address various aspects of the 3D crack problem—see Panasyuk, Andrejkiv, and Stadnik [189,190] for reviews which together cite some 500 related references. Focusing on singularity identification at the crack-surface intersection point ( $O$  in Fig. 21), Sih [191] provides a review through the 1970s. In chronological order, contributions on this aspect since include: Folias [192], Kawai, Fujitani, and Kumagai [193], Benthem [194], Bažant and Estenssoro [195–197], Sinclair [198], Benthem [199], Yamada and Okumura [200], Burton et al [201], Takakuda [181], Shaofu, Xing, and Qingzhi [202], Shivakumar and Raju [203], Zhu [204], Barsoum and Chen [205], Ghahremani [206], Leung and Su [207,208], Su and Sun [209], and Glushkov, Glushkova, and Lapina [183]. Together these papers are testimony to the challenge of the preceding asymptotic problem. While none of these papers solves the 3D crack problem completely analytically and correctly for all values of Poisson's ratio, a stress singularity at the intersection point has been clearly identified at this time. This identification relies on several papers, and on both largely analytical treatments and prima-

rily numerical ones. We summarize the singularity so found next, then offer some comments on other analyses that might appear to disagree with it to varying degrees.

For  $\bar{\phi} = \pi/2$  in Fig. 21, the crack front coincides with the negative  $z$  axis. At the outset, then, we note that for  $z < 0$  the 3D crack of Fig. 21 belongs to our first class of 3D geometries. Thus Aksentian [90] applies and the stress singularity for 2D plane strain should result at such locations. That is,

$$\sigma = O(r^{-1/2}) \quad \text{as } r \rightarrow 0 \quad \text{for } z < 0 \quad (5.48)$$

wherein  $\sigma$  continues as any stress component and  $r$  is the radial coordinate in Fig. 21. It follows that any investigation of the singular response at  $O$  should include the singularity in (5.48) if the crack front is approached away from  $O$ .

Returning attention to the singular response right at  $O$ , the investigation that has led to a clear identification of stress singularity there is Benthem [194]. In [194], stresses are assumed to be separable in spherical polar coordinates (Fig. 21), with

$$\sigma = \rho^{-\gamma} f(\theta) g(\psi) \quad \text{as } \rho \rightarrow 0 \quad (5.49)$$

Using Boussinesq-Papkovich-Neuber potentials then enables the 3D field equations of elasticity to be complied with and yields trigonometric functions for  $f(\theta)$ , associated Legendre functions for  $g(\psi)$ . Suitably selecting and combining these solutions satisfies exactly the symmetry conditions (5.46) and the stress-free crack conditions (5.45). The only remaining conditions, the stress-free surface conditions (5.47), are then satisfied approximately with sums of series of solutions complying with all other requirements (see [194] for details of the numerical method adopted to this end). Hence, largely an analytical approach which could be viewed as an extension to three dimensions of that in Williams [2] for two dimensions.

Results recover (5.48) on the crack front away from  $O$  as they should. They also recover the plane strain stresses with their inverse-square-root singularity ( $\gamma = 1/2$ ) when  $\nu = 0$ , the one value of Poisson's ratio for which plane strain stresses satisfy the stress-free surface conditions. For other values of  $\nu, \gamma < 1/2$  and the singularity is weaker. This general trend of  $\gamma = 1/2$  for  $\nu = 0$  with  $\gamma < 1/2$  for  $\nu > 0$  is confirmed in a number of investigations subsequent to Benthem [194]: Bažant and Estenssoro [195–197], Benthem [199], Yamada and Okumura [200], Burton et al [201], Takakuda [181], Shaofu, Xing, and Qingzhi [202], Shivakumar and Raju [203], Barsoum and Chen [205], Ghahremani [206], and Glushkov et al [183].

The precise values of the singularity exponent  $\gamma$  for  $\nu > 0$  in Benthem [194] are confirmed in Benthem [199] with what is in essence a direct numerical analysis. The independent approach in Benthem [199] leads to values that typically differ by 1/3% and have a maximum difference of 1 1/2%. Further confirmation of the precise values of  $\gamma$  for  $\nu > 0$  in Benthem [194] is provided by the analyses in Bažant and Estenssoro [195,197], Takakuda [181], and Ghahremani [206]. The average difference between numerical values given in the first three references and corresponding values

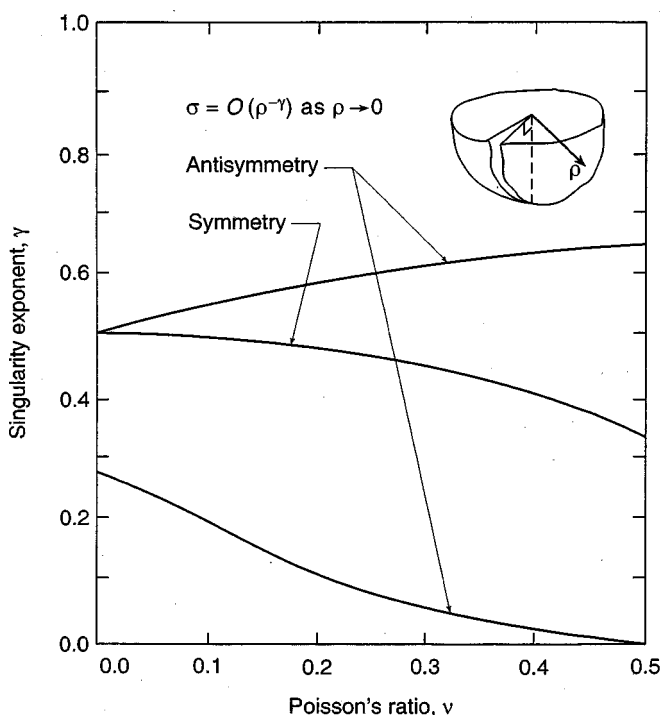


Fig. 25 Singularity exponents for varying Poisson's ratios for a quarter-plane crack in an elastic half-space

in Benthem [194] is less than 1/20%, while the maximum difference is less than 1/10%. In the fourth reference, a graphical comparison is made and shows all the  $\gamma$  values in Benthem [194] lying on a  $\gamma$ -value curve computed in Ghahremani [206]. All told, there is now excellent confirmation of the singularity exponents in Benthem [194]. Accordingly, we present these singularity exponents here in Fig. 25.

While, at this time, there would appear to be no doubt as to the existence of a stress singularity of the form of (5.49) with exponents as in Fig. 25, this does not mean that there cannot be other singular fields for the 3D crack problem. No completeness argument is advanced in the literature for stresses of the form of (5.49): Absent such, other singularities are not precluded. Conversely, absent a companion completeness argument, another form of singularity for the 3D crack problem does not invalidate the singularity identified in Benthem [194].

There are, in fact, quite a number of other approaches in the literature aimed at identifying alternative stress singularities to that of Benthem [194]. We review these efforts in chronological order next.

Folias [192] attempts the ambitious task of finding an analytical solution for a truly 3D, *global*, crack configuration. This configuration entails a through crack, in a plate of finite thickness, with crack fronts orthogonal to the stress-free plate faces and under transverse far-field tension. In the vicinity of where one of the crack fronts intersects a plate face, the 3D crack problem is contained. The analysis employs the symbolic method of Lur'e (Section 3.2, [210]). Results include an explicit expression for the singular part of  $\sigma_z$  at the crack-surface intersection, as well as an asymptotic charac-

terization of the stress and displacement fields there. In terms of the spherical polar coordinates of Fig. 21, the first has

$$\sigma_z = K \frac{\cos \psi \cos((1 + 2\nu)(\pi - \psi))}{\rho^{2\nu} \sqrt{\rho} \sin \psi} \cos \frac{\theta}{2} \text{ as } \rho \rightarrow 0 \quad (5.50)$$

where  $K$  is a constant (independent of  $\rho$ ,  $\psi$ , and  $\theta$ ), while the second has

$$\sigma = O(\rho^{-1/2-2\nu}), \quad u = O(\rho^{1/2-2\nu}), \text{ as } \rho \rightarrow 0 \quad (5.51)$$

where  $u$  is any displacement component. Away from the crack-surface intersection point, (5.50) recovers the inverse-square-root singularity that must occur at the crack front (that is, for  $\psi \rightarrow \pi$ ,  $\rho \neq 0$ ). For  $\nu = 0$ , (5.50) recovers an inverse-square-root singularity as  $\rho \rightarrow 0$ , the same singular character as in Benthem [194]. For  $\nu \neq 0$ , the singularity in (5.50) is stronger. This is in contrast to the singularity in Benthem [194]. Indeed for  $\nu > 1/4$ , even the displacements are unbounded. This has led to some discussion: Benthem and Koiter [211], Folias [212,213].

Unbounded displacements are even less physically appropriate than singular stresses. While singular fields with unbounded displacements are possible for the 2D crack, fortunately one can prove that they need never participate (via the completeness argument in Gregory [11]). Unfortunately, no such proof currently exists for 3D cracks. Therefore, the unbounded displacements of Folias [192] cannot be ruled out as possible participants in the 3D crack problem, despite their lack of physical appeal.

There is, though, a valid objection to the singularity given in Folias [192] in its present form. By virtue of  $z=0$  being free of shear tractions, the third stress equation of equilibrium has  $\partial \sigma_z / \partial z = 0$  at  $z=0$ . Equivalently, in terms of the spherical polar coordinates of Fig. 23,

$$\frac{1}{\rho} \frac{\partial \sigma_z}{\partial \psi} = 0 \text{ at } \psi = \pi/2 \quad (5.52)$$

From (5.50),

$$\frac{\partial \sigma_z}{\partial \psi} = K \frac{\sin \pi \nu}{\rho^{2\nu} \sqrt{\rho}} \cos \frac{\theta}{2} \text{ at } \psi = \pi/2 \quad (5.53)$$

Aside for the case  $\nu = 0$ , then, equilibrium is not complied with by the explicit singular stress given in Folias [192]. Of course, the method of solution construction adopted in [192] assures satisfaction of the equilibrium equations by the stress fields in toto. Thus there must be further contributions to the stress field in Folias [192], not to date explicitly extracted, that combine with (5.50) to restore this compliance. In order to do this, these further contributions must share the same dependence on  $\rho$  as in (5.50). Consequently there is the possibility they may completely remove singular fields which behave as in (5.51). Not to say that this has to happen, just that it could. As a result, Folias [192] cannot be relied on for singularity identification in the 3D crack problem.

Kawai, Fujitani, and Kumagai [193] attempts to identify local stress singularities for the 3D crack problem. This paper assumes the stresses can be represented as in (5.49) and Benthem [194]. Thereafter it determines forms for the

stresses and displacements so that the field equations of elasticity are complied with: These forms are similar to those in Benthem [194]. Then it proceeds to satisfy the symmetry conditions (5.46) and the free-surface conditions (5.47) exactly, the stress-free crack conditions (5.45) approximately: This is in contrast to Benthem [194] which satisfies the free-surface conditions approximately. Results include one singularity which is similar to that in Benthem [194] in that it shares diminishing strength with increasing  $\nu$  having started from an inverse-square-root singularity when  $\nu=0$ . Exponent values for this singularity, however, do differ appreciably from those in [194] (by 40% when  $\nu=1/2$ ). Results also include a stress singularity which is stronger than an inverse-square-root singularity for all values of  $\nu$ . If a valid result, this last would represent an additional and distinctly different singularity from that identified in Benthem [194].

The issue of validity in Kawai et al [193] stems from its use of series of associated Legendre functions to satisfy the stress-free crack conditions. In terms of the spherical polar coordinates of Fig. 21, the series involve, for example,

$$P_{\lambda}^{-\lambda+2n+2}(-\cos \psi) = O((\pi - \psi)^{\lambda-2n-2}) \text{ as } \psi \rightarrow \pi \tag{5.54}$$

for  $n=1,2,\dots$ , and  $\lambda < 2$ .<sup>30</sup> Stresses with such terms cannot converge to zero on a plane including  $\psi = \pi$ . Moreover, such terms lead to singular stress behavior at the crack front ( $\psi \rightarrow \pi$ ) away from the crack-surface intersection that is known *not* to occur. Hence, the stress singularities in Kawai et al [193] need to have it established that they are completely free of such terms in order for them to be admissible. To date this would not appear to have been done.

Sinclair [198] attempts to identify local stress singularities for the 3D crack problem. This paper assumes that stresses are separable in cylindrical polar coordinates. It satisfies the field equations of elasticity exactly with forms comprised of elementary functions. It also satisfies the stress-free crack and symmetry conditions, (5.45) and (5.46), exactly. However, it only attempts to satisfy the free-surface conditions (5.47) for  $\sigma_z$  with a term which is itself asymptotically zero as the crack tip on the surface is approached (the actual residual being  $O(r^{3/2})$  as  $r \rightarrow 0$  thereon). Results for the dominant singularity have

$$\hat{\sigma} = O(z^2/\sqrt{r}) \text{ as } r \rightarrow 0 \tag{5.55}$$

wherein  $\hat{\sigma}$  is any stress component other than  $\tau_{\theta z}$  and  $\tau_{rz}$ , these last being nonsingular (see Fig. 21 for the cylindrical polar coordinates used). Away from the crack-surface intersection point, the appropriate inverse-square-root singularity is recovered at the crack front. For  $\nu=0$ , the known inverse-square-root singularity is not recovered in the surface at  $z=0$ . The general trend of a weakening of singular response as the free surface is approached is reflected in (5.55), but now by a reducing singularity coefficient rather than a reducing singularity exponent.

The absence of the plane strain singularity for  $\nu=0$  does not necessarily invalidate a singularity identified for the 3D crack. While completeness (Gregory [11]) and uniqueness (Knowles and Pucik [12]) mean that any loading of the 3D crack which is independent of  $z$  must produce these plane strain fields when  $\nu=0$ , this does not have to be the case when loading is not independent of  $z$ .

The real objection to the simple analysis in Sinclair [198] lies in its satisfaction of the free-surface conditions. Boundary conditions are known to effect the nature of stress singularities considerably in elasticity. Hence, satisfying the free-surface conditions in only an asymptotic sense is quite likely to change the nature of any singularity found. Thus, while results in Sinclair [198] may indicate a possible trend for singularities in the 3D crack problem, they fall far short of actually identifying a possible stress singularity.

Shivakumar and Raju [203] attempts to identify two local stress singularities for the 3D crack problem. In this paper the singular stresses are assumed to admit representation by

$$\sigma = F(\theta, z)r^{-1/2} + G(\psi, \theta)\rho^{-\gamma} \text{ as } r \rightarrow 0 \text{ or } \rho \rightarrow 0 \tag{5.56}$$

where  $F$  and  $G$  are continuous functions.<sup>31</sup> Analysis is via finite elements with fitting used to estimate singularities present. This fitting is undertaken for each term in (5.56) separately. Away from the crack-surface, results recover the inverse-square-root singularity that must occur. For  $\nu=0$  they recover the known plane strain singularity (automatically, by the superposition employed). For  $\nu \rightarrow 0$ , they indicate that the function  $F$  is zero or negligibly small. For  $\nu > 0$ , they also estimate singularity exponents which are in good agreement with Benthem [194] (average difference 2/3%, maximum difference 3/2%).

Zhu [204] attempts to identify local stress singularities for the 3D crack problem. This paper assumes stresses are separable in cylindrical polar coordinates. Analysis is via a combination of two solutions. The first is for a crack in plane strain. The second removes surface tractions at  $z=0$  from the first. It is derived from a single harmonic potential (after Section 5.7, Green and Zerna [167]). The 3D aspects of the analysis are limited to the plane  $z=0$ . Within this plane, all field equations and boundary conditions in the 3D crack problem are satisfied. Unfortunately, in meeting the shear-free conditions on the crack flanks, continuity of crack flank displacements is required in the second solution. When surface tractions are applied to a cracked half-space, such continuity is generally not the case. Hence the analysis is demonstrably incomplete. Away from the crack-surface intersection point, the inverse-square-root singularity that must occur is recovered automatically by construction. For  $\nu=0$ , the known plane strain singularity is likewise recovered. For  $\nu \rightarrow 0$ , results show a persistence of the inverse-square-root singularity in the free surface at  $z=0$ . The coefficient of the singularity is reduced from that away from the

<sup>30</sup>See, eg, Ch 8, Abramowitz and Stegun [139], for the asymptotic behavior given in (5.54).

<sup>31</sup>Observe, therefore, that the second term in (5.56) is not the same as in Benthem [194]. In [194],  $G(\psi, \theta)$  contains terms which are  $O((\pi - \psi)^{-1/2})$  as  $\psi \rightarrow \pi$ .

surface by a factor of  $(1 - \nu - 2\nu^2)$ . This factor is 1 when  $\nu=0$ , appropriately,  $5/8$  when  $\nu=1/4$ , and 0 when  $\nu=1/2$ .

While all of analysis in Zhu [204] is correct, the 3D solution found is really only valid in the surface  $z=0$ . If instead it held for all  $z$  in the half-space, it would be possible to simply take the stresses it produced on the surface of a subregion within the half-space as prescribing tractions thereon and so pose a problem for which the fields in Zhu [204] are applicable. Absent a solution for other than  $z=0$ , however, there is no guarantee that the fields in Zhu [204] ever participate in an actual 3D crack problem. They could, though, in which case they would represent an additional and complementary singularity to that found in Benthem [194].

Leung and Su [207] attempts to identify local stress singularities for the 3D crack problem. This paper superimposes the singular crack-tip stresses in plane strain with stresses that are assumed to be separable in spherical polar coordinates. The latter have to have an inverse-square-root singularity to effect the removal of the stresses from the former on the surface at  $z=0$ . They are analyzed with finite elements. By construction, appropriate singular behavior results away from the crack-surface intersection point and for  $\nu=0$ . For  $\nu \rightarrow 0$ , a drop in the coefficient of the inverse-square-root singularity is indicated at the free surface.

Leung and Su [208] attempts the same identification as [207], but primarily by analytical means rather than numerical. After superposing the plane strain fields, the approach for the residual problem follows that in Zhu [204] and uses a single harmonic potential. In fact, the approach in Leung and Su [208] could be interpreted as an attempt to extend the results of Zhu [204] for the surface into the interior. In making this attempt, however, the approach follows that in Kawai et al [193] rather than that in Benthem [194]. As a result, in its present form it suffers from the same lack of convergence and from the introduction of inadmissible singular stresses on the crack front. Consequently, the results in Leung and Su [208] cannot be accepted at this time.

Su and Sun [209] attempts to identify local stress singularities in a global configuration entailing a through crack in a plate (the same geometry as in Folias [192]). This paper employs an interesting decomposition of the fields involved into a plane stress state, a shear stress state, and a Papkovitch-Fadle state. Each of these states is assumed to be separable in cylindrical polar coordinates. Series of solutions are employed. The analysis is analytical with the minor exception of the routine numerical determination of the eigenvalues used in the Papkovitch-Fadle expansion. Results recover the appropriate singular behavior away from the crack-surface intersection point and for  $\nu=0$ . For  $\nu>0$ , the dominant singular character identified is the same as in (5.55). As noted in (5.55) et seq,  $\tau_{\theta z}$  and  $\tau_{rz}$  are nonsingular. Hence they are not explicitly given in Su and Sun [209]. They are needed, though, to ensure satisfaction of the equilibrium equations by the singular stress components. Unfortunately, when these shear stress components are derived from the displacements given in Appendix I of Su and Sun [209], it transpires that they are not zero on the plate faces. This is in violation of the free-surface conditions. If this shortcoming in the promising

approach in Su and Sun [209] were to be rectified, it would appear that this paper would lead to the first essentially analytical solution for a singularity in the 3D crack problem. At this time, however, it cannot be accepted as such.

In sum for the 3D crack problem, the current state of research findings is as follows. Away from the crack-surface intersection point, an inverse-square-root stress singularity occurs, and only it occurs. "Away" includes arbitrarily close to the point, but not at it. Consequently, all singularities for the 3D crack problem may be viewed as characterizing the participation of this inverse-square-root singularity as the free surface is approached. Viewed in this light, Benthem [194] provides the only truly confirmed singularity identified to date, with

$$\sigma = O\left(\frac{\rho^{1/2-\gamma}}{\sqrt{\rho \sin \psi}}\right) \text{ as } \rho \rightarrow 0 \quad (5.57)$$

In (5.57), the spherical polar coordinates are as in Fig. 21 and the singularity exponent  $\gamma$  as in Fig. 25. For  $\nu=0$ ,  $\gamma=1/2$ . Then the crack-tip singularity for plane strain applies. For  $\nu \neq 0$ ,  $\gamma < 1/2$ . Hence the participation of the inverse-square-root singularity goes to zero in the free surface for the singularity identified in Benthem [194]. There may be other singularities for the 3D crack, some of which may not have this participation go to zero in the free surface. The existence of these alternative singularities would not invalidate the singularity in Benthem [194]. As of now, any such other singularities have yet to be properly identified.

A further instance of the third class of 3D geometries is the antisymmetric counterpart of the 3D crack problem. Herein the formulation is the same as for the 3D crack problem except that the symmetry conditions (5.46) are exchanged for antisymmetry conditions:

$$u = w = 0, \quad \sigma_y = 0, \quad \text{on } y = 0 \quad (5.58)$$

for  $x < 0$  and  $z < 0$ , where  $u$  and  $w$  are displacements in the  $x$  and  $z$  directions, respectively.

Benthem [199] analyzes the antisymmetric 3D crack via a finite difference approach. Singularity exponents appear to have converged to within about 2% in Benthem [199]. Two branches of singularity exponents for varying  $\nu$  are identified by this means. One branch is for a stronger singularity than the symmetric case, one weaker. The exponents for the stronger singularity are confirmed in Bazant and Estenssoro [196,197] (typically to within 2%). They are also confirmed in Ghahreimi [206]. Exponents for both the stronger and weaker singularities from Benthem [199] are included in Fig. 25 for varying Poisson's ratios.

Alternative singularities may exist for the antisymmetric 3D crack problem. Again these would not invalidate those identified in Benthem [199]. An indication of a possibility in this regard is given in Meda et al [214] which uses the very limited approach of Sinclair [198] to arrive at singular character as in (5.55). The same singular character is obtained by different means in Appendix II, Su and Sun [209], but insufficient details are furnished therein to enable checking.

As two last instances of the third class of 3D geometries, we consider two further crack-intersection configurations.

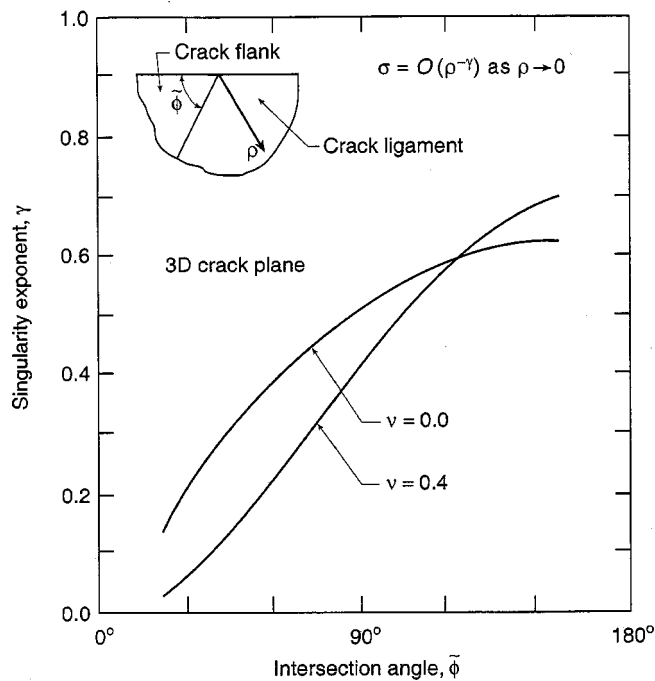


Fig. 26 Singularity exponents for varying angles of intersection for a symmetrically-loaded crack in an elastic half-space

The first further crack-intersection configuration entails crack fronts which are not orthogonal to the free surface ( $\tilde{\phi} \neq \pi/2$  in Fig. 21). Motivated by a search for an energy release rate  $G_I$  satisfying  $0 < G_I < \infty$  in the free surface, Bažant and Estenssoro [195–197] seek an angle  $\tilde{\phi}$  such that  $\gamma = 1/2$ . This leads to  $\tilde{\phi} > \pi/2$  for the symmetric case. Values of such  $\tilde{\phi}$  are given in Bažant and Estenssoro [197] for  $\nu$  ranging from 0.0 to 0.4. These values are confirmed in Burton et al [201] and Takakuda [181] (typically agreement is to within 1%). The antisymmetric case is also treated in Bažant and Estenssoro [197]. This leads to  $\tilde{\phi} < \pi/2$ . Singularity exponents other than  $\gamma = 1/2$  are tabulated in Takakuda [181] for  $0 \leq \nu \leq 1/2$  and other  $\tilde{\phi}$  under symmetric loading. For  $\nu = 0.0, 0.4$ , these results are illustrated in Fig. 26.

The second and final, further, crack-surface intersection configuration is as for the 3D crack problem but now with two materials comprising the half-space. Singularities for this 3D interface crack are identified in Bažant and Estenssoro [197], Barsoum and Chen [205], and Ghahremani and Shih [215].

#### 5.4 Other field equations

While it falls outside the stress singularities in classical elasticity reviewed so far, it is nonetheless appropriate in closing this review to offer a few comments on the effects of other field equations on singularities. It is appropriate because the singularities attending other field equations are quite often directly related to those in classical elasticity. The intent here is to indicate this sort of connection, rather than extensively explore it. Accordingly, references cited here are by way of example, rather than anything approaching a comprehensive listing.

Some remarks on the effects of other field equations on singularities are given in Part I, Section 2.1. These concern the possible removal of stress singularities by relaxing any of the three linearizations of classical elasticity. These three linearizations are: the small stress assumption that stresses remain below yield levels, the small strain assumption that strains are linearly related to displacement gradients, and the small deflection assumption that the loads act in their entirety on the undeformed state. Relaxing the first two linearizations entails switching to the field equations of *elastoplasticity* and *large strain elasticity*, respectively. A relaxation of the third can be made by applying the field equations of classical elasticity, together with loading conditions, *on deformed states* instead of undeformed. For each of these modifications to the field equations, analysis is nonlinear and consequently less tractable than that for classical elasticity. The general finding of such analysis is that relaxing any of the three linearizing assumptions of classical elasticity does lead to a different singular character. Further, typically the resulting singular character is less nonphysical (for example, the replacement of oscillatory stress singularities for the interface crack with a nonoscillatory singularity). Occasionally a singularity is even removed (for example, the singularity at an adhesive butt joint present in classical elasticity is absent from a large strain treatment).<sup>32</sup> However, the great majority of singularities in classical elasticity persist, albeit in altered forms, for any of these modifications to the field equations. Thus none of these modifications is really successful when it comes to removing stress singularities from classical elasticity.

Here we consider some other changes to the field equations of classical elasticity. We distinguish these modifications as follows: changes in the stress equations of equilibrium, changes in the stress-displacement relations, and changes to both. We consider each type of modification in turn next.

As a first simple change to the stress equations of equilibrium, we consider the effects of introducing *body-force fields*, heretofore taken as null. Then, for example, the first equilibrium equation for in-plane loading in (2.2) becomes

$$\frac{\partial \sigma_r}{\partial r} + \frac{1}{r} \frac{\partial \tau_{r\theta}}{\partial \theta} + \frac{\sigma_r - \sigma_\theta}{r} + F_r = 0 \tag{5.59}$$

where  $F_r$  is the radial component of the body-force field. What is apparent from (5.59) is that for body forces to effect stress singularities which behave as  $O(r^{-\gamma})$  as  $r \rightarrow 0$ , they themselves have to behave as  $O(r^{-\gamma-1})$ . Such body forces would not seem likely to be needed in practice. Hence stress singularities in elasticity can be expected to be unaffected by the presence of body-force fields.<sup>33</sup>

There is one possible exception to the foregoing in two dimensions. This is the line-load body force. For such a body-force field,

$$F_r = F_A / r, \quad F_\theta = 0 \tag{5.60}$$

<sup>32</sup>As explained in Part I, Section 2.1, the introduction of perfect plasticity does not really qualify as a modification that removes a singularity.

<sup>33</sup>Plate bending singularities are similarly unaffected by the presence of plate face loading: see Sections 4.3 and 4.4.

where  $F_A$  is a force per unit area. Then directly from (5.59) and the second of (2.2),

$$\sigma_r = \sigma_\theta = -F_A \ln(r/r_c), \quad \tau_{r\theta} = 0 \quad (5.61)$$

wherein  $r_c$  is some characterizing radius introduced to ensure dimensional consistency. The field in (5.61) also satisfies the stress equations of compatibility: It therefore complies with all the field equations of elasticity. Analogously in three dimensions, a point-load body force leads to a stress singularity which behaves as  $O(\rho^{-1})$  as  $\rho \rightarrow 0$ . Aside from like instances, however, stress singularities in elasticity can be expected to be the same with body forces as without.

As a second change to the stress equations of equilibrium we consider the introduction of inertial terms. Then these equations become *equations of motion*. This change can be viewed as mathematically equivalent to introducing a body-force field. For example, in (5.59), set

$$F_r = -\rho_m \frac{\partial^2 u_r}{\partial t^2} \quad (5.62)$$

wherein  $\rho_m$  is the mass density and  $t$  is time. Then the equation of motion in the radial direction is recovered. Similarly the equation of motion in the angular direction can be recovered. Accordingly we can expect singularities attending equations of motion to be similar to those for elastostatics with body forces.

As an initial instance of dynamic response, we consider the case of *vibrations* of elastic media. If the vibratory motion has frequency  $\omega$ , then one may take

$$u_r = \hat{u}_r(r, \theta) \sin \omega t \quad (5.63)$$

Assuming the same vibratory dependence for the other displacement component and the stresses enables  $\sin \omega t$  and the time dependence to be factored out of the equations of motion. Then we have exactly the same equations as for the introduction of body forces. Consequently no changes to stress singularities from those in classical elasticity are to be expected when vibrations are introduced. That this is so is demonstrated for antiplane shear in Sagochi [216]. It is further demonstrated for out-of-plane bending within fourth-order theory in Leissa, McGee, and Huang [121], and within sixth-order theory in Huang, McGee, and Leissa [134].<sup>34</sup>

For the more general case of *elastodynamic* response wherein motion is transitory rather than vibratory, the same sort of correspondence should occur whenever the stress and displacement fields are separable in their spatial and temporal dependences. This separable nature need not be with respect to a stationary coordinate system for a correspondence to hold. A demonstration is given in Achenbach and Bažant [218] for propagating cracks. For both antiplane shear and plane strain, the inverse-square-root stress singularity of elastostatics is recovered. Now, though, the  $\theta$ -dependence is only the same as the elastostatic case in the limit as the speed of crack propagation goes to zero.

Turning to changes to the stress-displacement relations, we first consider the effects of introducing temperature fields. The resulting field equations of *thermoelasticity* can be couched so that they differ from those of classical elasticity only in the stress-displacement relations (see, eg, Section 1.3, Nowacki [219]). The same field equations can be recast using the Duhamel-Neumann analogy (Section 1.9, [219]). Then they reveal that the singularities in stationary thermoelasticity are the same as in classical elasticity provided two possible additional sources of singularity are admitted. The first additional source is the action of a normal traction of magnitude  $c_T T$ , where  $c_T$  is a material constant (proportional to the material's linear coefficient of thermal expansion and its bulk modulus), and  $T$  is the temperature field present. The second additional source is an effective body-force field. In two dimensions, the latter can be expressed by

$$F_r = -c_T \frac{\partial T}{\partial r}, \quad F_\theta = -\frac{c_T}{r} \frac{\partial T}{\partial \theta} \quad (5.64)$$

where  $F_\theta$  is the  $\theta$ -component of the body force. It follows that, in two dimensions, the additional singularities so produced come from constant normal tractions and the possibility of a line-source temperature field. The first can produce logarithmic singularities as in Section 2.4. The second entails  $T$  of  $O(\ln r)$  as  $r \rightarrow 0$ , hence a line-load body force and logarithmic singular stresses as in (5.61). In three dimensions analogous results hold. For an elastic half-space with a constant temperature on a surface rectangle and zero temperature elsewhere on the surface, stresses can be obtained from Section 2.3, [219]. These stresses have logarithmic singularities at the corners of the rectangle (cf, [164]). At a point source in three dimensions, the temperature and stresses are  $O(\rho^{-1})$  as  $\rho \rightarrow 0$  (see, eg, Section 2.12, [219]). In addition, all the other singularities in classical elasticity can be present in thermoelasticity.<sup>35</sup>

A different type of modification to the stress-displacement relations results from varying elastic moduli. Three such variations are entertained to a limited degree here: variations with time, variations with position, and variations with direction.

Elastic moduli can vary with time so as to reflect the physical phenomena of creep and relaxation. When such *viscoelastic* variations are consistent with the constraints needed for the correspondence principle to hold, the singular character in classical elasticity carries over to viscoelasticity. If the singular stresses in elasticity are independent of elastic moduli, identical singular stresses occur in viscoelasticity. If the singular stresses in elasticity are dependent on elastic moduli, singular stresses have the same singularity strength or exponent in viscoelasticity. Now, though, the participation of different parts of the singularity coefficient can vary in different ways with time. A statement of the correspondence principle and a demonstration of its implications for the singular stresses attending a point load normal to a half-space

<sup>34</sup>While the inclusion of vibratory response leaves singularities unaltered, the presence of singularities can alter vibratory response: see Leissa [217].

<sup>35</sup>The situation is more complex than this limited discussion would indicate when multiple materials are present in thermoelasticity. Then the added discontinuities attending jumps in thermal conductivities can have associated stress singularities. See, for example, Yan and Ting [220] and Yang and Munz [221].

are provided in Lee [222]. Further demonstrations of the correspondence between elasticity and viscoelasticity singularities are given in Williams [223] for a crack.

When elastic moduli vary with position as piecewise constants, Sections 3, 4.2, and 4.3 summarize the numerous related studies in the literature for such *inhomogeneous elastic media*. The general finding of these studies is that the introduction of additional discontinuities attending abrupt changes in elastic moduli increases both the occurrence and the strength of stress singularities. This does not have to be so, though. Occasionally the singularity associated with a discontinuity already present in a configuration can be offset by the singularity associated with an added discontinuity in elastic moduli (see, eg, the butt joint in Section 3.3).

When elastic moduli vary with position other than as piecewise constants, there are relatively few studies in the literature. However, for the simple case of antiplane shear, it is straightforward to bound the effects of a radial dependence of the shear modulus. Taking the shear modulus to vary as

$$\mu = \mu_0 (r/r_c)^\varepsilon \quad (5.65)$$

for  $|\varepsilon| \ll 1$ , provides two extremes. For  $\varepsilon > 0$ ,  $\mu \rightarrow 0$  as  $r \rightarrow 0$ ; for  $\varepsilon < 0$ ,  $\mu \rightarrow \infty$  as  $r \rightarrow 0$ . Then, following the analytical path laid out in Section 4.1, leads to

$$\gamma = 1 - \frac{\pi}{\phi} - \frac{\varepsilon}{2}, \quad \gamma = 1 - \frac{\pi}{2\phi} - \frac{\varepsilon}{2} \quad (5.66)$$

as  $\varepsilon \rightarrow 0$ , for the dominant singularity exponents for non-mixed, mixed problems, respectively. Hence the singularity exponent is reduced when the modulus softens to zero ( $\varepsilon > 0$ ), and it is increased when the modulus stiffens to infinity ( $\varepsilon < 0$ ). This type of response is consistent with findings in general in this review, namely that increasing stiffness typically increases singular character. It is, though, for an extreme variation in moduli. And it is not that dramatic given this extreme variation. This suggests that the dependence of stress singularities on more realistic radial variations of elastic moduli may be slight if any.

To investigate this suggestion further, we take

$$\mu = \mu_0 + \mu_1 \frac{r}{r_c} \quad (5.67)$$

This choice requires  $u_z$  be taken as a series of separable functions with increasing powers of  $r$  in implementing the analytical approach in Section 4.1 instead of just a single separable term. Even so, the same results for exponents are obtained as in Section 4.1 (viz, as in (5.66) with  $\varepsilon = 0$ ). That is, the linear radial dependence of the shear modulus in (5.67) leaves singularity exponents unchanged from those for a constant shear modulus. By a like means, the same result can be expected to hold for elastic plates in extension.

The third and final variation in elastic moduli that we consider is to allow them to change with direction. Hence we admit *anisotropic* effects. Ting [224], Chapter 9, furnishes a clear exposition of singularity identification in anisotropic elasticity, together with an extensive set of related references. The general finding is that the additional discontinuities which can attend anisotropy can have associated stress sin-

gularities which increase the singular character over that found in classical elasticity. Occasionally additional singular stresses can offset those in isotropic elasticity (cf, a bimaterial versus a single material). An example of such offsetting is given in Ting [225].

As our last modification to the field equations, and one which effects both the stress equations of equilibrium and the stress-displacement relations, we consider the introduction of *couple stresses*. Field equations for a linearized theory including couple stresses may be found in Muki and Sternberg [226]. The general finding for such a theory is that the singularity strength remains the same as in classical theory for corresponding stresses, but dependence on  $\theta$  is modified. Demonstrations of this persistence of singular stresses are given in Muki and Sternberg [226] for the half-space under a discontinuous shear traction, normal and tangential line-loads, and a flat, lubricated, strip punch. A further demonstration is given in Sternberg and Muki [227] for a crack in plane strain.

## 6 CONCLUDING REMARKS

In classical elasticity, stress singularities occur under point loads, line loads, and so on. They can also occur away from any such concentrated loading. It is the occurrence of this latter type of singularity that is reviewed here.

When stress singularities occur away from concentrated loading, they do so in concert with a discontinuity: no discontinuity, no singularity. Hence we term them *discontinuity singularities*. The discontinuities for such singularities occur on boundaries. In classical elasticity, these discontinuities entail abrupt changes in boundary directions/boundary conditions/elastic moduli. In general, such discontinuities flag the possibility of singularities. In particular, step changes in uniform tractions or first derivatives of displacements flag the possibility of logarithmic singularities.

The presence of a discontinuity, however, does not necessarily mean that there is a stress singularity. For example, for the in-plane loading of an angular elastic plate, there are no singularities when the vertex angle is less than  $180^\circ$ , despite the presence of a sharp corner (see Sections 2.1 and 2.2). For the same plate as a half-plane with a step pressure applied on its edge, there are no singularities, despite the presence of an abrupt change in boundary conditions (Section 2.4). For the same plate with one face clamped the other free, there are no singularities when the vertex angle is less than  $45^\circ$  (Sections 2.1 and 2.2). This last example is despite the presence of a sharp corner, and an abrupt change in boundary conditions, and an abrupt change in elastic moduli (clamped conditions being attributable to attachment to a material with an infinite Young's modulus). Thus, while discontinuities flag possible stress singularities, they are not in themselves the real sources.

The real sources of discontinuity singularities are discontinuities in the stiffnesses in the cohesive or adhesive stress-separation laws which underlie the constitutive relations of elasticity. This may not be immediately apparent for some singularities. Some further explanation is given in Part I, Sections 2 and 5.

**Table 16. State of the art of stress singularity identification in classical elasticity**

Configuration	Single material		Bimaterial	
	Power	Log	Power	Log
In-plane loading of a plate	C	C	C	o
Antiplane shear of a wedge	C	C	C	C
Plate bending, 4th order theory	C	C	c	o
Plate bending, 6th order theory	c	o	o	O
Axisymmetric torsion of a cylinder	C	C	C	C
Axisymmetric axial loading at vertex	C	c	c	O
Axisymmetric axial loading at a cylindrical boundary	C	C	C	o
Three-dimensional away from 3D vertex	C	C	C	o

In two dimensions, the various discontinuity singularities actually identified to date in classical elasticity may be summarized as follows. For any stress component  $\sigma$ , as the singular point is approached, elasticity can have:

$$\begin{aligned}
 \sigma &= O(r^{-\gamma} \cos(\eta \ln r)) + O(r^{-\gamma} \sin(\eta \ln r)) \\
 \sigma &= O(r^{-\gamma} \ln r) + O(r^{-\gamma}) \\
 \sigma &= O(r^{-\gamma}) \\
 \sigma &= \text{ord}(\ln^2 r) + \text{ord}(\ln r) \\
 \sigma &= \text{ord}(\ln r) \\
 \sigma &= O(\ln r) \\
 \sigma &= O(\cos(\eta \ln r)) + O(\sin(\eta \ln r))
 \end{aligned}
 \tag{6.1}$$

as  $r \rightarrow 0$ , wherein  $\gamma$  is the singularity exponent ( $0 < \gamma < 1$ ), and  $\eta$  is the imaginary part of the eigenvalue involved. In (6.1),  $O$  is associated with locally homogeneous boundary conditions,  $\text{ord}$  with locally inhomogeneous ( $\text{ord}$  is defined in Part I, Section 1.2). For the former, the singularity may or may not participate depending on other far-field boundary conditions: hence the  $O$  notation. Typically, though, once such a singularity is identified as possible, it does participate. For the latter, the singularity's participation is guaranteed by the inhomogeneous part of the local boundary conditions: hence the  $\text{ord}$  notation.<sup>36</sup>

Numerous such singularities are identified in the literature for classical elasticity. Table 16 summarizes the state-of-the-art of these identifications for the various, essentially 2D, configurations that are reviewed here and involve one or two materials.

In Table 16, *power singularities* include the first three of (6.1). For the most part, the singularities involved are as in the third of (6.1). There are, though, quite a few instances of singularities as in the first of (6.1). There are relatively few as in the second of (6.1). In Table 16, then, *logarithmic singularities* include the fourth through sixth of (6.1). These are all weaker than power singularities. Accordingly they can be harder to detect absent an asymptotic appreciation of their

<sup>36</sup>The last stress of (6.1) is not strictly singular, being bounded as  $r \rightarrow 0$ . However, it is undefined as  $r \rightarrow 0$ , and consequently shares some of the difficulties associated with stress singularities.

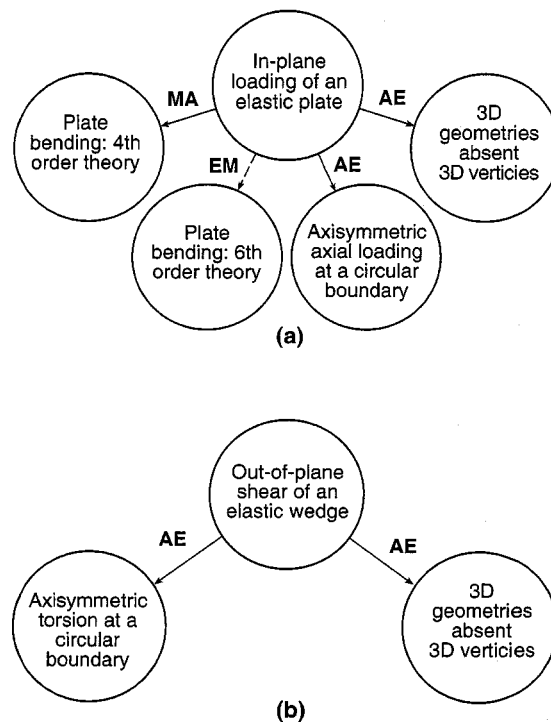


Fig. 27 Classes of configurations that are effectively equivalent with respect to singularity identification: a) configurations equivalent to plates in extension, b) configurations equivalent to wedges in antiplane shear

possible presence. This is the reason they are separated out from power singularities in Table 16. Of course, the presence of either type of singularity needs to be recognized if one is to avoid the futile exercise of stress-strength comparisons once either occurs.<sup>37</sup>

In Table 16, the following notation is adopted with respect to the state-of-the-art of identifications:

$$\begin{aligned}
 \mathbf{C} &= \text{largely closed, } \mathbf{c} = \text{partly closed} \\
 \mathbf{O} &= \text{largely open, } \mathbf{o} = \text{partly open}
 \end{aligned}
 \tag{6.2}$$

In (6.2), largely closed means there are few, if any, new singular configurations to be identified. Moreover, any such new configurations are not expected to occur often in practice. In contrast, partly closed means there are, in fact, quite a few more singular configurations to be identified. Further, in (6.2), largely open means the great majority of singular configurations have yet to be identified, whereas partly open means just a majority.

The bulk of singularity identifications in the literature are for in-plane loading of an elastic plate (Sections 2 and 3). As a result, identification for this configuration is largely complete. The partly open area of log singularities in bimetals is explained in Section 3.3. While there are fewer singularity identifications in the literature for antiplane shear, they are

<sup>37</sup>The few known instances of the last of (6.1) occurring are given at the end of Section 2.2.

nonetheless largely complete (Sections 4.1 and 4.2). This is a consequence of analysis for this configuration being relatively simple.

These two configurations lead to singularity identifications for a number of other configurations. The various ways they do this are illustrated in Fig. 27. Therein the following notation is used:

- AE**= asymptotically equivalent configuration  
**EM**= eigenvalue equations match (6.3)  
**MA**= mathematically analogous configuration

For further explanation, see Sections 4.3, 4.5, 5.1, and 5.2. Also in Fig. 27, an arrow with a solid line denotes that the correspondence holds for both single materials and bimaternal, whereas one with a broken line just for single materials (to date, anyway).

There are a few singularity identifications for trimaterials. These are mentioned in Sections 3.2 and 4.2.

There are 3D configurations other than those of Table 16 and Fig. 27 for which singularities are identified. An indication of the state-of-the-art with respect to singularity identification for these configurations is given in Sections 5.2 and 5.3.

A discussion of stress singularities for field equations other than those of classical elasticity may be found in Section 5.4. Typically, if a stress singularity occurs in classical elasticity, singular stresses persist with other field equations. Sometimes singularities persist with modified strengths, sometimes with the same. Examples of the former include elastoplasticity and large strain (nonlinear) elasticity. Examples of the latter include elastodynamics, viscoelasticity, thermoelasticity, and couple stress theory.

## ACKNOWLEDGMENTS

I am grateful for helpful input received from colleagues during the course of preparing this review: DB Bogy (UC Berkeley), JP Dempsey (Clarkson University), NW Klingbeil (Wright State University), BS Smallwood (Chrysler Corporation), and TCT Ting (University of Illinois, Chicago). I am also grateful for the careful typing of the manuscript by M Gibb and R Kostyak, and the painstaking preparation of the drawings by DC Little (all of Carnegie Mellon University). In addition, I am grateful to R.C. Benson (Penn State) for overseeing the extensive review process, as well as for the thoughtful input of reviewers, and the incorporation of resulting revisions by my wife, Della.

## REFERENCES

- [1] Sinclair GB (2004), Stress singularities in classical elasticity—I: Removal, interpretation, and analysis, *Appl. Mech. Rev.* **57**, 251–298.
- [2] Williams ML (1952), Stress singularities resulting from various boundary conditions in angular corners of plates in extension, *ASME J. Appl. Mech.* **19**, 526–528.
- [3] Dempsey JP, and Sinclair GB (1979), On the stress singularities in the plane elasticity of the composite wedge, *J. Elast.* **9**, 373–391.
- [4] Rao AK (1958), A study into the problem of diffusion of loads, Doctoral Dissertation, Univ of London, London, UK.
- [5] Johnson KL (1985), *Contact Mechanics*, Cambridge Univ Press, Cambridge, UK.
- [6] Winkler E (1867), *Theory of Elasticity and Strength*, (German), H Dominicus Press, Prague, Austria.
- [7] Oravas GA (1964), Review Number 4988, *Appl. Mech. Rev.* **17**, 684.
- [8] Euler L (1774), The pressure in planes from weights that settle (Latin), *Novi Commun Acad Petropolit* **18**, 283–329.
- [9] Nuller BM (1974), Deformation of an elastic wedge reinforced by a beam, *J. Appl. Math. Mech.* **38**, 823–829.
- [10] Ting TCT (1985), Asymptotic solution near the apex of an elastic wedge with curved boundaries, *Q. Appl. Math.* **42**, 467–476.
- [11] Gregory RD (1979), Green's functions, bi-linear forms, and completeness of the eigenfunctions for the elastostatic strip and wedge, *J. Elast.* **9**, 283–309.
- [12] Knowles JK, and Pucik TA (1973), Uniqueness for plane crack problems in linear elastostatics, *J. Elast.* **3**, 155–160.
- [13] Lighthill MJ (1975), *Introduction to Fourier Analysis and Generalized Functions*, Cambridge Univ Press, Cambridge, UK.
- [14] Kolosoff G (1910), On an application of the theory of complex variables to the two-dimensional problem of elasticity theory, Doctoral Dissertation, St Petersburg, Russia.
- [15] Kolosoff G (1914), On some properties of the plane problem of elasticity theory (German), *Z. Math. Phys.* **62**, 384–409.
- [16] Inglis CE (1913), Stresses in a plate due to the presence of cracks and sharp corners, *Soc. Nav. Archit. Mar. Eng., Trans.* **55**, 219–241.
- [17] Neuber H 1946, *Theory of Notch Stresses*, JW Edwards Co, Ann Arbor MI.
- [18] Kitover KA (1952), On the use of special systems of biharmonic functions for the solution of some problems in the theory of elasticity (Russian), *Prikl. Mat. Mekh.* **16**, 739–748.
- [19] Kalandiia AI (1969), Remarks on the singularity of elastic solutions near corners, *J. Appl. Math. Mech.* **33**, 127–131.
- [20] Seweryn A, and Molski K (1996), Elastic stress singularities and corresponding generalized stress intensity factors for angular corners under various boundary conditions, *Eng. Fract. Mech.* **55**, 529–556.
- [21] Dempsey JP (1978), On the stress singularities in the plane elasticity of the composite wedge, Doctoral Dissertation, Univ of Auckland, Auckland, New Zealand.
- [22] Gdoutos EE, and Theocaris PS (1975), Stress concentrations at the apex of a plane indenter acting on an elastic half plane, *ASME J. Appl. Mech.* **42**, 688–692.
- [23] Sinclair GB (1996), On the influence of cohesive stress-separation laws on elastic stress singularities, *J. Elast.* **44**, 203–221.
- [24] Rössle A (2000), Corner singularities and regularity of weak solutions for the two-dimensional Lamé equations on domains with angular corners, *J. Elast.* **60**, 57–75.
- [25] Rösel R (1987), On the wedge/notch eigenvalues, *Int. J. Fract.* **33**, 61–71.
- [26] Karp SN, and Karal FC (1962), The elastic-field behavior in the neighborhood of a crack of arbitrary angle, *Commun. Pure Appl. Math.* **15**, 413–421.
- [27] Sinclair GB, Khatod HN, and Rummel CW (2003), On the removal of stress singularities from sharp corners, *Proc of the 19 Canadian Congress of Applied Mechanics*, Vol. 1, Calgary, Alberta, 1, 94–95.
- [28] Williams ML (1953), Discussion of 'Stress singularities resulting from various boundary conditions in angular corners of plates in extension,' *ASME J. Appl. Mech.* **20**, 590.
- [29] Ricci L (1951), *Table of Minimum Roots of an Equation of Interest in Solid Mechanics* (Italian), Pubblicazioni No 296, Istituto per le Applicazioni del Calcolo, Rome, Italy.
- [30] Klingbeil NW (1996), private communication.
- [31] England AH (1971), On stress singularities in linear elasticity, *Int. J. Eng. Sci.* **9**, 571–585.
- [32] Smallwood BS (1996), private communication.
- [33] Dempsey JP (1995), Power-logarithmic stress singularities at bimaterial corners and interface cracks, *J. Adhes. Sci. Technol.* **9**, 253–265.
- [34] Sinclair GB (1999), Logarithmic stress singularities resulting from various boundary conditions in angular corners of plates in extension, *ASME J. Appl. Mech.* **66**, 556–560.
- [35] Browning RV, and Ju FD (1977), Stress singularities at an elastic crack with arbitrary surface loads, including possible fracture mechanics applications, *J. Math. Anal. Appl.* **58**, 482–496.
- [36] ANSYS personnel (1995), *ANSYS User's Manual*, Revision 5.2, Vol I, ANSYS Inc, Canonsburg, PA.
- [37] ABAQUS personnel (1997), *ABAQUS Standard User's Manual*, Revision 5.7, Vol I, Hibbitt, Karlsson and Sorensen, Inc, Pawtucket, RI.
- [38] Sinclair GB, and Epps BE (2002), On the logarithmic stress singularities induced by the use of displacement shape functions in bound-

- ary conditions in submodelling, *Commun. Numer. Methods Eng.* **18**, 121–130.
- [39] Dempsey JP (1981), The wedge subjected to tractions: A paradox resolved, *J. Elast.* **11**, 1–10.
- [40] Sinclair GB (1998), Further paradoxes in generalized Levy problems, *J. Elast.* **50**, 253–259.
- [41] Levy M (1898), On the elastic equilibrium of a masonry dam of triangular cross section (French), *Acad. Sci., Paris, C. R.* **127**, 10–15.
- [42] Timoshenko SP, and Goodier JN (1970), *Theory of Elasticity*, 3rd Edition, McGraw-Hill, New York, NY.
- [43] Fillunger P (1912), Three important plane states of stress for wedge-shaped bodies (German), *Z. Angew. Math. Mech.* **60**, 275–285.
- [44] Ting TCT (1984), The wedge subjected to tractions: A paradox re-examined, *J. Elast.* **14**, 235–247.
- [45] Sternberg E, and Koiter WT (1959), Discussion of “The wedge under a concentrated couple: A paradox in the two-dimensional theory of elasticity,” *ASME J. Appl. Mech.* **26**, 472–474.
- [46] Sneddon IN (1951), *Fourier Transforms*, McGraw-Hill, New York, NY.
- [47] Brock LM (1979), Frictionless indentation by a rigid wedge: The effect of tangential displacements in the contact zone, *Int. J. Eng. Sci.* **17**, 365–372.
- [48] Rao AK (1971), Stress concentrations and singularities at interface corners, *Z. Angew. Math. Mech.* **51**, 395–406.
- [49] Erdogan F, and Gupta GD (1972), Stresses near a flat inclusion in bonded dissimilar materials, *Int. J. Solids Struct.* **8**, 533–547.
- [50] Jones JP, and Whittier JS (1967), Waves at a flexibly bonded interface, *ASME J. Appl. Mech.* **34**, 905–909.
- [51] Lene F, and Leguillon D (1982), Homogenized constitutive law for a partially cohesive composite material, *Int. J. Solids Struct.* **18**, 443–458.
- [52] Ying X, and Katz IN (1987), A uniform formulation for the calculation of stress singularities in the plane elasticity of a wedge composed of multiple isotropic materials, *Comput. Math. Appl.* **14**, 437–458.
- [53] Dundurs J (1969), Discussion of “Edge-bonded dissimilar orthogonal elastic wedges under normal and shear loading,” *ASME J. Appl. Mech.* **36**, 650–652.
- [54] Bogy DB (1968), Edge-bonded dissimilar orthogonal elastic wedges under normal and shear loading, *ASME J. Appl. Mech.* **35**, 460–466.
- [55] Zak AR, and Williams ML (1963), Crack point stress singularities at a bi-material interface, *ASME J. Appl. Mech.* **30**, 142–143.
- [56] Dundurs J (1967), Effect of elastic constants on stress in a composite under plane deformation, *J. Compos. Mater.* **1**, 310–322.
- [57] Koguchi H, Inoue T, and Yada T (1996), Stress singularity in three-phase bonded structure, *ASME J. Appl. Mech.* **63**, 252–258.
- [58] Williams MI (1959), The stresses around a fault or crack in dissimilar media, *Bull. Seismol. Soc. Am.* **49**, 199–204.
- [59] Bogy DB (1971), Two edge-bonded elastic wedges of different materials and wedge angles under surface tractions, *ASME J. Appl. Mech.* **38**, 377–386.
- [60] Theocaris PS, and Gdoutos EE (1977), Stress singularities in cracked composite full-planes, *Int. J. Fract.* **13**, 763–773.
- [61] Ting TCT (1986), Explicit solution and invariance of the singularities at an interface crack in anisotropic composites, *Int. J. Solids Struct.* **22**, 965–983.
- [62] Ballarini R (1990), A rigid line inclusion at a bimaterial interface, *Eng. Fract. Mech.* **37**, 1–5.
- [63] Comninou M (1977), Interface crack with friction in the contact zone, *ASME J. Appl. Mech.* **44**, 780–781.
- [64] Dempsey JP, and Sinclair GB (1981), On the singular behavior at the vertex of a bi-material wedge, *J. Elast.* **11**, 317–327.
- [65] Comninou M (1977), The interface crack, *ASME J. Appl. Mech.* **44**, 631–636.
- [66] Comninou M (1976), Stress singularity at a sharp edge in contact problems with friction, *Z. Angew. Math. Phys.* **27**, 493–499.
- [67] Dundurs J, and Lee M-S (1972), Stress concentration at a sharp edge in contact problems, *J. Elast.* **2**, 109–112.
- [68] Wu K-C (1990), Line inclusions at anisotropic bimaterial interface, *Mech. Mater.* **10**, 173–182.
- [69] Chen YZ, and Hasebe N (1993), Singularity eigenvalue analysis of a crack along a wedge-shaped interface, *ASME J. Appl. Mech.* **60**, 781–783.
- [70] Van Vroonhoven JCW (1992), Stress singularities in bi-material wedges with adhesion and delamination, *Fatigue Fract. Eng. Mater. Struct.* **15**, 159–171.
- [71] Bogy DB, and Wang KC (1971), Stress singularities at interface corners in bonded dissimilar isotropic elastic materials, *Int. J. Solids Struct.* **7**, 993–1005.
- [72] Chen D-H, and Nisitani H (1993), Singular stress field near the corner of jointed dissimilar materials, *ASME J. Appl. Mech.* **60**, 607–613.
- [73] Pageau SS, Joseph PF, and Biggers Jr SB (1994), The order of stress singularities for bonded and debonded three-material junctions, *Int. J. Solids Struct.* **31**, 2979–2997.
- [74] Chaudhuri RA, Xie M, and Garala HJ (1996), Stress singularity due to kink band weakening a unidirectional composite under compression, *J. Compos. Mater.* **30**, 672–691.
- [75] Khrapkov AA (1968), First fundamental problem for a piecewise-homogeneous plane with a slit perpendicular to the line of separation, *J. Appl. Math. Mech.* **32**, 666–678.
- [76] Bogy DB (1971), On the plane elastostatic problem of a loaded crack terminating at a material interface, *ASME J. Appl. Mech.* **38**, 911–918.
- [77] Comninou M, and Dundurs J (1979), A closed crack tip terminating at an interface, *ASME J. Appl. Mech.* **46**, 97–100.
- [78] Wijeyewickrema AC, Dundurs J, and Keer LM (1995), The singular stress field of a crack terminating at a frictional interface between two materials, *ASME J. Appl. Mech.* **62**, 289–293.
- [79] Gharpuray VM, Dundurs J, and Keer LM (1991), A crack terminating at a slipping interface between two materials, *ASME J. Appl. Mech.* **58**, 960–963.
- [80] Fenner DN (1976), Stress singularities in composite materials with an arbitrarily oriented crack meeting an interface, *Int. J. Fract.* **12**, 705–721.
- [81] Yong-Li W (1992), Crack tip stress singularities in a bimaterial with an inclined interface, *Int. J. Fract.* **54**, R65–R72.
- [82] Wang W-C, and Chen J-T (1994), Singularities of an arbitrarily inclined semi-infinite crack meeting a bimaterial interface, *Eng. Fract. Mech.* **49**, 671–680.
- [83] Tan MA, and Meguid SA (1997), Stress singularities of a sharp notch terminating at a bimaterial interface, *Proc of 16th Canadian Congress of Applied Mechanics Vol 1*, Laval Univ, Quebec, Canada, 17–18.
- [84] Pinsan C, and Zhuping D (1991), Singular behavior and asymptotic stress field of a crack terminating at a bimaterial interface, *Acta Mech. Sin.* **7**, 344–350.
- [85] Bogy DB (1970), On the problem of edge-bonded quarter-planes loaded at the boundary, *Int. J. Solids Struct.* **6**, 1287–1313.
- [86] Hein VL, and Erdogan F (1971), Stress singularities in a two-material wedge, *Int. J. Fract. Mech.* **7**, 317–330.
- [87] Kubo S, Ohji K, and Nakai Y (1991), Free-edge singularities in edge-bonded elastic dissimilar wedges—geometrical conditions for appearance and disappearance of stress singularities, Report of the 61st Meeting of the Committee on Fracture Mechanics, Vol 39, Soc of Materials Science, Japan, 13–17 (this work is summarized in Murakami [95]).
- [88] Theocaris PS, and Gdoutos EE (1976), Stress singularities at equal angle biwedges and two-material composite half planes with rough interfaces, *ASME J. Appl. Mech.* **43**, 64–68.
- [89] Theocaris PS, and Gdoutos EE (1976), Stress singularities at vertices of composite plates with smooth or rough interfaces, *Arch. Mech. Stosow.* **28**, 693–704.
- [90] Aksentian OK (1967), Singularities of the stress-strain state of a plate in the neighborhood of an edge, *J. Appl. Math. Mech.* **31**, 193–202.
- [91] Avetisian AG, and Chobanian KS (1972), On the nature of stresses in the fixed vicinity of the junction surface brink of a composite elastic body loaded in conditions of a plane problem of the elasticity theory (Russian), *Dokl. Akad. Nauk Arm. SSR* **25**, 13–25.
- [92] Picu CR, and Gupta V (1996), Stress singularities at triple junctions with freely sliding grains, *Int. J. Solids Struct.* **33**, 1535–1541.
- [93] Inoue T, and Koguchi H (1996), Influence of the intermediate material on the order of stress singularity in three-phase bonded structure, *Int. J. Solids Struct.* **33**, 399–417.
- [94] Pageau SS, Gadi KS, Biggers Jr SB, and Joseph PF (1996), Standardized complex and logarithmic eigensolutions for  $n$ -material wedges and junctions, *Int. J. Fract.* **77**, 51–76 (See also: *ibid.*, **80**, 97).
- [95] Murakami Y (1992), Stress singularity for notch at bimaterial interface, *Stress Intensity Factors Handbook Vol 3*, Y Murakami et al (eds), Pergamon Press, Oxford, UK, 963–1062.
- [96] Chen D-H (1996), Logarithmic singular stress field in a semi-infinite plate consisting of two edge-bonded wedges subjected to surface tractions, *Int. J. Fract.* **75**, 352–378.
- [97] Courant R and Hilbert D (1953), *Methods of Mathematical Physics*, 1st English Edition, Vol I, Interscience Publ, New York, NY.
- [98] de Saint-Venant B (1878), On the torsion of prisms with bases made of circular arcs and radial lines, and on a singularity which can be found in certain uses of the logarithmic cylindrical coordinate system of Lamé (French), *Acad. Sci., Paris, C. R.* **87**, 849–854.

- [99] Sinclair GB (1980), On the singular eigenfunctions for plane harmonic problems in composite regions, *ASME J. Appl. Mech.* **47**, 87–92.
- [100] Thomson W, and Tait PG (1867), *A Treatise on Natural Philosophy*, Cambridge Univ Press, Cambridge, UK (This book is also available in two parts as *Principles of Mechanics and Dynamics*, Dover Publ, New York, NY).
- [101] de Saint-Venant B (1878), Sample calculations for the torsion of prisms with bases made of circular arcs and radial lines (French), *Acad. Sci., Paris, C. R.* **87**, 893–899.
- [102] Irwin GR, and Kies JA (1957), Fracture, *Proc of ONR Symp*, Washington DC, 563–571.
- [103] Wasow W (1957), Asymptotic development of the solution of Dirichlet's Problem at analytic corners, *Duke Math. J.* **24**, 47–56.
- [104] Ting TCT (1985), Elastic wedge subjected to antiplane shear tractions—A paradox explained, *Q. J. Mech. Appl. Math.* **38**, 245–255.
- [105] Sinclair GB (1999), A note on the removal of further breakdowns in classical solutions of Laplace's equation on sectorial regions, *J. Elast.* **56**, 247–252.
- [106] Ma C-C, and Hour B-L (1989), Analysis of dissimilar anisotropic wedges subjected to antiplane shear deformation, *Int. J. Solids Struct.* **25**, 1295–1309.
- [107] Sinclair GB (2000), Logarithmic stress singularities in two-dimensional and three-dimensional elasticity, *Proc of 20th Southeastern Conf of Theoretical and Applied Mechanics*, Callaway Gardens, GA, SM94.1–8.
- [108] Barnett DM (1967), The effect of shear modulus on the stress distribution produced by a planar array of screw dislocations near a bi-metallic interface, *Acta Metall.* **15**, 589–594.
- [109] Sendekyj GP (1973), Analysis of cracks in heterogeneous solids, *Fracture Mechanics of Ceramics*, Vol 1, RC Bradt, DPH Hasselmann, and FF Lang (eds), Plenum Press, New York, NY, 269–282.
- [110] Pageau SS, Joseph PF, and Biggers Jr SB (1995), Singular antiplane stress fields for bonded and debonded three-material junctions, *Eng. Fract. Mech.* **52**, 821–832.
- [111] Keer LM, and Freeman NJ (1970), Load transfer problem for an embedded shaft in torsion, *ASME J. Appl. Mech.* **37**, 959–964.
- [112] Love AEH (1944), *A Treatise on the Mathematical Theory of Elasticity*, 4th Edition, Dover Publ, New York, NY.
- [113] Kirchhoff G (1850), On the equilibrium and deflection of an elastic plate (German), *J. Reine Angew. Math.* **40**, 51–88.
- [114] Timoshenko SP, and Woinowsky-Krieger S (1959), *Theory of Plates and Shells*, 2nd Edition, McGraw-Hill, New York, NY.
- [115] Williams ML (1951), Surface stress singularities resulting from various boundary conditions in angular corners of plates under bending, *Proc of 1st US Nat Congress of Applied Mechanics*, Illinois Inst of Tech, Chicago, IL, 325–329.
- [116] Southwell RV (1950), On the analogues relating flexure and extension of flat plates, *Q. J. Mech. Appl. Math.* **3**, 257–271.
- [117] Dixon AC (1934), The problem of the rectangular plate, *J. Lond. Math. Soc.* **9**, 61–74.
- [118] Carrier GF and Shaw FS (1949), Some problems in the bending of thin plates, *Proc of 3rd Symp in Applied Mathematics of the Am Mathematical Soc*, Vol 3, Univ of Michigan, Ann Arbor, MI, 125–128.
- [119] Morley LSD (1964), Bending of clamped rectilinear plates, *Q. J. Mech. Appl. Math.* **17**, 293–317.
- [120] Hrudey TM, and Hrabok MM (1986), Singularity finite elements for plate bending, *J. Eng. Mech.* **112**, 666–681.
- [121] Leissa AW, McGee OG, and Huang CS (1993), Vibrations of sectorial plates having corner stress singularities, *ASME J. Appl. Mech.* **60**, 134–140.
- [122] Gregory RD, Chonghua G, and Wan FYM (1996), The cantilever strip under torsion, bending or flexure at infinity, *J. Elast.* **43**, 109–136.
- [123] Williams ML (1961), The bending stress distribution at the base of a stationary crack, *ASME J. Appl. Mech.* **28**, 78–82.
- [124] Williams ML (1957), On the stress distribution at the base of a stationary crack, *ASME J. Appl. Mech.* **24**, 109–114.
- [125] Irwin GR (1957), Analysis of stresses and strains near the end of a crack traversing a plate, *ASME J. Appl. Mech.* **24**, 361–364.
- [126] Sinclair GB (2000), Logarithmic stress singularities resulting from various boundary conditions in angular corners of plates under bending, *ASME J. Appl. Mech.* **67**, 219–223.
- [127] Nádai A (1925), *The Elastic Plate* (German), Julius Springer Publ, Berlin, Germany.
- [128] Sih GC, and Rice JR (1964), The bending of plates of dissimilar materials with cracks, *ASME J. Appl. Mech.* **31**, 477–482.
- [129] Huang CS (2002), Corner singularities in bi-material Mindlin plates, *Compos. Struct.* **56**, 315–327.
- [130] Reissner E (1945), The effect of transverse shear deformation on the bending of elastic plates, *ASME J. Appl. Mech.* **12**, A-69–A-77.
- [131] Hencky H (1947), On the treatment of shear rotations in flat plates (German), *Oesterr. Ing.-Arch.* **16**, 72–76.
- [132] Burton WS, and Sinclair GB (1986), On the singularities in Reissner's theory for the bending of elastic plates, *ASME J. Appl. Mech.* **53**, 220–222.
- [133] Yen DHY, and Zhou M (1989), On the corner singularities in Reissner's theory for the bending of elastic plates, *ASME J. Appl. Mech.* **56**, 726–729.
- [134] Huang CS, McGee OG, and Leissa AW (1994), Exact analytical solutions for free vibrations of thick sectional plates with simply supported radial edges, *Int. J. Solids Struct.* **31**, 1609–1631.
- [135] Knowles JK, and Wang N-M (1960), On the bending of an elastic plate containing a crack, *Z. Agnew Math. Phys.* **39**, 223–236.
- [136] Hartranft RJ, and Sih GC (1968), Effect of plate thickness on the bending stress distribution around through cracks, *Z. Agnew Math. Phys.* **47**, 276–291.
- [137] Wang N-M (1968), Effects of plate thickness on the bending of an elastic plate containing a crack, *Z. Agnew Math. Phys.* **47**, 371–390.
- [138] Hartranft RJ (1966), On some problems involving singularities in Reissner's theory of plate bending, Doctoral dissertation, Lehigh Univ, Bethlehem, PA.
- [139] Abramowitz M, and Stegun IA (1965), *Handbook of Mathematical Functions*, Dover Publ, New York, NY.
- [140] Bazant ZP, and Keer LM (1974), Singularities of elastic stresses and of harmonic functions at conical notches or inclusions, *Int. J. Solids Struct.* **10**, 957–964.
- [141] Thomson TR, and Little RW (1970), End effects in a truncated semi-infinite cone, *Q. J. Mech. Appl. Math.* **23**, 185–195.
- [142] Beagles AE, and Sändig A-M (1991), Singularities of rotationally symmetric solutions of boundary value problems for the Lamé equations, *Z. Angew. Math. Mech.* **71**, 423–431.
- [143] Love AEH (1939), Boussinesq's problem for a rigid cone, *Q. J. Math.* **10**, 161–175.
- [144] Hanson MT (1993), The elastic field for a sliding conical punch on an isotropic half-space, *ASME J. Appl. Mech.* **60**, 557–559.
- [145] Keer LM, and Parihar KS (1978), Elastic stress singularity at conical inclusions, *Int. J. Solids Struct.* **14**, 261–263.
- [146] Reissner E, and Sagoci HF (1944), Forced torsional oscillations of an elastic half-space: I, *J. Appl. Phys.* **15**, 652–654.
- [147] Tsuji T, Noda N, Shibuya T, and Koizumi T (1990), Stress singularity at the bottom of a V-notch in the inner surface of a circular pipe under torsion, *Int. J. Pressure Vessels Piping* **42**, 135–155.
- [148] Freeman NJ, and Keer LM (1967), Torsion of a cylindrical rod welded to an elastic half space, *ASME J. Appl. Mech.* **34**, 687–692.
- [149] Westmann RA (1968), Discussion of "Torsion of a cylindrical rod welded to an elastic half space," *ASME J. Appl. Mech.* **35**, 197–198.
- [150] Keer LM, and Freeman NJ (1969), Torsion of a finite elastic cylindrical rod partially bonded to an elastic half space, *Q. Appl. Math.* **26**, 567–573.
- [151] Barton MV (1941), The circular cylinder with a band of uniform pressure on a finite length of the surface, *ASME J. Appl. Mech.* **8**, A-97–A-104.
- [152] Zate AR (1964), Stresses in the vicinity of boundary discontinuities in bodies of revolution, *ASME J. Appl. Mech.* **31**, 150–152.
- [153] Sneddon IN (1946), The distribution of stress in the neighborhood of a crack in an elastic solid, *Proc. R. Soc. London, Ser. A* **A187**, 229–260.
- [154] Harding JW, and Sneddon IN (1945), The elastic stresses produced by the indentation of the plane surface of a semi-infinite elastic solid by a rigid punch, *Proc. Cambridge Philos. Soc.* **41**, 16–26.
- [155] Benthem JP, and Minderhoud P (1972), The problem of the solid cylinder compressed between rough rigid stamps, *Int. J. Solids Struct.* **8**, 1027–1042.
- [156] Agarwal VK (1978), Axisymmetric solution of the end-problem for semi-infinite elastic circular cylinder and its application to joined dissimilar cylinders under uniform tension, *Int. J. Eng. Sci.* **16**, 985–998.
- [157] Hartranft RJ, and Sih GC (1977), Stress singularity for a crack with an arbitrarily curved front, *Eng. Fract. Mech.* **9**, 705–718.
- [158] Sadowsky MA, and Sternberg E (1949), Stress concentration around a triaxial ellipsoidal cavity, *ASME J. Appl. Mech.* **16**, 149–157.
- [159] Green AE, and Sneddon IN (1950), The distribution of stress in the neighborhood of a flat elliptical crack in an elastic solid, *Proc. Cambridge Philos. Soc.* **46**, 159–164.

- [160] Kassir MK, and Sih GC (1966), Three-dimensional stress distribution around an elliptical crack under arbitrary loadings, *ASME J. Appl. Mech.* **33**, 601–611.
- [161] Galin LA (1948), Determination of displacements in three-dimensional contact problems of the theory of elasticity (Russian), *Prikl. Mat. Mekh.* **12**, 241–250.
- [162] Mindlin RD (1949), Compliance of elastic bodies in contact, *ASME J. Appl. Mech.* **16**, 259–268.
- [163] Hughes WF, and Gaylord EW (1964), *Basic Equations of Engineering Science*, Schaum Publ Co, New York, NY.
- [164] Love AEH (1929), The stress produced in a semi-infinite solid by pressure on part of the boundary, *Philos. Trans. R. Soc. London, Ser. A* **A228**, 397–420.
- [165] Turteltaub MJ, and Wheeler LT (1976), Line integral representations for the traction problem of the elastic halfspace and their application to a study of the singular effects of load jumps, *J. Elast.* **6**, 161–178.
- [166] Michell JH (1902), The inversion of plane stress, *Proc. London Math. Soc.* **34**, 134–142.
- [167] Green AE, and Zerna W (1968), *Theoretical Elasticity*, 2nd Edition, Oxford at Clarendon Press, UK.
- [168] Smith FW, and Alavi MJ (1971), Stress intensity factors for a penny shaped crack in a half space, *Eng. Fract. Mech.* **3**, 241–254.
- [169] Shah RC, and Kobayashi AS (1973), Stress intensity factors for an elliptical crack approaching the surface of a semi-infinite solid, *Int. J. Fract.* **9**, 133–146.
- [170] Liao CY, and Atluri SN (1989), Stress intensity factor variation along a semicircular surface flaw in a finite-thickness plate, *Eng. Fract. Mech.* **34**, 957–976.
- [171] Galin LA (1947), Pressure of a stamp with a flat base in the form of an infinite wedge on an elastic half-space (Russian), *Dokl. Akad. Nauk SSSR* **58**(2).
- [172] Rvachev VL (1959), The pressure on an elastic half-space of a stamp with a wedge-shaped planform, *J. Appl. Math. Mech.* **23**, 229–233.
- [173] Noble B (1959), The potential and charge distribution near the tip of a flat angular sector, Report NYU EM-135, New York Univ, New York, NY.
- [174] Aleksandrov VM, and Babeshko VA (1972), On the pressure on an elastic half-space of a wedge-shaped stamp, *J. Appl. Math. Mech.* **36**, 78–83.
- [175] Bažant ZP (1974), Three-dimensional harmonic functions near termination or intersection of gradient intersection lines: A general numerical method, *Int. J. Eng. Sci.* **12**, 221–243.
- [176] Walden H (1974), Solution of an eigenvalue problem for the Laplace operator on a spherical surface, Report X-582-74-41, Goddard Space Flight Center, Greenbelt, MD.
- [177] Morrison JA, and Lewis JA (1976), Charge singularity at the corner of a flat plate, *SIAM (Soc. Ind. Appl. Math.) J. Appl. Math.* **31**, 233–250.
- [178] Brothers PW (1976), The rigid rectangular punch on the elastic half-space, Masters thesis, Univ of Auckland, Auckland, New Zealand.
- [179] Keer LM, and Parihar KS (1978), A note on the singularity at the corner of a wedge-shaped punch or crack, *SIAM (Soc. Ind. Appl. Math.) J. Appl. Math.* **34**, 297–302.
- [180] Ioakimidis NI (1985), Determination of the order of singularity at the apex of a wedge-shaped crack, *Eng. Fract. Mech.* **22**, 369–373.
- [181] Takakuda K (1985), Stress singularities near crack front edges, *Bull. Japan Soc. Mech. Engineers* **28**, 225–231.
- [182] Xu L, and Kundu T (1995), Stress singularities at crack corners, *J. Elast.* **39**, 1–16.
- [183] Glushkov E, Glushkova N, and Lapina O (1999), 3D elastic stress singularity at polyhedral corner points, *Int. J. Solids Struct.* **36**, 1105–1128.
- [184] Parihar KS, and Keer LM (1978), Stress singularity at the corner of a wedge-shaped crack or inclusion, *ASME J. Appl. Mech.* **45**, 791–796.
- [185] Parihar KS, and Keer LM (1979), The singularity at the apex of a bonded wedge-shaped stamp, *ASME J. Appl. Mech.* **46**, 577–580.
- [186] Abramov BM (1937), The problem of contact of an elastic infinite half-plane with an absolutely rigid rough foundation, *C. R. (Dokl.) Acad. Sci. URSS* **17**, 173–178.
- [187] Abdel-Messieh YS, and Thatcher RW (1990), Estimating the form of some three-dimensional singularities, *Commun. Appl. Numer. Methods* **6**, 333–341.
- [188] Schmitz H, Volk K, and Wendland W (1993), Three-dimensional singularities of elastic fields near vertices, *Numer. Methods Partial Differ. Equ.* **9**, 323–337.
- [189] Panasyuk VV, Andrejiv AE, and Stadnik MM (1980), Basic mechanical concepts and mathematical techniques in application to three-dimensional crack problems: A review, *Eng. Fract. Mech.* **13**, 925–937.
- [190] Panasyuk VV, Andrejiv AE, and Stadnik MM (1981), Three-dimensional static crack problems solution (A review), *Eng. Fract. Mech.* **14**, 245–260.
- [191] Sih GC (1971), A review of the three-dimensional stress problem for a cracked plate, *Int. J. Fract. Mech.* **7**, 39–61.
- [192] Folias ES (1975), On the three-dimensional theory of cracked plates, *ASME J. Appl. Mech.* **42**, 663–674.
- [193] Kawai T, Fujitani Y, and Kumagai K (1977), Analysis of singularity at the root of the surface crack problem, *Proc of Int Conf on Fracture Mechanics and Technology*, Hong Kong, 1157–1163.
- [194] Benthem JP (1977), State of stress at the vertex of a quarter-infinite crack in a half-space, *Int. J. Solids Struct.* **13**, 479–492.
- [195] Bažant ZP, and Estenssoro LF (1977), General numerical method for three-dimensional singularities in cracked or notched elastic solids, *Proc of 4th Int Conf on Fracture*, Vol 3, Waterloo, Ontario, 371–383.
- [196] Bažant ZP, and Estenssoro LF (1977), Stress singularity and propagation of cracks at their intersection with surfaces, Structural Engineering Report 77-12/480, Dept of Civil Eng, Northwestern Univ, Evanston, IL.
- [197] Bažant ZP, and Estenssoro LF (1979), Surface singularity and crack propagation, *Int. J. Solids Struct.* **15**, 405–426 (See also: Addendum (1980), *ibid.* **16**, 479–481, and Erratum (1983), *ibid.* **19**, 661).
- [198] Sinclair GB (1979), Asymptotic singular eigenfunctions for the three-dimensional crack, *Proc of 7th Canadian Congress of Applied Mechanics*, Sherbrooke, Quebec, 295–296.
- [199] Benthem JP (1980), The quarter-infinite crack in a half-space: Alternative and additional solutions, *Int. J. Solids Struct.* **16**, 119–130.
- [200] Yamada Y, and Okumura H (1981), Analysis of local stress in composite materials by the 3D finite element, *Proc of Japan-US Conf on Composite Materials*, Tokyo, Japan, 55–84.
- [201] Burton WS, Sinclair GB, Solecki JS, and Swedlow JL (1984), On the implications for LEFM of the three-dimensional aspects in some crack-surface intersection problems, *Int. J. Fract.* **25**, 3–32.
- [202] Shaofu W, Xing Z, and Qingzhi H (1988), Functional variable displacement method in analysis of singularity near the corner point in a three-dimensional cracked solid, *Eng. Fract. Mech.* **31**, 191–200.
- [203] Shivakumar KN, and Raju IS (1990), Treatment of singularities in cracked bodies, *Int. J. Fract.* **45**, 159–178.
- [204] Zhu WX (1990), Singular stress field of three-dimensional crack, *Eng. Fract. Mech.* **36**, 239–244.
- [205] Barsoum RS, and Chen T-K (1991), Three-dimensional surface singularity of an interface crack, *Int. J. Fract.* **50**, 221–237.
- [206] Ghahremani F (1991), A numerical variational method for extracting 3D singularities, *Int. J. Solids Struct.* **27**, 1371–1386.
- [207] Leung AYT, and Su RKL (1996), Order of the singular stress field of through-thickness cracks, *Int. J. Fract.* **75**, 85–93.
- [208] Leung AYT, and Su RKL (1996), Analytical solution for mode I crack orthogonal to free surface, *Int. J. Fract.* **76**, 79–85.
- [209] Su XM, and Sun CT (1996), On singular stress of the crack tip of a thick plate under in-plane loading, *Int. J. Fract.* **82**, 237–252.
- [210] Lur'e AI (1964), *Three-Dimensional Problems of the Theory of Elasticity*, Interscience Publ, John Wiley and Sons, New York, NY.
- [211] Benthem JP, and Koiter WT (1976), Discussion of “On the three-dimensional theory of cracked plates,” *ASME J. Appl. Mech.* **43**, 374.
- [212] Folias ES (1976), Authors closure to discussion of “On the three-dimensional theory of cracked plates,” *ASME J. Appl. Mech.* **43**, 374–375.
- [213] Folias ES (1980), Method of solution of a class of three-dimensional elastostatic problems under mode I loading, *Int. J. Fract.* **16**, 335–348.
- [214] Meda G, Messner TW, Sinclair GB, and Solecki JS (1998), Path-independent H integrals for three-dimensional fracture mechanics, *Int. J. Fract.* **94**, 217–234.
- [215] Ghahremani F, and Shih CF (1992), Corner singularities of three-dimensional planar interface cracks, *ASME J. Appl. Mech.* **59**, 61–68.
- [216] Sagochi HF (1944), Forced torsional oscillations of an elastic half-space: II, *J. Appl. Phys.* **15**, 655–662.
- [217] Leissa AW (2001), Singularity considerations in membrane, plate and shell behaviors, *Int. J. Solids Struct.* **38**, 3341–3353.
- [218] Achenbach JD, and Bažant ZP (1975), Elastodynamic near-tip stress and displacement fields for rapidly propagating cracks in orthotropic materials, *ASME J. Appl. Mech.* **42**, 183–189.
- [219] Nowacki W (1968), *Thermoelasticity*, 2nd Edition, Pergamon Press, Oxford, UK.
- [220] Yan G, and Ting TCT (1993), The  $r^{-1/2}(\ln r)$  singularities at interface cracks in monoclinic and isotropic bimaterials due to heat flow, *ASME J. Appl. Mech.* **60**, 432–437.
- [221] Yang YY, and Munz D (1995), Stress intensity factor and stress dis-

- tribution in a joint with an interface corner under thermal and mechanical loading, *Comput. Struct.* **57**, 467–476.
- [222] Lee EH (1955), Stress analysis in visco-elastic bodies, *Q. Appl. Math.* **13**, 183–190.
- [223] Williams ML (1962), The fracture of viscoelastic materials, *Fracture of Solids, Proc of an Int Conf*, Maple Valley, WA, 157–188.
- [224] Ting TCT (1986), *Anisotropic Elasticity*, Oxford Univ Press, New York, NY.
- [225] Ting TCT (1998), The remarkable nature of cylindrically uniform anisotropic elastic materials, *Proc of 13th US Natl Congress of Applied Mechanics*, TA7.
- [226] Muki R, and Sternberg E (1965), The influence of couple-stresses on singular stress concentrations in elastic solids, *Z. Angew. Math. Phys.* **16**, 611–648.
- [227] Sternberg E, and Muki R (1967), The effect of couple-stresses on the stress concentration around a crack, *Int. J. Solids Struct.* **3**, 69–95.



**Glenn Sinclair** received his undergraduate education from the University of Auckland in New Zealand. He graduated with a BS in Mathematics in 1967 and a BE in Engineering Science in 1969. He then attended Caltech, graduating with a PhD in Applied Mechanics in 1972. He has since served on the faculty of Yale University, the University of Auckland, Carnegie Mellon University, and Louisiana State University, where he is currently the Francis S Blummer Professor of Mechanical Engineering. His research is primarily concerned with fracture mechanics, tribology, and numerical methods. Recent interests focus on finding means of improving modeling so that stress and pressure singularities are removed from both solid and fluid mechanics problems, and submodeling procedures and verification techniques for finite element analysis.